OF RIGID POLYMER MATERIALS BY
SEMEN MIKHAYLOVICH KOKOSHVILI

JPRS L/9371

28 October 1980

Translation

METHODS OF DYNAMIC TESTING OF RIGID POLYMER MATERIALS

By

Semen Mikhaylovich Kokoshvili

FBIS FOREIGN BROADCAST INFORMATION SERVICE

APPROVED FOR RELEASE: 2007/02/08: CIA-RDP82-00850R000300040051-8

NOTE

JPRS publications contain information primarily from foreign newspapers, periodicals and books, but also from news agency transmissions and broadcasts. Materials from foreign-language sources are translated; those from English-language sources are transcribed or reprinted, with the original phrasing and other characteristics retained.

Headlines, editorial reports, and material enclosed in brackets [] are supplied by JPRS. Processing indicators such as [Text] or [Excerpt] in the first line of each item, or following the last line of a brief, indicate how the original information was processed. Where no processing indicator is given, the information was summarized or extracted.

Unfamiliar names rendered phonetically or transliterated are enclosed in parentheses. Words or names preceded by a question mark and enclosed in parentheses were not clear in the original but have been supplied as appropriate in context. Other unattributed parenthetical notes within the body of an item originate with the source. Times within items are as given by source.

The contents of this publication in no way represent the policies, views or attitudes of the U.S. Government.

APPROVED FOR RELEASE: 2007/02/08: CIA-RDP82-00850R000300040051-8

JPRS L/9371

28 October 1980

METHODS OF DYNAMIC TESTING OF RIGID POLYMER MATERIALS

Riga METODY DINAMICHESKIKH ISPYTANIY ZHESTKIKH POLIMERNYKH MATERIALOV in Russian 1978 signed to press 29 Jun 78 pp 4-182

[Book by Semen Mikhaylovich Kokoshvili, Institute of Mechanics of Polymers, Lithuanian Academy of Sciences, Izdatel'stvo Zinatne, 1300 copies, 182 pages, UDC 620.178.7]

CONTENTS

ANNOTATION

[Text] This book deals with dynamic testing techniques that give results used as the basis for designing polymer parts and components that operate under impact loading conditions. Particular attention is given to tests of rings and beams, and also to the use of the split pressure bar method proposed by Hopkinson. The theoretical basis of methods of dynamic testing is outlined, and a detailed description is given of techniques for loading by electromagnetic fields and an electric discharge in liquid. The book contains reference material on the mechanical behavior of polymer materials over a wide range of temperatures and strain rates. Methods are given for constructing and verifying models of viscoelastic behavior of polymers. Tables 8, figures 148, references 170.

PREFACE

The introduction of modern synthetic materials requires extensive investigation of their mechanical properties, and above all demands development of sound methods of testing under various loading conditions. Practically and theoretically sound techniques and generalized reference books are available for static tests of reinforced plates, but in the field of dynamic tests an acute need is felt for just such developments. Dynamic tests for present-day polymer and composition materials are especially necessary as a consequence of the sharp sensitivity of these materials to changes in loading rate.

This book generalizes the experience of dynamic testing of polymer and composite materials that has been accumulated in the Laboratory of

Dynamic Properties of Polymer Materials at the Institute of Mechanics of Polymers, Lithuanian SSR Academy of Sciences. Considerable attention is given to methods of high strain-rate testing. However, the materials of research done by the author are naturally of special interest, in particular the development of methods of loading by electromagnetic fields and the electrohydraulic effect, improvement of the Hopkinson split pressure bar system, investigation of the properties of ring specimens and beams made up of reinforced plates. Although the data in the book are based on the study of polymer behavior, it is hoped that the proposed methods for dynamic loading and registration of high strain-rate processes will find application in the investigation of other structural materials.

All comments will be appreciated, and should be addressed to the author or the science editor at: 226006, Riga, Institute of Mechanics of Polymers, Lithuanian SSR Academy of Sciences, 23 Ayzkraukles Street.

V. P. Tamuzh
(science editor)

INTRODUCTION

A typical peculiarity of the behavior of polymer materials is the considerable time dependence of their mechanical properties. Inelastic behavior of polymers can be observed even in cases where the loading time amounts to days or is measured in microseconds. A fairly complete description of the principles governing mechanical properties of polymers is attained in complex mechanical tests that include changes in strain rates and temperatures.

Methods of mechanical tests of materials, regardless of the form of stressed state of the investigated object, can be differentiated into static, quasistatic and dynamic methods.

Static testing methods for polymer materials are based on using standard loading devices and recording equipment. The range of strain rates that are covered by these methods is fairly wide. In creep studies, strain rates are of the order of 10^{-6}-10^{-1} s^{-1}, and in the case of uniform tension -- 10^{-3}-10^{-1} s^{-1}. Static testing methods are not considered in this book.

Quasistatic testing methods cover strain rates of the order of 10^{-1}-10^{4} s^{-1}. These methods are realized by identical loading devices and identical recording facilities. The loading devices must meet the requirement of transmitting high energy to the specimen over a time that varies over wide limits (from a few milliseconds to microseconds). The recording equipment is quick-response sensors, wide-band amplifiers and oscillographic devices.

In describing the loading facilities, particular attention was given to devices that use electric energy, which have a number of advantages over

conventional loading devices, one of these advantages being the capability of loading the surface of a specimen by forces with a given distribution. Methods of transmitting electric energy to a specimen are based on loading by powerful electromagnetic pulsed fields or by action through a transfer medium (free electric discharge in a liquid). Both loading methods have found application fairly recently in mechanical tests, and have a good outlook. Loading and recording facilities selected with consideration of anticipated strain rates, and also with consideration of the shape and dimensions of the specimen, comprise the testing method. The same test involving short-term loading can be taken as quasistatic or dynamic, depending on loading duration and the geometric dimensions of the specimen.

Dynamic testing is done with loading of the specimen by an intense short-duration pulse load that produces a nonuniform stressed state in the specimen as a consequence of stress wave propagation. Dynamic methods involve loads in which considerable inertial forces act on the specimen.

Investigation of wave propagation is the most developed method of dynamic testing. In a number of cases dynamic methods do not involve wave propagation, even though they are based on accounting for inertial forces. One form of the method is testing of a thin ring under the action of internal uniform pulse pressure.

The use of quasistatic testing methods is based on the assumption of uniformity of the stressed state of the specimen in time at any point, i. e. without consideration of wave processes. Therefore the results of quasistatic experiments are processed just as for static tests, although we will show that the loading and recording facilities of the methods to be compared are quite different. Quasistatic tests are done over a wide range of strain rates. Close to the upper limit of this range, the tests differ more and more from the static case. For example, the influence that inertial forces have on the process of deformation becomes more pronounced and apparent, as shown by recordings of the transient process.

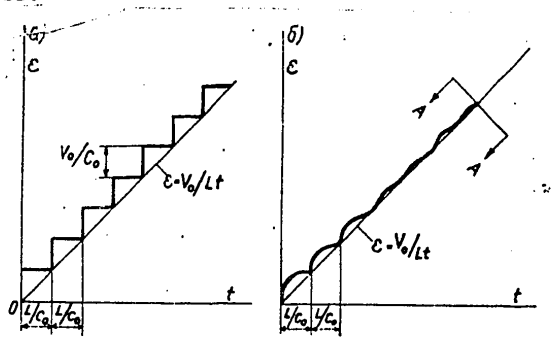

Fig. I.1. Displacement-time dependence in cross section x = L/2 for an elastic (a) and a viscoelastic (b) rod

As an example, Fig. I.1 shows two solutions of the problem of stretching of a uniform elastic rod of length L with one end fixed and the other moving at constant velocity V_0. The straight line $\varepsilon = V_0 t/L$ is the result of the quasistatic approach to the solution. The graph showing the step function is the solution of the dynamic problem for cross section $x = L/2$ of the rod. The dynamic and static solutions coincide at times Ln/c_0 ($n = 0, 1, 2...$), where c_0 is the rate of propagation of longitudinal elastic waves in the rod. Experiments with a polymer rod show that viscosity effects are the cause of the observed ε-t dependence shown analogously in Fig. I.1, b. Region A-A can be taken as a transition zone. When this region covers a considerable part of the process of deformation, the test should be considered dynamic. Let us note that depending on the length of the rods, the same testing conditions may lead to different results that must be treated in accordance with quasistatic or dynamic methods. A combination of dynamic and quasistatic processes of deformation in mechanical tests is observed in a system made up of two long rods separated by a test specimen in the form of a thin gasket. Loading such a system by a pulse of certain length leads to quasistatic deformation of the gasket. At the same time, lengthwise nonuniform stressed state of the rods makes it necessary to treat their deformation as a dynamic process. This testing arrangement is realized by the Hopkinson split pressure bar method. Material testing by this method can be classified as intermediate between quasistatic and dynamic studies.

Conclusions about the stressed state of a specimen at strain rates that approach the limit of applicability of these techniques require additional proofs. Adequately precise definition of the quasistatic nature of deformation is complicated (compared with the above example) by nonlinear behavior of the test material, the need for accounting for radial movements of the specimen and so on. The final decision on the validity of the quasistatic approach to the treatment of test results is based on solution of the problem of propagation and interaction of stress waves in the specimen (see Fig. I.1). Testing by the Hopkinson split pressure bar method is substantiated by solution of the problem of wave propagation in the split bar. While efforts on the part of experimenters to eliminate the influence of wave processes in dynamic tests could hardly be expected to succeed, a change to new unconventional testing methods does make it possible to disregard wave effects in a specimen up to very high strain rates. One such method, on which development began quite recently, is testing of a thin ring with loading by a uniformly distributed impulsive foce. The dynamic response of the ring specimen to such loading makes it necessary to consider the ring as a mechanical oscillatory system, which requires registration of accelerations to compute the stresses in the ring.

New testing methods are now supplemented by quasistatic tests in the complex-stressed state. Such methods are still in the early developmental stage. In view of the complexity of solving problems on propagation of combined waves and the undeveloped state of the art, it could be assumed that there is no sound basis for quasistatic testing methods

in the complex-stressed state. Nevertheless we feel that it is necessary to examine the corresponding techniques. The first attempts to develop a biaxial version of the Hopkinson split pressure bar are especially promising in our opinion. It is apparently in this direction that further development of methods of dynamic and quasistatic tests will take place.

Has there been progress in the traditional method of testing for impact toughness which is standardized in the Soviet Union and elsewhere? Absolutely. More and more frequent use is now being made of standard methods that include registration of force and displacement. The impact toughness method is still the most accessible technique for qualitative evaluation of materials that are being compared. The breaking energy is calculated in accordance with the method of impact toughness testing without consideration of forces of inertia, i. e. such tests can be called quasistatic.

Dynamic and quasistatic studies are aimed at getting fairly exact mechanical characteristics. Generalization of the results of these tests in the form of models of mechanical behavior is of first-rank importance since engineering calculations are based on them. Materials of theoretical and experimental studies of wave propagation in rods can be used to verify a model obtained with consideration of the results of quasistatic experiments. The justification procedure is done in the following sequence: the problem of wave propagation in the rod is solved on the basis of the proposed model (which must necessarily conform to an equation of motion of hyperbolic type), and then an experiment is done to study wave phenomena in the rod. A decision as to applicability of the model is made on the basis of comparison of theory and experiment.

One of the important features of the mechanical behavior of polymers is considerable dependence of all mechanical parameters on strain rate. The way that strain rate affects the mechanical properties of polymers of different classes cannot be reduced to a single formulation. For example, studies of the mechanical properties of amorphous and crystalline polymers has shown that their mechanical behavior depends on the nature of the relaxation process that predominates during deformation.

The problems to be solved in this book were determined on the basis of the foregoing presentation:

1) the development of modern facilities for loading and registration;

2) verification of quasistatic methods of mechanical testing on the basis of theories of wave propagation;

3) construction of a model of mechanical behavior that reflects response of the material over a wide range of times of loading action, and verification of this model by studying wave propagation;

4) establishment of principles that govern the influence of strain rate on deformation and strength of polymers.

The author takes this opportunity to express sincere gratitude to the science editor of the book, Professor V. P. Tamuzh, and also to Professor G. S. Shapiro, Doctor of Technical Sciences V. V. Kovriga, Candidate of Technical Sciences V. V. Viktorov and Candidate of Physical and Mathematical Sciences R. A. Basin for discussing the results. The author thanks P. V. Tikhomirov for assistance, and also Yu. Ya. Riba, P. P. Kalninya and D. A. Abolinyu.

PART I

LOADING AND RECORDING FACILITIES FOR DYNAMIC TESTS

Dynamic tests utilize facilities that differ in the form of cumulative energy. Loading facilities that utilize mechanical energy (swinging and rotating hammers) and compressed gas energy (pneumatic hammers) have been fairly well developed. To hurl masses with velocity of the order of several kilometers per second, gas guns are used [Ref. 4, 64, 65]. Work has been successfully begun on using electrical energy accumulated in capacitors for dynamic tests.

Recording of dynamic quantities is made difficult by the brevity of the process, and therefore the use of rapid-action facilities enables reduction of response lag in accordance with the anticipated strain rates. At very high strain rates it is advisable to use non-contact measurement instrumentation distinguished by a comparatively small mass and short measurement base.

Without going into the question of reproducing equipment, let us note that modern cathode-ray oscillographs (S1-29, S1-33, S-37, etc.) that have taken the place of galvanometer oscillographs only partly meet the requirements of researchers because of the inadequate screen. The DL-905 instrument made by Datalab, which stores a pulse and reproduces it by a two-coordinate chart recorder in the necessary time scale could serve as the ideal reproducing device for dynamic tests.

Chapter 1

LOADING DEVICES

Depending on the kind of cumulative energy, facilities for quasistatic and dynamic tests can be classified as follows: 1) mechanical; 2) pneumatic and hydraulic; 3) using explosive energy; 4) using electrical energy. The use of these latter as loading devices has begun fairly recently, and therefore the most space in this chapter has been devoted to their description. A detailed description is given of two loading

methods based on the interaction of pulsed electromagnetic fields and use of the electrohydraulic effect.

1.1. Traditional* Loading Devices

The simplest device in this category is the *drop hammer*. This mechanism transmits the energy of free fall of a massive body to the specimen. Because of the restricted height from which the mass descends onto the specimen, the rate of impact of the free body on the specimen does not exceed 10 m/s. To increase the initial impact velocity, a slingshot device is used in which the energy of a stretched rubber band supplements the energy of free fall [Ref. 109]. The Ansler hammer was one of the first devices based on using free fall of a system with the specimen that stops when a mass fastened to the specimen impacts against projections of a massive base. Stretching of the specimen is accomplished by inertial forces. To increase the capacity of the device, it is necessary to increase the mass fastened to the specimen.

A more up-to-date design is proposed in Ref. 28, in which the weight is a hollow cylinder and stretching is accomplished by impact of the weight against a crosshead fastened to the specimen. The design proposed by N. N. Davidenkov is improved in Ref. 20.

Another extensive group of facilities using the energy of free fall is pendulum hammers with principal parameters defined by State Standard GOST 14703-73 (hammers, pendulum, for determining impact toughness of plastics). In recent years Japan, East Germany and other nations have been producing hammers for research purposes on which tests for cantilever bending and impact stretching can be done in addition to two-support bending tests. Such hammers are equipped with devices for measuring elongation of the specimen and the impact force; however, in some cases the results do not meet research requirements. The Soviet Union makes BKM-5-1 and BKM-5-3 hammers. Interchangeable pendulums and supports on the model BKM-5-1 allow tests for two-support bending, impact stretching, cantilever bending and shear.

Among the disadvantages of hammers with a falling weight are: 1) the limited impact velocity, which cannot be increased without increasing the dimensions of the hammer; 2) bending of the specimens due to pendulum travel on a circular arc; 3) repeated impacts of the loading element with the specimen. Nevertheless, the hammers meet requirements for getting estimates of the characteristics of materials to be compared by standard techniques.

Rotary hammers are based on using the energy of a flywheel accelerated to a predetermined speed. The Werkstoffprüfmaschinen testing machine plant

*For more detailed information on the loading devices here termed "traditional," we refer the reader to monographs in the reference list: 20, 22, 28, 29, 36, 109.

in Leipzig, East Germany, makes the series-produced PCO facility. In testing, one end of the specimen is held in a fixed clamp, and a light crosshead is fastened to the other end. The striker of the hammer is restrained by a pawl. When the rotor reaches the set speed, a signal energizes an electromagnet that releases the pawl. The striker thus freed swivels about a pivot under the action of centrifugal force, and occupies its working position by the instant when it meets the crosshead. The disadvantages of the hammer are the same as for the drop hammers. Adequate precision of results can be achieved with reliable registration of forces and deformation, and estimation of bending deformations with stretching of the specimen. Despite the capability for impact tests with velocity up to 50 m/s, sufficiently reliable results can apparently be obtained at velocities that do not exceed 7-8 m/s.

The inadequacy of the rotary hammer has been eliminated to a great degree in the design described in Ref. 37. An overall view of the unit is shown in Fig. 1.1. Specimen 1 with dynamometer 2 is fastened and centered in cylindrical guide 3 hinged to lever 4. At the instant

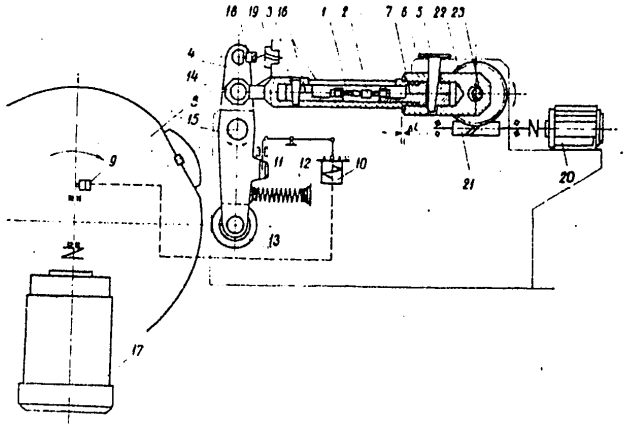

Fig. 1.1. Diagram of rotary hammer [Ref. 37]. See the text for details.

preceding impact, wedge 5 with springs 6 produces slight tension (about 10 kgf) on the specimen with dynamometer through clamp 7. When rotor 8 has reached the required speed, a controlling signal from the control panel through arcless breaker 9 releases the lever from pin 11 by means of electromagnet 10. Under the action of spring 12, the lever puts connected roller 13 under the thrust of striker 14 and, turning about pivot 15 through an angle determined by gap Δl, transforms the rotary motion of the rotor to translational motion of clamp 16 that has a velocity range of 2-30 m/s. After destruction of the specimen, motor 17 automatically switches to self-braking, and in the case of a single strike lever 4 is held by a special catch (not shown) in a position that

prevents idle knocking of the striker against roller 13 during deceleration of the rotor (5-6 s). Lever 4 is set in the initial position by worm gear 18, 19. Gap Δl can be regulated by motor 20 through worm gear 21, 22 and eccentric shaft 23. By regulating this gap, the force that arises in the specimen upon impact can be varied with fixed rotor speed.

Hydraulic and pneumatic facilities based on the use of energy transmitted by a liquid or compressed gas enable testing over a fairly wide range of strain rates. These devices are not industrially produced in the Soviet Union, and therefore a number of laboratories have developed original installations [e. g. see Ref. 16]. In the United States, some recent developments of the MTS system are used in quasistatic tests.

Pneumatic facilities [Ref. 7, 20, 70] enable testing to a fairly high strain rate (10^4 s^{-1}). It should be mentioned that A. A. Il'yushin [Ref. 86] was the first in the USSR to develop a pneumatic installation with technical parameters that satisfy modern requirements right up to the present. Ref. 94 deals with a hydraulic facility that operates over a wide range of velocities, and can be used for both static and dynamic testing ($\dot{\varepsilon} = 50$ s^{-1}).

The simplest design of a pneumatic facility (hammer) includes the following principal elements: a cylinder, a piston, a system for emptying the cylinder and a device for fastening the the specimen. To increase the speed of hammer action, the emptied part of the cylinder must have a minimum volume. The speed of the piston depends on its mass and the elements attached to it, and on the speed of operation of the valve that bleeds pressure in the cylinder. A low-pressure line is provided for regulating the position of the piston before the test (fastening the specimen, pretensioning, compression and so on). Systems with replaceable diaphragms that rupture for rapid discharge of gas from the cylinder have given a good account of themselves as emptying devices. Ref. 70 describes a device in which two diaphragms are ruptured (in two stages). First a blade slits one of the diaphragms, which leads to a rise in pressure on the other diaphragm. The abrupt bursting of the second diaphragm empties the cylinder at the appropriate rate. The kinematics of pneumatic facilities are considered in Ref. 70, 94.

The use of energy of powder and explosives for dynamic testing was started long ago because of a number of advantages of the method. Ordinary firearms are the simplest means used for impact loading of a specimen. Davis [Ref. 29] noted that different force-time relations can be realized by changing the shape of the tip of the bullet. A disadvantage of the method of direct impact of a bullet against the end of the specimen is that contact phenomena arise that are difficult to account for in processing results. This disadvantage has been eliminated in the loading methods described in Ref. 45, 77. G. M. Kozlov [Ref. 45] has proposed a facility in which a tubular specimen is subjected to tension upon impact of a lead bullet traveling at 300-800 m/s through a bullet guide connected to the loaded end of the specimen. Ref. 77 describes a facility that can strain a specimen at rates up to 1200 m/s.

The use of explosives for loading a specimen does not require special devices, excepting those cases where the force is transmitted through a transfer medium (for example a liquid). Ref. 41 describes methods of loading a specimen by forces of inertia of a mass with detonation of an explosive charge on its surface, Ref. 141 demonstrates the use of explosives as a source of energy for loading a Hopkinson bar, and Ref. 169 shows the use of explosives for studying surface waves.

The use of explosives is accompanied by electromagnetic pickups, and as a result registration of the stressed state is done either at a point removed from the blast point, or the surface of the specimen is studied by high-speed photography. We should point out the similarity of loading by explosives and by electrical devices, which is especially apparent when forces are transmitted through a transfer medium.

1.2. Magnetic-Pulse Facility

It is comparatively recently that electric energy has been used for mechanical tests. The basic principle of dynamic machines -- accumulation of considerable energy and release over a short time -- has been most successfully realized in facilities intended for dynamic and quasi-static testing. Energy is accumulated by capacitor banks, and discharge is accompanied by release of the energy. The device used for accumulating and releasing energy is called a pulse current generator. Two methods are known for transmitting the discharge energy of capacitors to a test specimen. The first is based on deformation of specimens by rather high-power pulsed electromagnetic fields [Ref. 9, 21, 34, 44, 136]. The technique is most simply realized by special inductors. Upon discharge, electrodynamic forces repel a metal body that is freely set on the inductor and is used as the striker on the test specimen. The other method of transmitting energy consists in using the so-called electrohydraulic effect, resulting in intensive pulse pressure in a liquid as a consequence of electric discharge.

The use of facilities based on electric energy stored in capacitors is dictated mainly by high efficiency and the capability for producing short and fairly intensive loads. An electric diagram of a pulse generator is

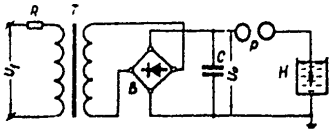

Fig. 1.2. Electric diagram of a pulse generator: T--high-voltage step-up transformer; B--high-voltage rectifier; C--capacitors; P--spark gap

shown in Fig. 1.2. The element for electrical-to-mechanical energy conversion (denoted by H on the diagram) in this case is based on free discharge in a liquid. The most important characteristics of the generator are the installed power and energy of the discharge, and also the period of the discharge. The discharge energy is

$$E=\frac{U_0^2}{2}C,$$

where U_0 is the working voltage. The frequency of capacitor discharge determines the shape of the pulse acting on the test specimen.

MIU-40/5 facility. The schematic electric diagram of a facility used at the Institute of Mechanics of Polymers, Lithuanian SSR Academy of Sciences, is shown in Fig. 1.3. The circuit operates as follows.

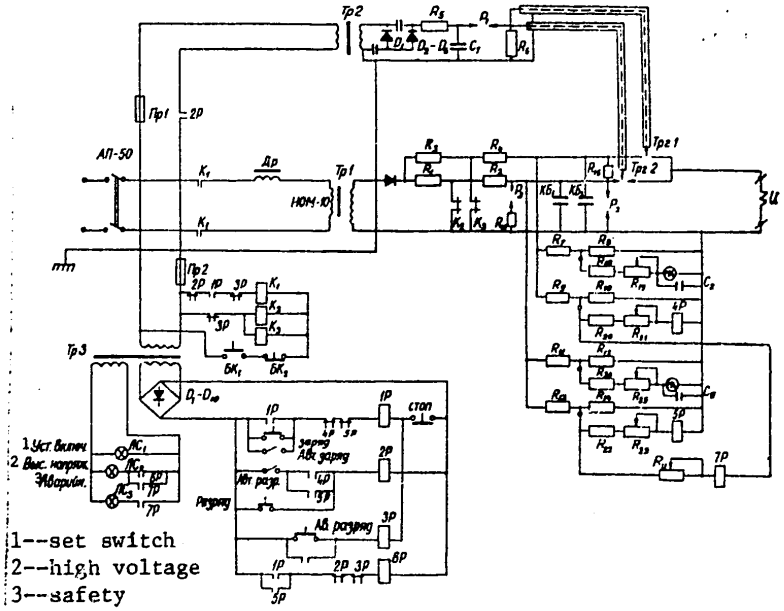

Fig. 1.3. Electric schematic of the MIU-40/5 facility at the Institute of Mechanics of Polymers [see explanation in text]

Pressing the "charge" button [*заряд*] engages contactor K1 that sends voltage to step-up transformer Tp1. The secondary voltage of the transformer is rectified by high-voltage rectifier BB and is fed through current-limiting resistors R_1-R_4 to sections of the capacitor bank *КБ1* and *КБ2*. The charging voltage level is monitored by microammeters connected in the circuits of each of the sections of the capacitor bank. Charging of the capacitor banks is stopped by pressing the "STOP" button [*СТОП*]; when this is done, capacitor K1 is disconnected. The "discharge" button [*разряд*] is pressed to discharge the sections of the capacitor bank to the inductor. Doing this energizes the ignition system consisting of elements *Тр2*, *Д1*,..., *Д6*, *С1*,..., *С6*, *R5*, *С7*, *Р1* and *Р6*. The ignition system produces a high-voltage pulse of 25 kV that is fed to the ignition electrodes of transformers Tp1, Tp2. The pulse ionizes the gap between the electrodes, resulting in discharge of the capacitor bank to the inductor. A more detailed description of the principal components of the circuit is given below.

Capacitor bank. The MIU-40/5 facility uses IMU-140-5 capacitors distinguished by low self-inductance. The capacitor bank is made in the form of two sections of ten capacitors each. The choice of two parallel operating sections of the capacitor bank facilitates the work of the dischargers. The possibility of non-simultaneous firing of both dischargers is prevented by a special ignition circuit. In each section, the capacitors are interconnected by three-layer flat busbars made of copper plates 6 mm thick.

Dischargers (Tp2). The facility uses two dischargers operating in parallel. Dischargers of coaxial type are used to reduce self-inductance. Teflon is the insulating material. Practical tests have shown that discharge tracks can be observed on the electrodes after 150-200 operations. The discharger leads are interconnected by a three-layer system of flat busbars to which leads are attached for connecting the load.

Step-up transformer, high-voltage rectifier. The primary of transformer Tp3 (see Fig. 1.3) is connected to a 220 V line. The MIU-40/5 uses an NOM-10 voltage transformer with secondary voltage of 10 kV and power of 750 W. The time for charging the capacitor bank to the full working voltage is about two minutes. The high-voltage rectifier rectifies the secondary voltage of the step-up transformer. The rectifier is based on silicon semiconductor diodes. The working voltage of the rectifier is 28 kV, which is much higher than the voltage rating of the transformer. The rectifier operates in a half-wave circuit.

Ignition device. The capacitor bank is discharged when a high-voltage pulse produced by a special system utilizing low-power step-up transformer Tp2 (see Fig. 1.3) with secondary voltage of 4 kV is sent to the controlling electrodes of a trigatron. For reliable firing of trigatrons the voltage pulse must have a steep leading edge, therefore the ignition voltage U_{ign} is chosen 2-3 times as high as the charging voltage of the capacitor bank. The voltage of the secondary winding of the transformer is stepped up by multiplying the voltage of *Д1*,..., *Д6* and *C1*,..., *C6* by a factor of six. Ignition capacitor C7 is charged to a certain level of voltage (24 kV), the capacitance of 0.8 μF ensuring a sufficient discharge frequency of C6, and thus providing a steep front for the initiating pulse. When the voltage across capacitor C7 reaches 20 kV, breakdown of the spark gap takes place in discharger P1, whose second electrode is connected through resistor R to the zero wire. When this happens, a high-voltage pulse is also sent to the controlling electrodes of trigatrons *Tp21* and *Tp22*. The selected discharge frequency of the ignition capacitor, which is 5-10 times as high as the frequency of the main current of the capacitor bank, is conducive to simultaneity of trigatron firing and discharge of both section of the capacitor bank.

The control circuit of the facility is based on DC electromagnetic relays supplied by step-down transformer Tp3 with rectifier *Д7-Д10* connected in a bridge circuit. Also connected to the transformer secondary is the supply to the signal circuits (*ЛС-1*...*ЛС-3*). When АП-50 is switched on,

voltage is fed to the facility that goes through normally closed contacts of relay 3P to the windings of safety discharge contactors K2 and K3. Pressing pushbutton *заряд* sends voltage to intermediate relay 1P through normally closed contacts of relays 4P and 5P. Intermediate relay 1P energizes contactor K1, which sends line voltage to the primary winding of step-up transformer Tp1. This results in charging of sections *КБ1* and *КБ2* of the capacitor bank. The resistance of R4 and R2 is experimentally determined for simultaneously charging these sections to a given voltage.

The voltage level across the capacitors is monitored by two microammeters connected to high-potential voltage dividers R7, R8 and R11, R12. Resistances of R19 and R25 are used for calibrating the microammeters with respect to a laboratory voltmeter. Capacitors C8 and C9 that shunt the microammeters protect them from pulse interference during discharge of the capacitor bank. Charging of the capcitor bank can be terminated by pressing pushbutton *СТОП*. This interrupts the supply to relay 1P and K1, and disconnects transformer Tp1 from the line. Charging is also terminated automatically when a certain voltage is reached, that is set by potentiometers R21 and R23 through which voltage relays 4P and 5P are supplied from voltage dividers R9,..., R14. Potentiometers R21 and R23 are selected so that at their maximum resistance the operation of relays 4P and 5P occurs at a voltage of 5 kV on the capacitor bank, i. e. the maximum permissible voltage. The next major operation on the facility -- discharge -- takes place after pressing the pushbutton *разряд*. This energizes intermediate relay 2P that supplies the ignition unit.

1.2.1. Loading by Electrodynamic Forces

The magnetic pulse facility can be a generator of a powerful pulsed magnetic field if an inductor is connected to its output terminals, and the magnetic field induces eddy currents in metal components in the near vicinity. Interaction between the magnetic field of the inductor and the induced field leads to mechanical body forces in the inductor and the components directed in accordance with the well known left hand rule. As a result of this interaction, the component is pushed away from the securely fastened inductor. Another method that is used for transmitting energy to a specimen from capacitors is based on repulsion of 2 conductors with currents in opposed directions. At present, both of these methods of transferring the energy of strong magnetic fields to a test specimen can be considered fairly well developed. The former is realized by single-turn inductors (Fig. 1.4); the latter is based on the use of

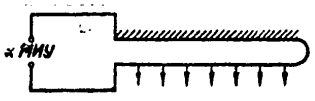

Fig. 1.4. Diagram of specimen loading by a single-loop inductor: к *ИМУ* = to magnetic-pulse facility

many-turn inductors paired with massive bodies. The accelerated masses may be plates [Ref. 9, 21, 34, 44], cylinders, etc. The working principle of the single-turn inductor is as follows. A one-piece or composite band

is shaped into a loop. One half of this loop is secured to a massive base, and the other half rests freely on the surface of the specimen. The ends of the inductor are connected to the leads of the magnetic-pulse facility. Discharge of the capacitors of the magnetic-pulse facility to the single-turn inductor leads to electrodynamic forces of repulsion between the two halves of the inductor. The use of the single-turn inductor for testing beams and rings is described in more detail in the next section. Discharging the capacitors of the magnetic-pulse facility produces electromagnetic pickups that complicate the recording process in tests with single-turn inductors. For this reason, recording must be done on the surface of the specimen at a point rather far removed from the inductor, or else the stressed and strained state that arises in the specimen under the action of inertial forces must be recorded (i. e. at the instant of termination of the discharge and hence when the influence of electrodynamic forces is absent). Complete independence of recordings from pickups due to discharge is attained when the force is transmitted to the specimen by using many-turn inductors to hurl massive bodies. To eliminate interference in this case, it is only necessary to choose the distance covered by the thrown body L before it meets the specimen such that the relation

$$\frac{L}{V_0} \geqslant T$$

is satisfied, where V_0 is the mean velocity of the hurled body, T is the time of discharge. The impulse of the force acting on the thrown mass is found from the formula [Ref. 43]

$$F = \frac{2\pi\mu_0 n^2 (R_1+R_2)}{\gamma^2 (R_2-R_1)} e^{-2\nu\gamma} I^2 \operatorname{sh}^2 \frac{\gamma l}{2}; \qquad (1.1)$$

$\nu = \left(\frac{H}{2}+\delta\right)\frac{1}{R_2}$; $\gamma = \frac{H}{b+c}$; μ_0 is the coefficient of induction; R_2, R_1 are the outside and inside radius of the inductor respectively; $h = H/R_2$; H is the thickness of a turn of the inductor; δ is the distance from the inductor to the mass to be thrown; I is the current in the inductor; n is the number of turns; c is the width of the insulation; b is the width of a turn. The velocity with which the mass is thrown is $V = F/m$.

At the Institute of Mechanics of Polymers, Lithuanian SSR Academy of Sciences, research has been done on throwing a mass by an inductor that is a copper plate in which Micarta is cemented into a milled spiral gap. Copper bars 8 mm in diameter were welded to the plate as leads of the inductor. The design of the projectile-mass is shown in Fig. 1.5. The way that the velocity of this projectile depends on the parameters of the inductor (Table 1.1) and the charging voltage of the capacitors is shown in Fig. 1.6 and 1.7. These figures also show the results of calculation by formula (1.1).

TABLE 1.1

Inductor parameters	Variants		
	I	II	III
Number of turns	3	6	6
Inside diameter $2R_1$	0	0	0
Outside diameter $2R_2$	70	70	70
Turn thickness H, mm	2.0	2.5	2.0
Turn width h, mm	9.0	5.0	9.0
Insulation width c, mm	1.0	1.0	1.0
Inductance, mH	0.244	0.833	1.640
Resistance, Ω	8.6	27.5	34.4

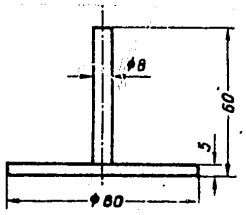

Fig. 1.5. Shape and dimensions of projectile-mass

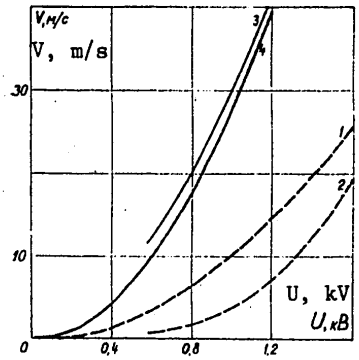

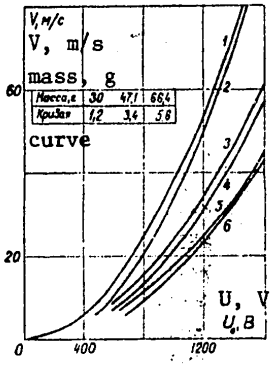

Fig. 1.6. Curves for projectile velocity as a function of voltage across the capacitors: 1 and 4--calculation; 2 and 3--experiments using inductors I and III (see Table 1.1). Projectile mass 30 g.

Fig. 1.7. Curves for projective velocity as a function of voltage across the capacitors and the value of the mass: 2, 4, 6--calculation; 1, 3, 5--experiment

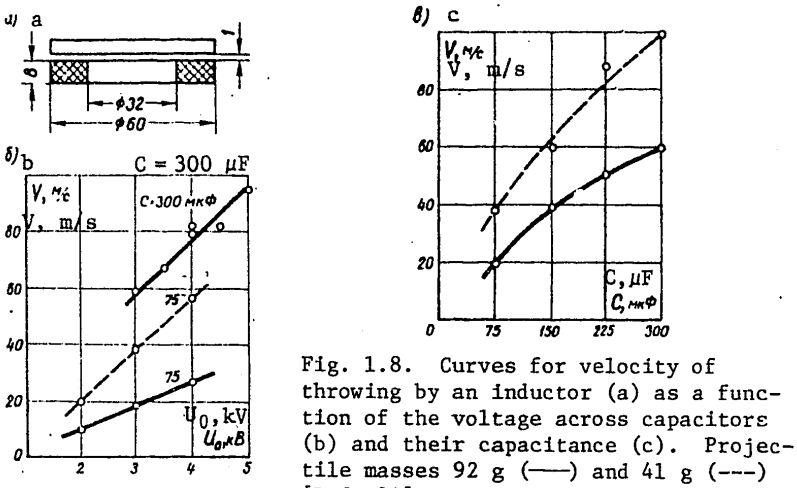

Fig. 1.8. Curves for velocity of throwing by an inductor (a) as a function of the voltage across capacitors (b) and their capacitance (c). Projectile masses 92 g (——) and 41 g (---) [Ref. 91].

Curves for the velocity of the projectile mass as a function of capacitance of the capacitors as plotted by G. V. Stepanov [Ref. 91] using an inductor consisting of 28 turns of PE 2.0 wire are shown in Fig. 1.8.

1.2.2. Loading by an Electric Discharge in Liquid

A method of producing high pulse pressures in a liquid by an electric discharge was discovered by L. A. Yutkin [Ref. 111] and called the electrohydraulic effect. The use of the electrohydraulic effect for testing began fairly recently [Ref. 3]. At the present time, electrical energy is converted to mechanical energy by two equivalent techniques: by exploding a wire in the liquid, or by an electric discharge in the liquid [Ref. 14, 40].

Electric discharge in liquid. The process of electric discharge in a liquid is characterized by a number of sequentially occurring effects. First electric breakdown takes place between electrodes with the formation of a spark channel in which high temperature leads to the formation of a gas-vapor cavity with high internal pressure that causes abrupt expansion until the pressure inside the cavity is equal to the hydrostatic pressure of the ambient liquid. Then the radius of the cavity fluctuates, attenuating in time. The abrupt enlargement of the gas-vapor cavity produces a shock wave in the ambient liquid.

In addition to formation of a shock wave and external fluid flow around the gas-vapor cavity, the discharge is accompanied by acoustic, ultrasonic, x-ray [Ref. 18] and other phenomena that have no significant influence on the process of deformation of the test speicmen, but do affect the recordings made during testing. The numerical values of the pressures on the shock wave front during free electric discharge in a liquid depend on many factors. Among these, we note the size of the

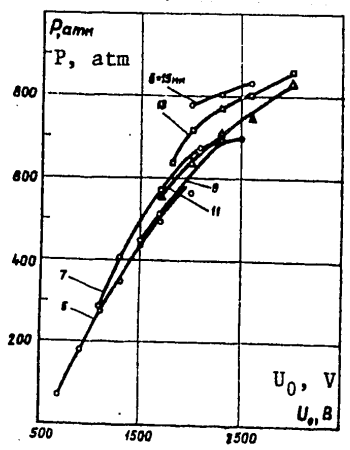

Fig. 1.9. Pressure in liquid accompanying electrohydraulic effect as a function of the discharge gap δ and initial voltage acorss the capacitors. The pressure was measured at a distance of 200 mm from the initiator.

discharge gap, the voltage across the capacitors, the inductance and capacitance of the capacitors.

Fig. 1.9 shows the way that pressure depends on the discharge gap and voltage across the capacitors of the MIU-40/5 facility. The pressure was determined at a distance of 200 mm from the discharge source by measurement of deformation on the surface of an aluminum rod with its end immersed in the liquid.

Chapter 2

RECORDING DEVICES

Recording during dynamic testing is faced with a number of difficulties due to the brevity of the processes to be recorded. The measurements are influenced by the time lag of the recording sensors, wave phenomena in the specimen, and the frequency responses of the recording and amplifying equipment Development of correct and sufficiently reliable recording methods is aimed primarily at eliminating the influence of these effects on the parameters to be recorded.

2.1. Measurement of Load and Pressure

The load must be recorded in addition to strain measurements for plotting stress-strain diagrams in quasistatic and dynamic tests. When forces are transmitted to the specimen through an intermediate medium, the pressure is measured. Linear forces are determined by sensors (strain gages, piezoelectric sensors, capacitive, inductive, dielectric). The

main requirement to be met by the dynamometer is that readings must be independent of strain rate, i. e. the static and dynamic calibration should coincide. Force registration by dynamometers reduces to measuring deformation of an elastic element by sensors of a type determined by the anticipated magnitude of the force as well as the time of its action. The elastic element of the dynamometer may be the thickened portion of the specimen [Ref. 7, 20] or a special structural component that goes beyond the limits of the specimen. The simplest dynamometer of the latter type is a long waveguide rod. The main requirements to be met by dynamometers that are a thickened portion of the specimen are: the stresses in the thickened part must not exceed the yield point of the material, which should show pure elasticity. Therefore the given method of force measurement is used only in testing metals. The values of the force measured on the thickened part of a specimen in quasistatic tests of polymers cannot be considered reliable because of the dependence of the mechanical properties of the specimen material on strain rate.

2.1.1. Piezoelectric Dynamometers

Dynamometers may be placed on the striker or in direct proximity to the stationary clamp. Combining the dynamometer with a massive striking body is most justified in recordings that accompany tests for dynamic bending.

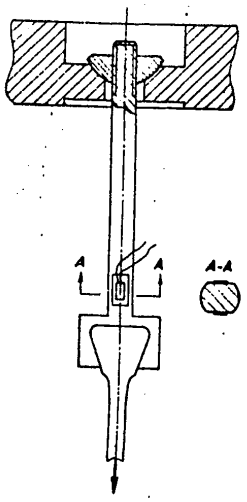

Fig. 2.1. Diagram of the simplest dynamometer

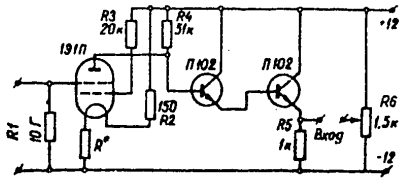

Fig. 2.2. Circuit of the simplest piezoelectric amplifier [Ref. 66]: *exog* = input

The simplest dynamometer located beyond the limits of the specimen is shown in Fig. 2.1. The construction of the elastic element depends on the method used for measuring deformation. The dynamometer has the

simplest construction when deformations of the elastic element are measured by strain gages placed as close as possible to the clamp.

Regardless of the measurement method, the dynamometers must meet the following requirements: 1) the frequency of their normal modes must be sufficiently high; 2) the readings of the dynamometer must depend linearly on the applied load. These requirements are interrelated since they reduce to the necessity for high rigidity of the dynamometer, which in turn leads to a reduction in sensitivity of strain gage registrations. As a result, a trend was noted long ago to force measurement by piezoelectric pickups with sensitivity 2-3 orders of magnitude greater than that of recording by strain gages under conditions of identical dynamometer sensitivity. A definite advantage of using piezoelectric sensors is the capability for measuring weak forces, which is very important in tests of low-modulus materials, filaments and so on. Another advantage of piezoelectric dynamometers that is no less important is practically total shielding from pickups due to ionization of the air when explosives are used, and also with the use of electric energy stored in capacitors.

Piezoelectric measurements are based on the piezoelectric effect, and on the charge that arises when a load acts on a piezoelectric element. Quantitatively, the piezoelectric effect is determined by the relation

$$q = \alpha P, \tag{1.2}$$

where $\alpha = \text{const}$ is the piezoelectric constant. The piezoelectric effect is displayed by materials among which quartz occupies a special place due to high mechanical strength. A number of ceramics that have lower mechanical strength have a piezoelectric constant an order of magnitude greater than that of quartz (Table 2.1).

The emf that arises upon impact loading in a piezoelectric element can be recorded by a reproducing device without intermediate amplification. However, for purposes of static graduation of the piezoelectric element an amplifier with high-impedance input is needed to reduce the rate of bleeding of the charge from the element.

Piezoelectric amplifiers have practically zero lag. Fig. 2.2 shows a schematic diagram of the simplest amplifier [Ref. 66]. The standard PM-1 set (East Germany) includes a piezoelectric amplifier with high-impedance input. The device can be used for static graduation of piezoelectric elements, and has a wide frequency passband. Standard dynamometers called force sensors or pressure sensors are also produced in the United States and Denmark. Practically all standard force sensors have a low level of measurable force, and therefore are used mainly in testing materials for harmonic oscillations (from 0.5 g to 5-10 kg).

Dynamometers for tensile tests. In contrast to designs with annular piezoelectric elements in standard non-Soviet dynamometers, the devices

TABLE 2.1

(1) Параметры	(2) Кварц	(3) Титанат бария			(4) Цирконат-титанат свинца			(5) Ниобат свинца	
		ТБ-1	ТБК-3	БКС	ЦТС-19	ЦТС-21	ЦТС-22	НБС-1	НБС-3
(6) Плотность ρ, г/см^3	2,65	5,3	5,3	5,2	7,0	7,0	7,0	5,6	5,5
(7) Пьезомодуль $d\left(\frac{C}{N}\cdot 10^{12}\right)$	2,2	$\alpha=45$ $\beta=100$	$\alpha=45$ $\beta=85$	$\alpha=20$ $\beta=50$	$\alpha=100$ $\beta=200$	$\alpha=25$ $\beta=65$	$\alpha=50$ $\beta=100$	$\alpha=65$ $\beta=165$	$\alpha=40$ $\beta=100$
(8) Акустическая жесткость, г/см^2·с·10^{-4}	152	220—245	240—265	230—260	210—260	245—265	250—280	200—240	200—230
(9) Прочность на сжатие, кгс/см^2	35000	3000	2500	3000	3000	3000	3000	2000	2000
(10) Прочность на растяжение, кгс/см^2	1000	250	—	—	—	—	—	—	—
(11) Прочность на изгиб, кгс/см^2	1270	600	—	—	—	—	—	—	—

KEY:
1--Parameters
2--Quartz
3--Barium titanate
4--Lead zirconate-titanate
5--Lead niobate
6--Density ρ, g/cm^3
7--Piezoelectric constant $\alpha\cdot(10^{12}$ C/N)
8--Acoustic stiffness, g/cm^2·s·10^{-4}
9--Compressive strength, kgf/cm^2
10--Tensile strength, kgf/cm^2
11--Bending strength, kgf/cm^2

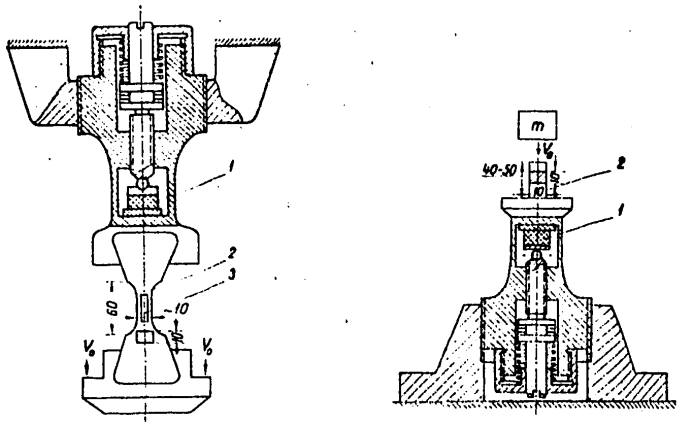

Fig. 2.3. Construction of piezoelectric dynamometer for tensile tests: 1--piezoelectric sensor; 2--specimen; 3--strain gage

Fig. 2.4. Construction of piezoelectric dynamometer for compressive tests: 1--piezoelectric sensor; 2--specimen

described below use piezoelectric elements in the form of disks that can take considerable forces. The time lag of the force sensor is evaluated on the basis of dynamometer design data, including the clamp for holding the specimen if the dynamometer is intended for force registration under tension. Fig. 2.3 and 2.4 show dynamometer designs in which the piezoelectric sensor is located as close as possible to the specimen in the clamp, which leads to an increase in the natural frequency of the dynamometer [Ref. 50, 51]. The piezoelectric element is installed in a window in the elastic element, which is combined with the clamp and precompressed by a screw. As the specimen is stretched, deformation of the elastic element relieves the pressure on the precompressed piezoelectric sensor, and an emf arises. Piezoceramic pellets 8 mm in diameter and 5 mm thick are used as the piezoelectric element. The natural frequency of the dynamometer depends on its geometric dimensions.

Dynamometers for compressive tests have a design analogous to that described above. The only difference is that there are no clamps, which increases the natural frequency of the dynamometer. Fig. 2.5 shows a typical oscillogram produced by a dynamometer with natural frequency of 50 kHz [see Fig. 2.4].

2.1.2. Waveguide-Dynamometers

The lag time of dynamometers described in the preceding section limits their applicability in tests with strain rates of about 20-50 s^{-1}. The range of applicability is expanded by using waveguides, the main purpose being to prevent the natural vibrations of the dynamometer from being

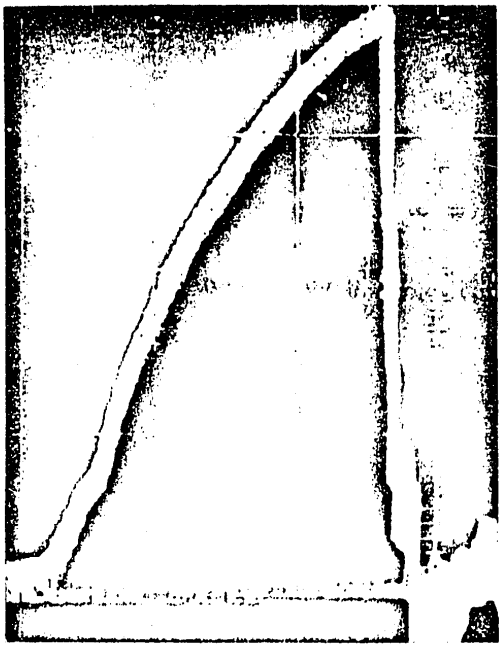

Fig. 2.5. Typical force-time oscillogram produced by a dynamometer [see Fig. 2.3]. Testing of glass-textolite at $\dot{\varepsilon} = 5\ s^{-1}$ (AST fabric -- 50%, EDT resin -- 50%).

passed on to the specimen. A diagram of force measurements by waveguides is shown in Fig. 2.6. The length of the waveguide is selected so that

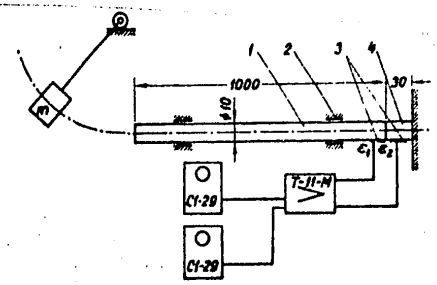

Fig. 2.6. Diagram of force registration by a waveguide in compression tests: 1--waveguide rod; 2--support; 3--strain gage; 4--specimen

the reflected waves from the left end do not reach the specimen during testing. If the length of the specimen is more than an order of magnitude less than the length of the waveguide, a quasistatic state may be rapidly reached in the specimen, whereas there is no such state in the waveguide throughout the course of the experiment. The simplest version of a waveguide is a specimen with an elongated dynamometric section [Ref. 76, 92]. The advantage of a force sensor with a long waveguide rod

is obvious, and shows up in the absence of distortions caused by natural vibrations of the force sensor and elements of the facility [Ref. 23].

Methods have been developed at the Institute of Mechanics of Polymers, Lithuanian SSR Academy of Sciences, for recording quasistatic compression with a strain rate of up to 100 s^{-1} by using a waveguide [Ref. 53]. Given below is the experimental technique and a comparison of the results of measurements by the dynamometers described in 2.1.1 and by waveguides. Stress-strain diagrams obtained by these devices are shown in Fig. 2.7, showing the feasibility of plotting a reliable diagram right up to $\dot{\varepsilon} = 100\ s^{-1}$.

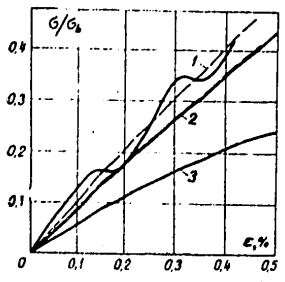

Fig. 2.7. Diagrams of σ/σ_b vs ε in which the values of σ were found by a waveguide (---) and by a piezoelectric dynamometer (——) in compression tests: 1--strain rate 26 s^{-1}; 2--5 s^{-1}; 3--10^{-3} s^{-1}; σ_b is the static breaking point.

A steel rod (waveguide) 10 mm in diameter and 1 m long [see Fig. 2.6] was placed in Teflon bearings and put into contact with a test specimen resting against a rather massive plate. The specimens were bars with a cross section of 10×10 mm and length of 30-40 mm. The loading device was an MK-30 pendulum hammer. The signals from strain gages A and B cemented close to the contacting ends of the rods were amplified by a T11-M device and fed to the inputs of two S1-29 memorizing oscilloscopes. Considering that the steel rod was elastically deformed, the experimental relation between strain and time (ε_I-t) on the end of the steel rod was transformed to a relation between force and time (P-t). Dynamic stress-strain diagrams were plotted from relations ε_{II}-t for a polymer rod, and from P-t curves.

Pressure sensors. The necessity for pressure measurement arises in cases where loading is done by an explosive charge or by underwater explosion of a wire. In either case the dynamic pressure is transmitted to the specimen through an intermediate medium (liquid) in which the pressure is recorded. Pressure sensors produced by a number of non-Soviet enterprises and companies have a fairly wide range of measurable pressure. The natural frequency of the sensors is no more than 45 kHz. Quick-response instruments based on waveguides have been used for recording pulse pressures over the last few years. A version of pressure recording using a waveguide is shown in Fig. 2.8. The waveguide material is chosen so that the acoustic stiffness ρc (Table 2.2) of the piezoelectric element is not appreciably different from that of the waveguide. The sensor for measuring pulse pressure [Ref. 66] (see Fig. 2.8) consists of a waveguide and piezoelectric element that have the same acoustic resistance.

TABLE 2.2

Waveguide material	$\rho c \cdot 10^{-4}$ g/s·cm^2	Piezoelectric material	$\rho c \cdot 10^{-4}$ g/s·cm^2
Bismuth	214	НБС-1	200-240
Cadmium	240	НБС-3	200-230
Zinc	296	ЦТС-19	290
Aluminum	169	quartz	152
Steel-3	454	-	-

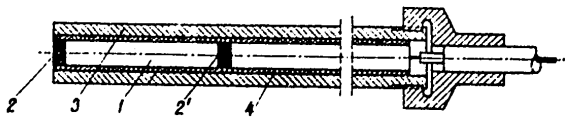

Fig. 2.8. Piezoelectric pressure sensor: 1--elastic rod (waveguide); 2, 2'--versions of placement of piezoelectric elements; 3--casing; 4--insulating tube

The sensor for measuring pulse pressure, including the piezoelectric element, can be statically calibrated.

The simplest version of the pressure sensor is a metal rod waveguide with cemented strain gages (results of application of the sensor will be considered later on).

2.1.3. Capacitive and Dielectric Pressure Sensors

Below we describe methods of recording dynamic forces and pressures that have not been extensively used because of the complexity of realization and limits of applicability. Nevertheless, we will consider them in this section since experimental practice does not exclude cases where just such methods are the only ones that can be realized.

A capacitive sensor of diaphragm type is described in Ref. 36. The pulse pressure to be measured by the sensor compresses its elastic element (e. g. a mica ring), whose thickness determines the gap in a capacitor. The sensor is connected in a tank circuit to which high-frequency voltage is sent from a stabilized quartz-crystal oscillator. The tank is tuned slightly off the frequency of the oscillator. Change in the capacitance of the sensor under the action of a load increases or decreases the mismatch of the tank frequency. The amplitude of the rf voltage on the tank varies as a function of the magnitude of the force acting on the diaphragm, and as a result the carrier frequency is amplitude-modulated, and

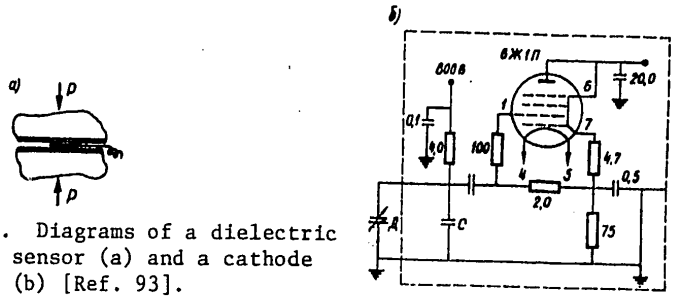

Fig. 2.9. Diagrams of a dielectric pressure sensor (a) and a cathode follower (b) [Ref. 93].

then goes to an oscilloscope input through a bandpass amplifier and detector.

Dielectric pressure sensor [Ref. 79, 93]. This is a capacitor formed by aluminum foil (0.01 mm thick, 12 mm in diameter) and adjoining metal surfaces with a dielectric film between them (see Fig. 2.9, a). Preliminary electrical polarization of the dielectric compressed between plates under a potential of 800 V through a resistor of 4.3 MΩ ensures constancy of the charge accumulated on the capacitor of the sensor and the capacitive divider. The dynamic component of the voltage across the sensor due to the change in capacitance with compression of the dielectric is sent through a cathode follower (Fig. 2.9, b) to the input of the oscilloscope.

2.2. Measurement of Displacements and Deformations

The basis of photoelectric methods of measurement in quasistatic and dynamic tests is the use of photoelectric devices -- photocells and photomultipliers -- that convert radiation in the visible, ultraviolet and infrared regions of the spectrum to an electric signal. This conversion is based on the photoemissive effect in which a flux of radiation incident on the surface of certain semiconductors and metals produces emission of electrons (the physical nature of this effect is described in Ref. 71). Reasons for using photocells and photomultipliers in dynamic and quasistatic tests are: 1) practically zero response time; 2) capability of total shielding of the measurement system from pickups caused by the discharge of capacitors and ionization of air when explosives are used; 3) high sensitivity; 4) capability of direct static calibration.

The simplest circuit for photocell connection is shown in Fig. 2.10. Displacement is registered by a display component (flag) fastened to a moving element that varies the light flux from the source. Between the flag and the photocell is a diaphragm (Fig. 2.11), which is a metal plate with a specially shaped opening. Because of the difference in sensitivity of cathode sections relative to the center, the opening has a shape like that shown in Fig. 2.11 to make the sensor readings linear. Sensors for registration of displacements in quasistatic tests differ with respect to the distances between the photocell and the light source. In the diagram

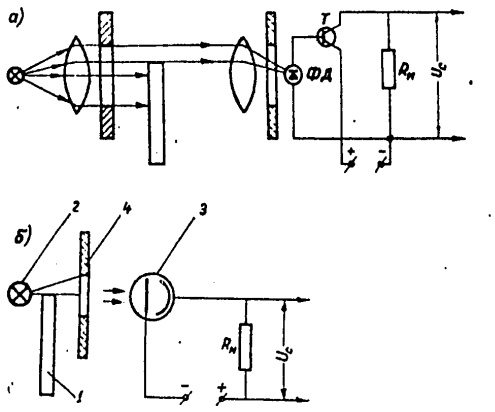

Fig. 2.10. Systems for recording displacements by photocells with an optical lens system (a), and without one (b): 1--display element; 2--light source; 3--photocell; 4--diaphragm; ФД--photodiode

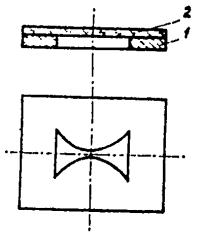

Fig. 2.11. Construction of diaphragm (1) with frosted glass (2)

of Fig. 2.10, b, this distance is set at a minimum, and the light source and photocell are accommodated in two housings fastened by bolts. The clearance between the housings permits passage of the flag. A diagram of a displacement sensor in which the light source is more distant from the photocell and the photomultiplier is shown in Fig. 2.10, a. In contrast to the previously described sensor, this one is equipped with a lens system. Registration of displacements by photocells and photomultipliers with the use of flags is applied in the case of quasistatic testing of materials. The indicator flag may be a moving part of the loading device.

2.2.1. Photoelectric Methods

Use of the method described above is limited to impact velocities at which vibration of the indicator component begins to distort the results, and moreover it cannot be used to register small displacements (of the order of 0.01 mm).

The interferometric method of measuring longitudinal extension of a specimen under tension enables determination of quantities with very high precision. Ref. 156 describes the use of an interferometric method for measuring elongation and the angle of turn of a specimen subjected to torsion and tension. Fig. 2.12, a shows a system for recording elongation of a specimen in quasistatic tests. The measurement links were

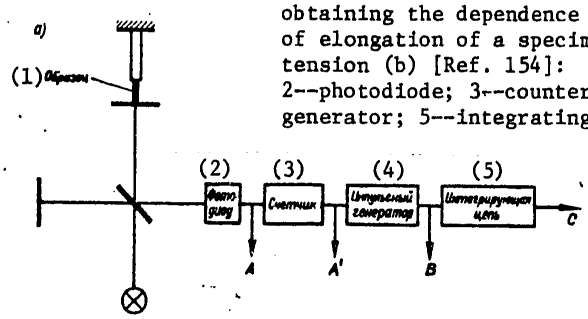

Fig. 2.12. System for interferometric registration of elongation of a specimen (a) and stages of obtaining the dependence in time of elongation of a specimen under tension (b) [Ref. 154]: 1--specimen; 2--photodiode; 3--counter; 4--pulse generator; 5--integrating circuit

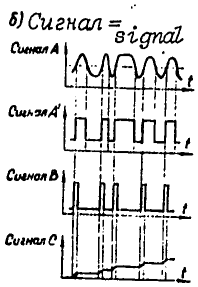

interferometers. Fig. 2.12, b shows the corresponding signal diagrams obtained in the circuit elements of Fig. 2.12, a. The signals from the photodiodes are sent to a binary-decimal counter, which is a device based on discrete measurement by coding of the quantity to be measured (designs of counters are described in Ref. 71). The pulses have the same amplitude and rise time and are used to trigger an oscillator in which each trigger pulse produces a pulse of constant amplitude and duration at the output. Thus the passage of each interference band produces a pulse of predetermined amplitude and duration. The pulses are fed to an integrator, and from there to an oscilloscope. The interference photoelectric method used for recording deformations in tests of materials [Ref. 5, 115, 116] is now under intensive development, and certainly deserves attention.

Registration of deformations is done as follows. A diffraction grating is formed on the surface of the specimen, at which a laser beam is aimed. Upon reflection from the grating, the beam is diffracted and split into several beams that satisfy the Bragg condition (see Ref. 115):

(2.2)

where λ is the wavelength of laser emission, Θ_n is the angle of deflection of the n-th order beam, d_0 is the lattice constant for the grating on the undeformed specimen. As the specimen is strained, the lattice constant changes, causing a change in angle Θ_n. Thus the registration of

deformations during testing reduces to measurement of the angle Θ_n. The theory of the diffraction grating is considered in Ref. 115. The system for converting the input quantity to recorded strain is not different from that given above for all practical purposes.

2.2.2. Strain-Gage Methods

The change in resistivity of electrically conductive materials under the action of mechanical forces (strain-gage effect) is the basis for recording deformation by metallic strain wires. The most pronounced strain effect is displayed by semiconductor materials (germanium, silicon, indium antimonide, etc.). Both metallic and semiconductor strain wires are currently in use as strain gages. The principal equation of the strain effect for a metallic strain gage is

$$\frac{\Delta R}{R} = S\varepsilon, \tag{2.3}$$

where ε is relative deformation of the wire, R and ΔR are deformations [sic] of the unstrained wire and the increment in its resistance under the action of a force; S is a coefficient of strain sensitivity (ranging from 1.9 to 2.9 for high-resistance wires).

Two kinds of metallic strain gages -- wire and foil -- are produced by Soviet industry. Wire strain gages are made from annealed constantan (GOST 492-52). The strain gages have a comparatively low coefficient of strain sensitivity (about 2.1). Other disadvantages of wire strain gages are an inadequate range of measured deformations (less than 0.3-0.5%), sensitivity to transverse deformation and low permissible current.

Foil strain gages are made from constantan foil 2-10 μm thick. Their main advantage is lower sensitivity to transverse deformations than wire strain gages. The use of annealed iron for foil strain gages increases the maximum measurable relative deformation to 10% [Ref. 35].

Of the semiconductor materials that have been studied at the present time the most suitable for making strain gages are germanium and silicon. The strain gages made from these materials are called gedistors and kremnistors respectively. Gedistors are not nearly as good as kremnistors in their operational parameters. The coefficient of strain sensitivity of semiconductor strain gages reaches 200, which gives a signal at the output of a bridge circuit of the order of a few volts with power of hundreds of milliwatts, obviating the need for amplifiers.

Measurement and amplification circuits for registration of deformation by strain gages. The strain gage senses the deformations to be measured and transforms them. In order to register changes of resistance, they must be converted to the corresponding current or voltage. To do this, the strain gage is connected in an electric measurement circuit that is capable of performing these transformations. Two strain-gage conversion

circuits have been developed: the potentiometric circuit and the bridge circuit. These produce electric signals with a change in resistance of the sensor. When metallic strain gages are used, these signals may be so weak that they are not felt by the recording device (oscilloscope). In such cases, resort must be had to special amplifying devices that raise the signals to the necessary levels.

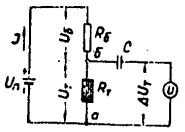

Fig. 2.13. Potentiometric strain gage amplifier circuit [Ref. 110]

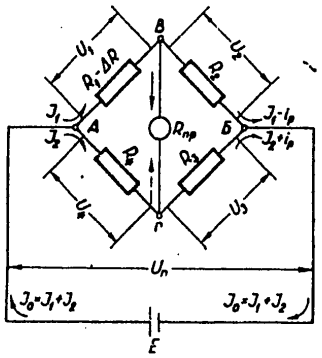

Fig. 2.14. Strain gage amplifier bridge circuit [Ref. 110]

The potentiometric conversion circuit is simplest (Fig. 2.13). The two-armed voltage amplifier consists of strain gage R_T and ballast resistor $R_б$ connected in series. The circuit is connected to a DC source with voltage $U_п$. Thanks to a capacitor that blocks the constant singal component, the potentiometric circuit becomes suitable for measuring dynamic processes. The voltage ΔU_T at the output of the amplifier depends on the voltage of the supply circuit $U_п$ and the resistance of strain gage R_T. The relation between ΔU_T and ΔR_T takes the form [Ref. 110]:

$$\Delta U_T = \Delta R_T \frac{U_п R_б}{(R_б + R_T)^2}, \tag{2.4}$$

and since $U_б = I(R_б + R_T)$, $\Delta R_T = S\varepsilon R_T$, it reduces to the form

$$\Delta U_T = I \frac{R_T \varepsilon S}{1 + \frac{R_T}{R_б}}. \tag{2.5}$$

In practice we take $R_T = R_б$, whence $\Delta U_T = 1/2 I R_T \varepsilon S$. We can see from (2.5) that increasing the supply current of the sensor causes a proportional increase in amplitude of the signal being recorded. Brief high-current loading of the strain gage (impermissible with prolonged duty) during dynamic tests is extensively used [Ref. 20, 35]. The sensor does not have time to change temperature in this period.

The bridge circuit for resistance measurement (Fig. 2.14) is based on a very important property of the bridge: at a certain resistance ratio in the arms ($R_1R_3 = R_2R_4$) the voltage at the output vanishes even when there is input voltage. The state of electrical equilibrium of the bridge is

very easily upset with the slightest change in the given position, so that measurements with the circuit are very sensitive.

Strain amplifiers. There are three types of standard strain amplifiers used in strain measurement: DC amplifiers, alternating voltage amplifiers and carrier frequency voltage amplifiers. The DC amplifier has considerable advantages over the other types, the main advantages being absence of frequency and phase distortions due to the fact that there are no reactive elements in the circuit. However, the DC type has the greatest zero drift, which is not very detrimental for recording rapid processes. Three-channel and ten-channel transistorized DC amplifiers have a passband of from 0 to 20 kHz.

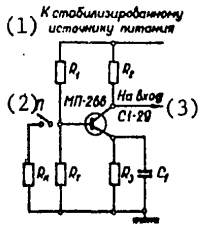

Fig. 2.15. Simplest transistorized strain amplifier circuit [Ref. 35]:
1--to stabilized power supply
2--switch
3--to S1-29 oscilloscope input

Alternating voltage amplifiers, while highly sensitive over a wide frequency range, are subject to strong influence from various kinds of interference. The use of carrier frequency voltage amplifiers for recording fast processes is limited since the limiting frequency of the carrier signal (close to 50 kHz) as a consequence of elevation of the carrier frequency causes an increase in phase shifts that impede balancing of the bridge with respect to the reactive component and reduce its sensitivity. The described strain measuring equipment [Ref. 20] is based on series produced oscilloscope EO-7 supplemented by a block of input amplifiers with carrier frequency oscillator and commutating device, and a series produced rectifier with electronic stabilization of the anode voltage.

The working principle of the amplifier shown in Fig. 2.15 is as follows [Ref. 35]. Strain gage R_T is connected in the measurement circuit in a potentiometric arrangement. The nonlinearity of the input circuit is less than 0.5% at a deformation of about 10%. Calibration is by vertical devlection of the oscilloscope beam when the strain gage is shunted by a calibration resistor. No phase or amplitude-frequency distortions are observed at a pulse rate of up to 500 kHz.

Influence that the base of the strain gage has on recordings in quasi-static tests. The mechanical distortions that accompny rapid processes are due to various effects, the most significant being wave propagation. Let us consider the influence that these distortions have on registration of the deformation of a strain gage resistor of length l cemented on the surface of a specimen subjected to impact. A mechanical quantity -- deformation -- is converted to an electrical quantity -- change in

resistance of wire. If ε is deformation at the point with coordinate x, then the complete equation of strain gage resistance is

$$\frac{\Delta R}{R}=\frac{S}{l}\int_0^l \varepsilon dx, \tag{2.6}$$

where S is the coefficient of strain sensitivity, and R is the initial resistance of the strain gage.

For a plane wave propagating at velocity c_0, deformation is $\varepsilon = f(x - c_0 t)$. The function $f(\xi)$ depends on boundary conditions. For the case where a load is applied to the end of the rod that causes a constant strain rate,

$$\varepsilon=\frac{\dot{\varepsilon}_0}{c_0}(c_0 t-x). \tag{2.7}$$

Limits of integration in (2.6) equal to 0 and $c_0 t$ correspond to the time interval during which the pulse front passes through the sensor, which gives on the first stage at $t \leqslant L/c_0$:

$$\frac{\Delta R}{RS}=\frac{\dot{\varepsilon}_0}{c_0 l}\int_0^{c_0 t}(c_0 t-x)\,dx=-\frac{\dot{\varepsilon}_0}{2l}c_0 t^2. \tag{2.8}$$

Denoting $\tau = l/c_0$, we rewrite (2.8) as

$$\frac{\Delta R}{RS}=-\frac{\dot{\varepsilon}_0 t^2}{2\tau};\quad t\leqslant\tau. \tag{2.9}$$

The stage is terminated at $t = \tau$:

$$\left.\frac{\Delta R}{RS}\right|_{t=\tau}=-\frac{\varepsilon_0\tau}{2}. \tag{2.10}$$

The readings of the strain gage on the second stage, i. e. $t \geqslant \tau$:

$$\frac{\Delta R}{RS}=\frac{\dot{\varepsilon}_0 t}{lc_0}\int_0^l (c_0 t-x)\,dx=-\frac{\dot{\varepsilon}_0}{2}(2t-\tau),$$

i. e. the solution is the piecewise function

$$\begin{aligned}\frac{\Delta R}{RS}&=-\dot{\varepsilon}_0\frac{t^2}{2\tau};\quad t\leqslant\tau.\\ \frac{\Delta R}{RS}&=-\dot{\varepsilon}_0 t+\dot{\varepsilon}_0\frac{\tau}{2};\quad t>\tau.\end{aligned} \tag{2.11}$$

Both stages are matched both with respect to amplitude and with respect to the first derivative:

$$\left.\frac{\Delta R}{RS}\right|_{t=\tau} = -\frac{\dot{\varepsilon}_0\tau}{2};\quad \frac{d}{dt}\left(\frac{\Delta R}{RS}\right)_{t=\tau} = \dot{\varepsilon}_0. \tag{2.12}$$

It can be concluded from (2.11) and (2.12) that: 1) distortion of strain registrations as deformation uniformly increases is expressed in the fact that on the first stage at $t \leqslant \tau$ the signal $\varepsilon = \dot{\varepsilon}_0 t$ is converted to the function $\dot{\varepsilon}_0 t^2/2\tau$ as a consequence of the fact that the leading edge of the wave passes through the sensor in finite time τ; 2) for times longer than τ, the recorded strain rate coincides with the actual value. Electrical distortions on the second stage (at $t \geqslant \tau$) are expressed in the fact that the recorded signal is less than the actual strain by an amount $\dot{\varepsilon}_0\tau/2$; 3) in contrast to other loading conditions (for example $\varepsilon = \text{const}$, $\varepsilon = Ae^{-t/\tau}$), under uniform deformation the function $\varepsilon(t)$ does not have a discontinuity of the first derivative.

The amplitude error of measurements as a function of strain rate $\dot{\varepsilon}_0$, base of the strain gage l and velocity of wave propagation c_0 in the investigated material is computed from the formula

$$\eta = \frac{\dot{\varepsilon}_0\tau}{2}\cdot\frac{100\%}{\varepsilon_{\text{макс}}} = \frac{\dot{\varepsilon}_0 l\cdot 100\%}{2c_0\varepsilon_{\text{макс}}}, \tag{2.13}$$

where $\varepsilon_{\text{макс}}$ is the maximum value for the strain gage at which it retains its linear readings. It can be concluded on the basis of (2.13) that the strain gage base l must be selected in accordance with the anticipated strain rates.

2.3. Measurement of Velocities

Methods of testing at low (less than 10 m/s) and moderately high velocities (up to 100 m/s) differ not only in the necessity of using wide-band equipment for the high-speed tests (with passband of more than 4 MHz), but also in construction.

Discrete registration of velocities is based on using oscilloscope pips that are generated by two or more electric contacts with known distance between them. Discrete velocity sensors (which are called electrocontact sensors) are most justified in measurement of the velocity of the body striking against the specimen. Ref. 36 describes the electric circuit for measuring the velocity of a striker up to 5 m/s used in the construction of a horizontal hammer with rubber striker accelerator. The system includes two independent electric circuits, one of which triggers an oscilloscope, while the other sends pulses from an electromagnetic sensor to the oscilloscope during motion of the striker preceding impact.

Ref. 79 describes a method of measuring velocities exceeding 300 m/s by electrocontact sensors (Fig. 2.16) made in the form of steel wires 0.5 mm

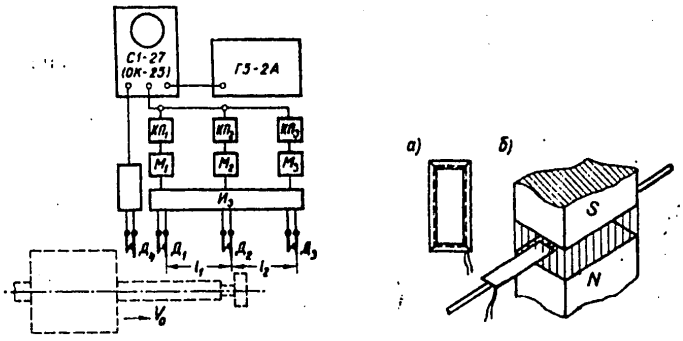

Fig. 2.16. Diagram of discrete registration of the velocity of a projectile [Ref. 79]

Fig. 2.17. Induction sensor [Ref. 69]: a--construction; b--sensor in a magnetic field

in diameter stretched perpendicular to the direction of motion of the striker. The measurement circuit includes multivibrators that operate in the slave mode. The multivibrators receive trigger pulses from a three-armed voltage divider when the wires are broken by the striker immediately before collision and after breaking the specimen. The multivibrators generated pulses with duration of 9.1 μs sent through cathode followers to the oscilloscope input. The slave sweep of the oscilloscope was triggered from a potentiometric circuit when the sensor was opened. The use of three sensors enables measurement of two time intervals and computation of two velocities, which improves the reliability of the measurements.

Discrete registration of velocities is satisfactory only in the case of measurement of kinematic quantities, in particular the velocity of a large mass striking against a specimen, since the velocity of this mass during the experiment is taken as constant. In case of necessity of establishing the velocity of a cross sectional surface or point of the specimen, continuous registration is advisable, a particular advantage of which is that where necessary the velocity registration data can be supplemented or replaced by displacement data by means of an integrating circuit. Two methods are known for continuous velocity registration, based on using inductive and capacitive sensors.

The inductive sensor (Fig. 2.17) is a rectangular mica frame on which 20-30 turns of fine wire are wound. The frame is fastened to a rod (wire), and one end is placed in the uniform magnetic field of a permanent magnet. With displacement along the long axis, an emf proportional to the velocity of displacement is induced in the frame. The signal from the sensor is sent without intermediate amplification to the input of a

cathode-ray oscilloscope. The small dimensions of the sensor, and consequently its low mass, enable investigation of wave propagation in rods [Ref. 48, 49, 69, 155]. In case of necessity, the signal from the sensor goes to the input of an RC integrator. This gives a recording of displacement as a function of time [Ref. 38]. The range of displacement measurements is limited to a quantity somewhat shorter than the sensor. The sensitivity of the sensor depends on magnetic field intensity, the distance between poles of the magnet, the number of turns and the width of the sensor. The use of the sensors is limited by the finiteness of their mass. High accelerations cause development of considerable inertial forces capable of deforming and destroying the sensor. The simplest method of calibrating inductive sensors is to compare recordings of the velocity V of some cross section of an elastic rod with data of strain measurements in the same cross section of the rod by a strain gage. In doing this, a relation is used from the one-dimensional theory of wave propagation:

$$-V = c_0 \varepsilon,$$

where c_0 is the velocity of elastic wave propagation.

Capacitive sensor. Recordings by capacitive sensors are zero-lag as a consequence of the fact that the sensor is non-contact. The convenience of measuring velocity or displacement of a free surface has led to use of a capacitive sensor in a system called the Hopkinson bar. A sensor was first used for this system by Davis [Ref. 29] who applied it for determining the displacement of the free end of a rod used as the grounded plate in a flat capacitor (the other plate was stationary while the rod was dynamically loaded). The change in capacitance of the capacitor thus formed in proportional to displacement of the end of the rod.

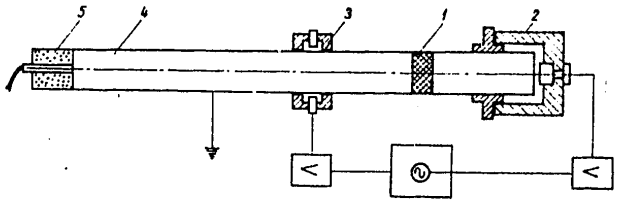

Fig. 2.18. Kolsky bar [Ref. 46]: 1--specimen; 2--flat sensor; 3--cylindrical capacitor sensor; 4--rod (waveguide); 5--explosive charge with cap

Further improvements in the method of determining stresses by recording the rate of displacement by capacitive sensors are given by H. Kolsky [Ref. 46]. Fig. 2.18 shows a diagram of what is sometimes called the Kolsky bar. This design includes two rods between which a pellet specimen is placed. Pulse pressure is applied to the free end of one of the

rods. The pulse propagating through the rod compresses the specimen. The incident pulse is recorded by a cylindrical capacitive sensor, which enables determination of the relation between velocity and time. A flat sensor measures the displacement of the free end of the anvil rod.

Further development of electric circuits, including capacitive sensors, has shown that the most convenient for dynamic measurements is an arrangement in which the potential difference across the sensor electrodes U_0 is proportional to the velocity of displacement. The signal amplitude from the capacitive sensor is [Ref. 93]

$$\Delta U = U_0 R \frac{dC}{dt} = kU_0 RV \frac{d^2}{x_0^2},$$

where R is the load resistance of the measurement circuit, V is the velocity of the free surface, $C = kd^2/x_0^2$ is the capacitance of the sensor, k is a constant, d/x_0 is the ratio of the diameter of the free electrode to the gap between electrodes. An increase in U_0, R and d/x_0^2 increases the sensitivity of the sensor. The maximum voltage U_0 is limited by the electric strength of the air gap. The permissible value of U_0 can be increased to several kilovolts by using a thin layer of dielectric to insulate the electrode from the surface of the specimen. Circuits for velocity measurement at $U_0 = 1500$ V were developed in Ref. 93. Electrodes with dimensions $d = 25$ mm, $x_0 = 2$ mm were used for measurements. The same voltage was applied to a guard ring with inside diameter of 28 mm and outside diameter of 96 mm. To prevent electric breakdown, a triacetate

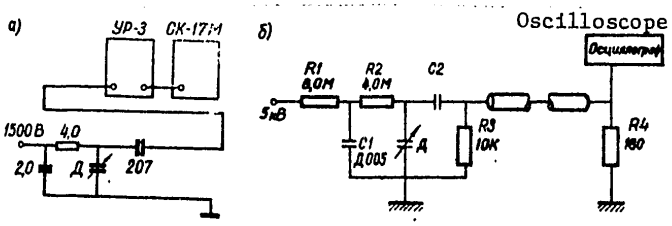

Fig. 2.19. Electric diagram for measurement of velocity by a capacitive sensor with initial voltage of 1500 V across the plates [Ref. 93] (a), and with initial voltage of 5000 V [Ref. 167] (b)

film 0.2 mm thick protected the electrodes of the sensor, the guard ring and the surface of the specimen (see Fig. 2.19, a). From the sensor, the signal went to the input of an oscilloscope through an amplifier with input impedance of 75 ohms. Ref. 124 and 167 give circuits for measuring velocity by a capacitive sensor with voltage of 5 kV applied to the plates (Fig. 2.19, b).

In concluding our survey of methods of velocity registration in dynamic tests, let us note that new non-contact facilities have been developed in recent years that are based on the use of laser interferometry [Ref. 11, 32, 33, 113, 163].

* * *

Since no universal facility has as yet been developed for testing materials over a wide range of strain rates, studies are done on two or three testing machines. Quasistatic tests are done by well developed facilities that use energy of various kinds (compressed gas, accelerated mass). The main disadvantage of devices based on accumulation of mechanical energy (hammers with a falling weight, pendulum and rotary hammers) is bending that cannot be eliminated. Pendulum and rotary hammers are intended for testing specimens with geometric dimensions that do not always satisfy the researcher. Hydraulic and pneumatic devices at present are the only facilities for quasistatic tests over a fairly wide range of strain rates.

Devices that use electrical energy have a number of advantages over the conventional loading devices: the capability of transmitting loads with distribution over the surface of the specimen that can be predetermined, and universality that ensures wide variation of the kinds of tests. An important advantage of the devices is also the capacity for transmitting considerable energy to a specimen over a quite brief time interval. The studies given in Part I of different modes of operation of the magnetic-pulse facility show the feasibility of throwing considerable masses at high velocities, and transmitting intense forces by electromagnetic fields as well as by free discharge in a liquid.

Dynamic tests are done for fairly precise determination of functions that characterize the stressed and strained state of a test specimen under short-term intense loads. This purpose may be attained when the tests are accompanied by correct and exact measurements, and therefore the recording facilities must meet requirements that minimize response time. Dynamometric devices combined with the clamp of a loading device with maximum frequency of up to 50 kHz may find application in quasistatic tests with strain rates of no more than 50 s^{-1}. Dynamometers in the form of waveguides permit testing of materials at rates up to $\dot{\varepsilon} = 10^3$ s^{-1}. Noncontact methods of measurements by capacitors and interferometry have practically no limits of applicability with respect to $\dot{\varepsilon}$.

PART II

Dynamic Tests of Rigid Polymer Materials

Testing of rod specimens is complicated by the presence of wave phenomena, stress concentration, local strains and so on. Therefore attempts have been made recently to develop reliable methods for taking consideration of these effects, if not eliminating them entirely.

The most developed method is the Hopkinson split-bar system based on the use of specimens of the simplest shape (pellets), enabling consideration of wave phenomena in the specimen. In the case of axisymmetric loading of a thin ring by a distributed dynamic load, wave processes in the specimen can be disregarded, which makes the method especially valuable. The method of dynamic bending of beams gives important information on the

resistance of polymer materials to shearing loads when studying transverse impact. The investigation of mechanical properties cannot in any way be considered complete without studying the behavior of polymer materials in the complex-stressed state.

In doing tests and developing methods, particular attention was given to substantiating the quasistatic treatment of the results of experiments, which is based on solving problems of wave propagation.

Chapter 3
THE HOPKINSON SPLIT BAR METHOD

A method of calculating dynamic stresses in an elastic rod by measuring the velocity of the free end was proposed by Hopkinson [see Ref. 46], and later improved by Davis [Ref. 29] who provided a velocity sensor for the method, and made a careful analysis of wave propagation in the rod. In 1949 H. Kolsky suggested using the Hopkinson bar to measure stresses and strains of a specimen in the form of a thin gasket. This marks the beginning of development of the Hopkinson split bar method for testing materials at considerable strain rates (up to $\dot{\varepsilon} = 10^4\ s^{-1}$). By the efforts of experimenters [Ref. 5, 116, 126, 132, 145, 147, 168] a technique was developed based on using modern loading devices and recording facilities. The Hopkinson split bar [HSB] method occupies an intermediate position between quasistatic and dynamic tests, since the stressed state of the specimen is uniform within its range of applicability, and the recordings that accompany an experiment are made with consideration of wave processes in long metal rods. Fairly well developed variants of the HSB method are compressive, torsional and tensile. Research has started on development of a biaxial variant of the technique.

All variants of the HSB method are based on using a system of split bars. These systems comprise two elastic rods (a pressure transmitter and an anvil) between which the specimen is placed. Recorded data on strains ε_I and ε_{II} enable determination of the stress and strain in the specimen. The rods are chosen of such a length that stress waves reflected from the free ends do not introduce distortions. An indisputable advantage of the method (as compared with conventional techniques) is the capability of: 1) tuning out interference due to the response time of the force sensor, vibrations of the installation, the foundation, etc.; 2) determining considerable deformations of a specimen measured in tens of percent; 3) preventing bending of a specimen in tensile and compressive tests; 4) correct validation of an experiment based on a simple scheme of force transmission to a specimen through rods.

Stresses and strains in the specimen in tests by the HSB method are calculated on the basis of a one-dimensional theory of wave propagation. According to the one-dimensional theory of elastic waves in semi-infinite rods, strain and stress are related to velocity by the expressions

$$\sigma = -\rho c_0 V; \tag{3.1}$$

$$\varepsilon = -\frac{V}{c_0}, \tag{3.2}$$

where ρ is the density of the rod material.

Let a rod consist of two sections with area F_1 and F_2, i. e. at some coordinate the rod is broken by a discontinuity of cross section. If the rod is loaded by stress σ^J, then a reflected wave will propagate from the coordinate of sudden change in F:

$$\sigma^R = -\frac{F_2 - F_1}{F_2 + F_1}\sigma^J, \tag{3.3}$$

and a transmission wave will enter the rod with area F_2 with stress

$$\sigma^T = \frac{2F_2}{F_1 + F_2}\sigma^J. \tag{3.4}$$

If the sections of rods F_1 and F_2 are made of different materials with acoustic stiffnesses $\rho_1 c_1$ and $\rho_2 c_2$, then the functions relating σ^R and σ^T to σ^J, according to the one-dimensional theory, take the form

$$\sigma^R = -\frac{\rho_2 c_2 F_2 - \rho_1 c_1 F_1}{\rho_1 c_1 F_1 + \rho_2 c_2 F_2}\sigma^J;$$

$$\sigma^T = \frac{2\rho_2 c_2 F_2}{\rho_1 c_1 F_1 + \rho_2 c_2 F_2}\sigma^J. \tag{3.5}$$

The correspondence between (3.5) and experimental results is demonstrated in Ref. 78, 132. The simplest refinement of the one-dimensional theory is a Love equation [see Ref. 22] derived by the Hamilton principle with consideration of the kinetic energy of radial motion. De Vault [Ref. 127] gives asymptotic forms of the solution of the Love equation.

At present no rigorous solutions have been found for the three-dimensional problem of wave propagation due to the complexity of simultaneously accounting for boundary conditions on the ends of the rod and its lateral surfaces. The solutions of Poghammer and Chree for a one-dimensional circular rod [see Ref. 22] are considered the best approximation. The complicated form of the frequency equation brings about certain difficulties for getting numerical results. Besides, since the solutions are represented as infinite waves, they cannot describe the propagation of discontinuities. Less rigorous theories are an attempt to simplify the mathematical description while retaining the most important conclusions of the three-dimensional theory. The precision of this theory is usually evaluated by comparing the corresponding spectra with those derived on the basis of the Poghammer-Chree theory. At present, the

exact equations are being successfully solved by numerical methods. In spite of the fact that in many cases they do not permit direct comparison of results with the exact Poghammer-Chree solution, the reliability of numerical results can be validated by existing methods of evaluating the accuracy of numerical methods.

Data found on the basis of the elementary theory do not agree with experimental data where the time of action of the load is commensurate with or less than the time taken by a wave to travel a distance comparable to the diameter of the rod. To describe the dispersion nature of wave propagation in rods, methods have been developed that give asymptotic solutions of exact equations of motion with mixed boundary conditions (displacements and stresses are given on the ends). It was found that the exact theory and all approximate theories (with the exception of the one-dimensional theories) lead to the same asymptotic solution for the head part of the pulse corresponding to the first mode of oscillations. These solutions take the form of an Airy integral, and are found on the assumption that flat cross sections are not curved during wave propagation, and therefore radial, circular and shear stresses are equal to zero. The curvatures of cross sections were first considered in an examination of waves in rods of rectangular cross section under the action of a suddenly applied load [Ref. 30]. An asymptotic solution of the problem for circular rods based on exact equations was found in Ref. 31 for the case of loading by stepwise pressure or by a velocity pulse. Numerical solutions have been found for the problem of wave propagation in an elastic rod when the end is loaded by pressure that depends on coordinate [Ref. 39].

Exact equations were used in Ref. 107, 108 for calculating dynamic stresses in a split bar. The results of this work can be expressed in the form of recommendations on loading a Hopkinson split bar and using it for recordings: 1) the head part of the pulse in a cross section not far from the end of the rod that is struck contains higher modes of vibrations that die out with distance from the end. Deformations on rods are measured in cross sections not more than twenty diameters from the ends; 2) the end face of the bar in the HSB system should be loaded by uniformly distributed pressure; excitation of higher modes increases when the rod is loaded by a concentrated load; 3) specimens for tests by the HSB method must be of such a shape and size that the free surfaces of the end faces of rods in contact with a specimen have minimum areas; 4) the HSB must not be loaded by an abrupt intense pulse of a length commensurate with the diameter of the specimen.

3.1. Governing Principles of the HSB Method

Let us consider loading of a system of three rods (Fig. 3.1). The load is applied to the end of a rod. With regard to the one-dimensional theory of propagation of elastic waves, deformation in some section of the rod on the wave is related to mass velocity by the expression

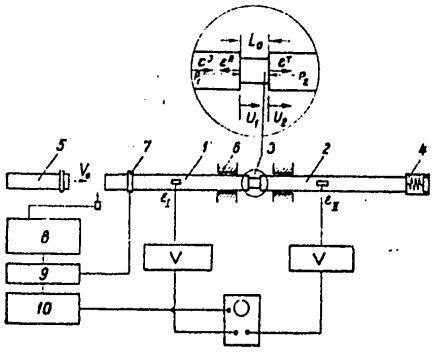

Fig. 3.1. Diagram of the Hopkinson split bar method: 1--pressure transmitting rod; 2--anvil rod; 3--specimen; 4--damper; 5--striker; 6--supports; 7--piezoelectric crystal; 8--system for measuring the striker velocity; 9, 10--amplifier and transducer of the signal from the piezoelectric crystal for triggering the oscilloscope; ε_I, ε_{II}--strain gages

$$\varepsilon = -\frac{1}{c_0}\cdot\frac{\partial U}{\partial t}, \tag{3.6}$$

whence $U = -c_0\int_0^t \varepsilon dt'$, where c_0 is the velocity of propagation of elastic waves in the rod. The displacements of the ends of the rods U_1 and U_2 are found from the formulas

$$\begin{aligned} -U_1 &= c_0\int_0^t \varepsilon^J dt' + c_0\int_0^t \varepsilon^R dt' = c_0\int_0^t (\varepsilon^J+\varepsilon^R)\,dt';\\ U_2 &= -c_0\int_0^t \varepsilon^T dt', \end{aligned} \tag{3.7}$$

where ε^J, ε^R, ε^T are the deformations in the incident, reflected and transmission waves. Deformation of the specimen ε_s, considering its stressed state to be uniform, is defined as follows:

$$\varepsilon_s = \frac{U_2-U_1}{L} = -\frac{c_0}{L}\int_0^t (\varepsilon^J+\varepsilon^R-\varepsilon^T)\,dt', \tag{3.8}$$

where L is the initial length of the specimen. Since ε^J, ε^R, ε^T, we rewrite (3.8) in the form

$$\varepsilon_s = -\frac{2c_0}{L}\int_0^t \varepsilon^R dt'. \tag{3.9}$$

Let us go on to determine the stress in the specimen. For forces P_1 and P_2 (see Fig. 3.1)

$$P_1=EF\,(\varepsilon^J-\varepsilon^R);\quad P_2=EF\varepsilon^T, \tag{3.10}$$

where E and F are respectively the modulus of elasticity and the cross section of the rods. Since $P_1 = P_2$, we get $\sigma_S = (P_1 + P_2)/2F_S$. The stress in the specimen as a consequence of continuity of forces on the ends of the specimen is

$$\sigma_s=\frac{EF}{2F_s}(\varepsilon^T+\varepsilon^J-\varepsilon^R)=\frac{EF}{F_s}\varepsilon^T, \tag{3.11}$$

where F_S is the cross sectional area of the specimen. Expressions (3.9) and (3.11) are the starting relations in the case of utilization of the HSB method. The purpose of the method is to calculate σ_S and σ_S from data of registration of ε^R and ε^T. Equality of the forces on the ends of the specimen occurs in cases where the accelerations and the inertial forces that they produce are vanishingly small. Otherwise they must be taken into consideration.

Computing stress σ_S according to a two-dimensional theory. The formula for computing stress with consideration of axial and radial inertia of the specimen from the HSB method is given in Ref. 126. However, this relation can be derived in a simpler way. Suppose that the axial and radial velocities of a specimen in the form of a cylinder of height L and radius R = D/2 are related to axial strain rate $\dot{\varepsilon}_S$ by the expressions

$$\begin{aligned}\dot{U}_x&=\dot{U}_1-\dot{\varepsilon}_s x;\\ \dot{U}_r&=-\nu_s r\dot{\varepsilon}_s,\end{aligned} \tag{3.12}$$

where ν_S is the Poisson ratio, $\dot{U}_1$ is the velocity of cross section with ordinate x = 0. The x-axis is directed along the axis of the split bar. We take the cross sectional areas of the specimens and rods to be the same ($F = F_S = \pi R^2$). The coordinate origin is at the center of the end face of the pressure-transmitting rod in contact with the specimen. Let us use the Hamilton principle

$$\dot{\Pi}+\dot{K}=Q_i\dot{q}_i, \tag{3.13}$$

where $\dot{\Pi}$ and $\dot{K}$ are the rates of change of the potential and kinetic energy of the system, Q_i are generalized external forces, $\dot{q}_i$ are generalized velocities. For $\dot{\Pi}$, Q_i, $\dot{q}_i$ we have

$$\begin{aligned}\dot{\Pi}&=\sigma_s\dot{\varepsilon}\Omega;\\ Q_i\dot{q}_i&=F_s\,(p_1\dot{U}_1-p_2\dot{U}_2)=\\ &=F_s[\,(p_1-p_2)\,\dot{U}_1+p_2L\dot{\varepsilon}_s],\end{aligned} \tag{3.14}$$

where Ω is the volume of the specimen ($\Omega = F_s L$); p_1 and p_2 are the pressures on the ends of the rods (at $x = 0$ and $x = L$ respectively). In (3.14) it is taken into consideration that $\dot{U}_2 = \dot{U}_1 - \dot{\varepsilon}_s L$.

The derivative of kinetic energy is

$$\dot{K} = \rho_s \Omega \left(\frac{\nu_s^2 R^2}{2} \dot{\varepsilon}_s \ddot{\varepsilon}_s + \dot{U}_1 \ddot{U}_1 - \frac{\dot{U}_1}{2} \ddot{\varepsilon}_s L - \ddot{U}_1 \frac{\dot{\varepsilon}_s L}{2} + \frac{L^2}{3} \dot{\varepsilon}_s \ddot{\varepsilon}_s \right). \tag{3.15}$$

Let us set up the Hamilton equation with consideration of (3.14) and (3.15):

$$\begin{aligned} L\dot{\varepsilon}_s \left[\dot{\sigma}_s + \left(\frac{L^2}{3} \ddot{\varepsilon}_s - \frac{\dot{U}_1 L}{2} + \frac{\nu_s^2}{2} R^2 \ddot{\varepsilon}_s \right) \right] = \\ = \left([(p_1 - p_2)\, \dot{U}_1 + p_2 \dot{\varepsilon}_s L] - \rho_s L \left(\dot{U}_1 - \ddot{\varepsilon}_s \frac{L}{2} \right) \dot{U}_1 \right. . \end{aligned} \tag{3.16}$$

Applying the d'Alembert principle to the specimen we get

$$(p_1 - p_2) = \rho_s L \left(\dot{U}_1 - \frac{\ddot{\varepsilon}_s}{2} L \right). \tag{3.17}$$

With consideration of (3.17), we rewrite (3.16) as

$$\sigma_s = -p_2 - \rho_s \ddot{\varepsilon}_s \left(\frac{L^2}{3} + \frac{\nu_s^2}{2} R^2 \right) + \rho_s \frac{\dot{U}_1 L}{2}; \tag{3.18}$$

(3.18) can be written in the form

$$\sigma_s = -p_2 - \rho_s \ddot{\varepsilon}_s \left(\frac{\nu_s^2 R^2}{2} - \frac{L^2}{6} \right) + \rho_s \frac{L}{2} \dot{U}_2. \tag{3.19}$$

In contrast to Davies and Hunter [Ref. 126], we arrived at (3.19) without additional assumptions. The inertial component in (3.19) is minimum if the geometric dimensions of the specimen conform to the relation

$$L = \sqrt{3} \nu_s R. \tag{3.20}$$

In this case the real stress in the specimen will differ from that calculated in accordance with the one-dimensional theory (formula (3.11)) by an amount $\rho_s \ddot{U}_2 L/2$. If the geometric dimensions of the specimen conform to relation (3.20), then measurement of acceleration $\ddot{U}_2$ enables determination of σ_s. Formula (3.20) reflects the validated geometric dimensions of the specimen, while (3.19) shows the influence of its radial inertia on the quantity σ_s.

3.2. Hardware of Variants of the HSB Method

Compressive variant of the HSB. The hardware that has currently evolved for [this] variant of the HSB method includes (see Fig. 3.1): 1) the Hopkinson split bar proper comprising the pressure transmitter and the anvil rod, between which the specimen is placed; 2) the damper block intended for absorbing the energy of the anvil; 3) the striker intended for loading. The striker is accelerated by the loading device (for example a pneumatic unit). The rods must be uniform, i. e. it is impermissible to use rods with recesses, collars or attached components. Sensor readings should verify that the rods are coaxial in the assembled form. Experience has shown that 20 mm is the optimum diameter for the rods. The class of machining of the rods is no less than the sixth. The rods are held in a centering support system (for example Teflon journal bearings). The triggering device is a piezoelectric crystal cemented to the surface of the pressure transmitter close to the end that will take the impact. The signal from the piezoelectric transducer is sent through an amplifier to a pulse oscillator that triggers the oscilloscope. Strain gages are used to register deformations in the rods.

For direct recording of deformation ε_s, an RC integrator is connected in the measurement channel between the output of the strain amplifier and the input of the oscilloscope. Placement of the strain gages at equal distances from the specimen enables direct registration of the stress-strain diagram.

The Institute of Mechanics of Polymers, Academy of Sciences of the Lithuanian SSR uses a facility that realizes the HSB method for tension and compression (Fig. 3.2). The loading device is a pulse current generator (magnetic-pulse facility). The working mode of the pulse generator during tests is free electric discharge in a liquid. The Hopkinson bar proper is made up of a system of Duralumin rods 20 mm in diameter and 1 m long held in Teflon bearings that are installed in a rigid vertical stand. The rods are checked for coaxiality by oscillograms of ε_I and ε_{II} in the absence of a specimen.

The pressure transmitter is loaded by two methods. The first method is implemented by a striker placed in the discharge chamber (see Fig. 3.2, b). Upon free discharge of the capacitors, a pressure wave arises in the liquid that pushes the striker.

The second method of loading the pressure transmitting rod is by impact of a plate (Fig. 3.2, a) that buckles under the action of hydraulic pressure. Pulses ε^J of variable duration are produced by varying the thickness of the plate, the material of the plate, and the voltage of the capacitors.

In contrast to conventional arrangements for the HSB method, there is no damping block in the variant shown in Fig. 3.2. The oscilloscopes

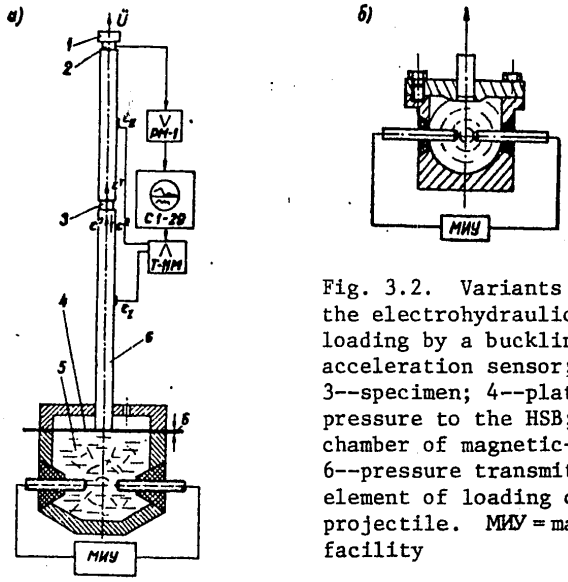

Fig. 3.2. Variants of HSB loading by the electrohydraulic effect: a--loading by a buckling plate (1--acceleration sensor; 2--anvil rod; 3--specimen; 4--plate that transmits pressure to the HSB; 5--discharge chamber of magnetic-pulse facility; 6--pressure transmitting rod); b--element of loading device sith repelled projectile. МИУ = magnetic-pulse facility

are triggered from the electromagnetic pickup that accompanies free discharge of the capacitors of the magnetic-pulse facility. The time delay for registration of the ε_I sensors is 100 μs. During this time the oscilloscope beam settles down and reaches a stable zero line.

In addition to the usual registration of deformations ε_I and ε_{II} by strain gages, the variant of the HSB method that we have developed adds registration of accelerations by a sensor placed on the free end of the anvil rod. This acceleration sensor consists of a light aluminum frame into which a quartz pellet with two inertial masses is pressed (Fig. 3.3). The sensor has a natural frequency of 80 kHz. The sensor is calibrated as follows. The anvil rod with the acceleration sensor is loaded by an intense pulse (see Fig. 3.3). An amplifier is used to record acceleration of the end of the rod, and a strain gage cemented in the middle of the rod is used to record deformation. Considering that the acceleration sensor registers the quantity $2\partial V/\partial t$, while the strain gage measures the quantity $\varepsilon = -V/c_0$, calibration reduces to establishing correspondence between the function V and its time derivative.

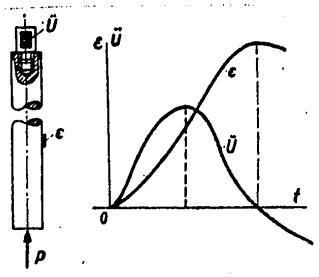

Fig. 3.3. Calibration of acceleration sensor

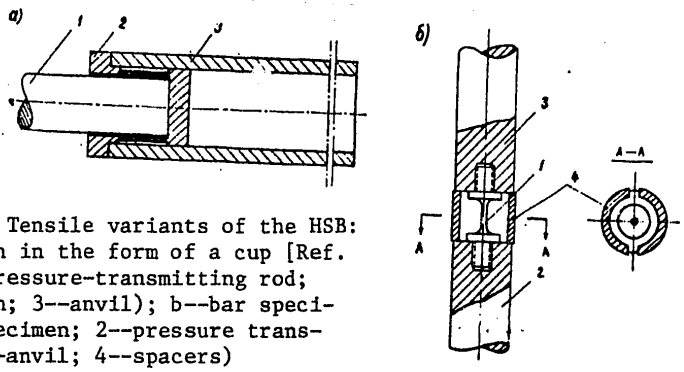

Fig. 3.4. Tensile variants of the HSB: a--specimen in the form of a cup [Ref. 147] (1--pressure-transmitting rod; 2--specimen; 3--anvil); b--bar specimen (1--specimen; 2--pressure transmitter; 3--anvil; 4--spacers)

Tensile variant of the HSB. One of the first variants of the HSB for stretching metal specimens was proposed by Lindholm and Yeakley [Ref. 147]. A diagram of this variant is shown in Fig. 3.4. The shape of the specimen in the tensile version differs considerably from the shape of the specimen for compression. The specimen takes the shape of a cup with a massive bottom that is struck by the pressure-transmitting rod. The anvil is a tube. Direct measurements of deformations on the specimen have shown that the method is not applicable to tests of polymers at strain rates greater than 100 s^{-1}. The massive bottom of the cup specimen and its thin walls result in very low values of the natural frequency ω_0 of the specimen. Attempts to increase ω_0 by reducing the mass of the bottom of the cup and increasing the thickness of the walls have been unsuccessful.

Ref. 140 describes a variant of the Hopkinson bar method adapted for stretching in which the pressure-transmitting rod is welded to a long test bar of the same diameter. This variant is not suitable for testing polymers.

Fig. 3.4, b shows a diagram of a tensile variant with a rod specimen that is threaded onto the rod system of the HSB. The threaded part is not required if the specimen is cemented to the ends of the rods. Placed between the rods under slight tension are two spacers that prevent compression of the specimen when the rods are loaded by compression. Tests with the arrangement shown in Fig. 3.4, b are done as follows. A compression pulse traveling through the pressure-transmitting rod passes through the tempered spacers to the anvil rod, is reflected from its free end, and stretches the specimen.

Torsional variant of the HSB. The one-dimensional theory of the torsional variant of the Hopkinson bar method is no different from the theory for the tensile and compressive variants. The hardware for the

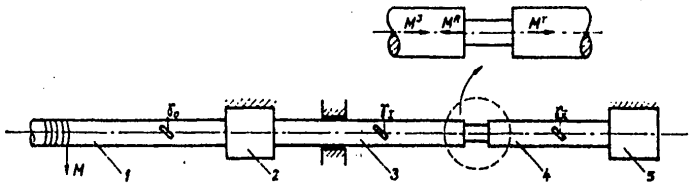

Fig. 3.5. Torsional version of the HSB: 1--accumulator rod; 2--arresting device; 3--torque-transmitting rod; 4--anvil rod; 5--damper block

torsional variant is considerably different from that for the other forms (Fig. 3.5). The HSB system is supplemented by another rod called an accumulator. Before starting the experiment, torque is statically applied to the accumulator. The stored energy of the accumulator is transmitted to the Hopkinson bar system upon operation of a special arresting device. (The two elastic rods with identical mechanical and geometric characteristics are termed the anvil rod and the torque-transmitting rod respectively.) For practical purposes, there is no difference in processing of recordings by strain gages in the torsional variant as compared with processing the results of the compressive and tensile variants.

Based on the theory of composite rods, we can write for the stress and shear strain of the specimen:

$$\tau_s = -G\frac{r_s}{r}\frac{I}{I_s}\gamma^T; \quad \gamma_s = -2\frac{r_s}{r}\frac{c_G}{L}\int_0^t \gamma^R dt', \tag{3.12}$$

where γ^T and γ^R are the transmitted and reflected shear strain respectively, r_S, r are the radii of the specimen and the rods respectively, I_S, I are the moments of inertia of the cross sections of the specimen and the rods, G is the shear modulus for the rods, τ_S, γ_S are the tangential stresses and corresponding shear strains of the specimen, and c_G is the velocity of shear waves in the rod.

The torsional variant of the Hopkinson rod is based on loading the specimen by the quick release of the stored torque. The stored energy is released in different ways [Ref. 121, 154]. The simplest way is to break a link that fixes the position of the pretorqued accumulator rod. The pulse rise time is dependent on the time of breakage of this component of the structure. In our opinion, Ref. 67 describes the most successful device for attaining a quite rapid release of torque by an exploding foil. A ring with ears is cut from thin aluminum foil and cemented to a massive frame and to the accumulator rod. Electric voltage of 2 kV is applied to the ears of the foil ring.

The arresting device of Ref. 154 for torque release is based on using compressed gas energy. The arresting device is a piston rod that rests against an eccentric connected to a torque transmitter. The eccentric is rapidly released as the piston moves downward under the action of the gas. The specimen for tests in the torsional variant of the method may also take the form of a pellet. Tubular specimens with thickened ends have been used [Ref. 154]. The ends of the specimen are cemented to the ends of the rods and the torque transmitter respectively. The methods of registration in the torsional method are no different from those described above.

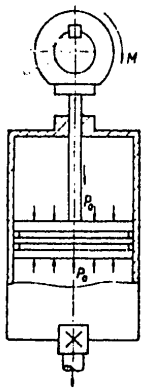

Fig. 3.6. Diagram of pneumatic arresting device

3.3. Validation of the HSB Method

The stressed and strained state of the specimen is calculated according to formulas (3.9) and (3.11) on the assumption that the specimen is quasistatically strained. Given below are the results of works to validate this assumption for tests by the HSB method in the permissible range of strain rates.

The advantage of the HSB method over other techniques is that the simplicity of the loading arrangement enables clear formulation of the mathemetical problem of wave propagation and interaction in the composite rods. Solution of such a problem provides the basis for using the assumption of quasistatic deformation within reasonable limits of strain rates on the specimen.

Bell's experiments. Experiments done by Bell [Ref. 5] were the formulation of problems for further research, and convincingly demonstrated that the assumption of quasistatic distribution of strains in a specimen does not hold at high strain rates (~10^3 s^{-1}) in appreciably nonlinear materials. Bell compared two methods of strain measurement. Data from calculations by expression (3.9) were compared with characteristics found by the method of a diffraction grating applied directly to an aluminum alloy specimen with appreciably nonlinear stress-strain diagram. Since the stress-strain diagram does not depend on strain rate, the given material is taken as a standard. Fig. 3.7 shows the results of comparison of deformations of a specimen calculated by formula (3.9) and by direct measurement by a diffraction grating cemented to the middle of the specimen. The experiment is done on specimens with ratio of L/D = 1, 1/2, 3/4 and 1/4. It is concluded on the basis of these experiments that nonlinearity of the material leads to formation of slow waves and causes deviation of the actual stressed state of the specimen from quasistatic. Bell's experiment has compelled researchers to be cautious in using the HSB method for tests of nonlinear materials at strain rates $\dot{\varepsilon} > 10^3$ s^{-1}.

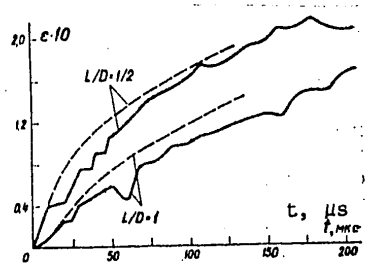

Fig. 3.7. Strain-time curves for two ratios of L/D found by direct recording (——) and calculated from (3.9) using the conventional HSB method (---). Standard test material (with unit stress-strain diagram) [Ref. 5].

Tests by the HSB method are theoretically substantiated in a number of works [Ref. 74, 117, 122, 126]. According to Davies and Hunter [Ref. 126], the minimum value of stresses with consideration of the one-dimensional theory and radial inertia will be reached if the dimensions of the specimen conform to relation (3.20). The influence that nonlinear axial wave phenomena, the ratio L/R and friction over the end faces of the specimen have on registered parameters in experiments with the Hopkinson bar is checked out in Ref. 117.

Shown in Fig. 3.8 and 3.9 are the results of numerical solution of the problem of dynamic compression of a specimen in the HSB. Data of Bell's

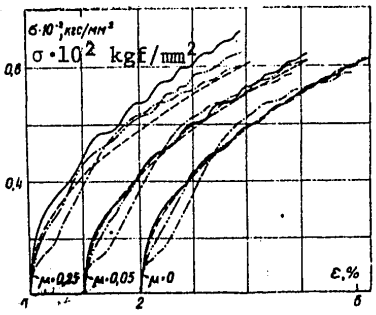

Fig. 3.8. Results of calculation of the stress-strain diagrams of the standard material at different values of the coefficient of friction and ratios L/D: ——— 0.3; -·-·- 0.6; -·-·-·- 1.2; ---- initial stress-strain diagram. The mean strain rate is 400 s^{-1} [Ref. 117].

experiment [Ref. 5] were used as the input in getting the solution. The specimen material is nonlinearly elastic, i. e. it has a unit stress-strain diagram (see Fig. 3.8). The problem was solved with consideration of friction on the ends of the material in the form of a Heaviside step function. Radial motion of the specimen is taken into consideration. Fig. 3.8 also shows the results of solution for the cases L/D = 0.6, 1.2, and 0.3 (Poisson ratio $\nu_s = 0.35$). The problem was solved with variation of the coefficient of friction μ from 0 to 0.25. The average strain rate of the specimen $\dot{\varepsilon} = 400\ s^{-1}$.

Fig. 3.9. Stress-strain curves for the standard material $L/D = 0.3$, $\mu = 0$ at different values of $\dot{\varepsilon}$, s^{-1}: 1--400; 2--800; 3--1600; 4--3300 [Ref. 117]

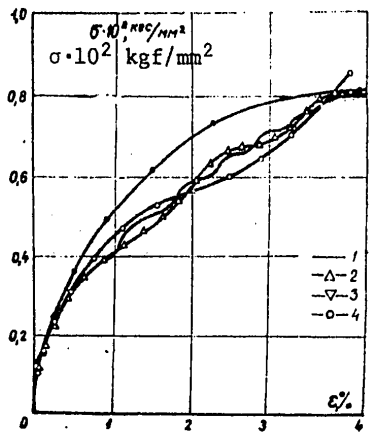

Fig. 3.9 reflects the relations given in Ref. 117 at a ratio $L/D = 0.3$ and different values of $\dot{\varepsilon}$. Thus careful machining of the ends of the specimen, lubrication, and selection of L/D according to (3.20) will lead to results that can be treated as quasistatic at strain rates of less than 10^3 s^{-1}.

The final purpose of using the HSB method is to get a stress-strain diagram, and the reliability of this diagram may be doubtful if it is found at strain rates of the order of 10^3 s^{-1} or more using one-dimensional ratios (3.9) and (3.11) becuase of the unaccounted influence of axial and radial inertia of the specimen. The stress-strain diagram is constructed by eliminating time from stress-time and strain-time diagrams. These two functions must be strictly matched in time to get reliable stress-strain diagrams.

We verify the applicability of one-dimensional relations of the HSB method twice. First the condition of equality of forces on the ends is checked by the ordinary registrations of the method. To evaluate the inertial component of stress and strain, accelerations of the free anvil end are recorded and deformation on the specimen is recorded directly by strain gages.

The first step in solving the problem is direct verification of the condition of equality of forces on the ends of the specimen, which can be written as

$$\varepsilon^J = \varepsilon^R + \varepsilon^T$$

and visually examined on oscillograms. Fig. 3.10 shows reworked oscillograms of $\varepsilon^{I,R}$-t, ε^T-t for our tests done on polycarbonate compression. The experiments were done with loading of the split bar by different

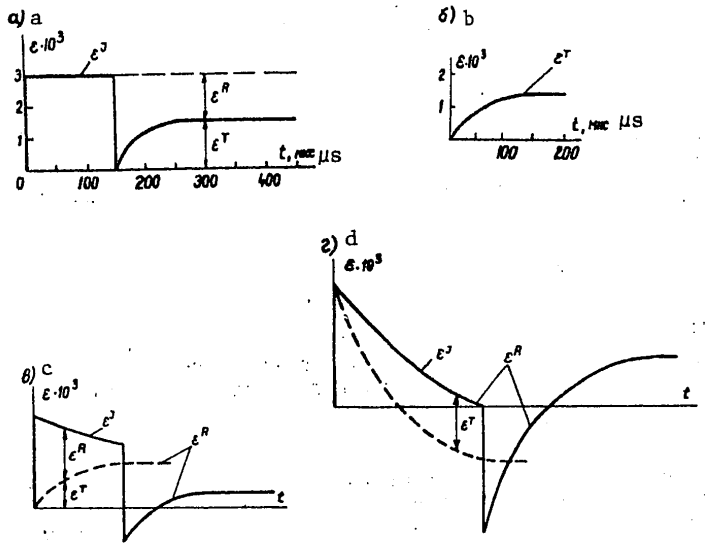

Fig. 3.10. Typical oscillograms of $\varepsilon^{J,R}$-t and ε^{T}-t plotted in polycarbonate testing for compression according to the diagram of Fig. 3.2, b: a--plots for ε^{J} and ε^{R} at a value of the projectile mass of m = 0.5 kg; c--the same at m = 0.2 kg; d--the same at m = 0.1 kg; b--plot common to all cases for ε^{T}-t, L/D = 0.5.

values m of projectile masses (0.5, 0.2 and 0.1 kg). The form of ε^{J} depends considerably on the value of m. It can readily be shown that satisfying the law of conservation of momentum gives

$$\varepsilon^{J} = -\frac{V_0}{c_0} e^{-\frac{Mt}{mL_1 c_0}}, \qquad (3.22)$$

where V_0 is the initial velocity of the projectile mass, M, L_1 are the mass and length of the pressure-transmitter rod in the HSB system.

From Fig. 3.10 we see that the simplest analysis of equality of forces on the end of the specimen with respect to relation $\varepsilon^{J} = \varepsilon^{R} + \varepsilon^{T}$ can be done for the case where testing is done by throwing considerable masses (see Fig. 3.10, a). For this purpose it is necessary to superimpose the oscillogram of ε^{T} on that of ε^{J}. It should be noted that the oscillograms are given for an elastic-viscoplastic material with conditional dynamic yield stress $\sigma_s = 1100$ kgf/cm^2. An increase in the strain rate due to an increase in the amplitude of the incident pulse ε^{J} leads to a rise in the rate of deformation and also brings it closer to a constant value, i. e. where $\varepsilon^{R} >> \varepsilon^{T}$. The rise in the strain rate is also

associated with oscillations superimposed on the recorded plots (not shown in Fig. 3.10). These are due to acceleration (axial and radial) of the specimen, and lead to disruption of the condition of equality of forces on the ends, particularly in cases where the testing time is commensurate with the period of these oscillations.

Fig. 3.10, c shows an oscillogram obtained with loading of the rod by a mass of 0.2 kg. Finding the function ε^R and establishing applicability of the formula $\varepsilon^J = \varepsilon^R + \varepsilon^T$ are still simple in the given case, although more complicated than that previously considered. To do this, we make the plots shown in Fig. 3.10, c. Compared with the case of loading with $m = 0.3$, the strain rate here falls in time more appreciably, the lower the projectile mass. The exponent in (3.22) becomes considerable at $M/m \gg 1$. The oscillograms shown in Fig. 3.10, d correspond to this case (verification of correspondence of the forces on the ends is shown by the dotted line). In contrast to the first two cases, here the strain rate is a function that changes rather strongly in time.

A transition to high strain rates (of the order of 10^3 s^{-1}) leads to the development of forces of inertia resulting in violation of the condition $p_1 = p_2$, which leads to infeasibility of the one-dimensional relation, and replacement by (3.19). If the geometric dimensions of the specimen are selected in accordance with (3.20), then

$$\sigma_s = \sigma^T + \rho_s \frac{L}{2} \dot{U}_2. \tag{3.23}$$

This expression implies that by supplementing the results of registration of σ^T with data that characterize acceleration of the free end of the anvil rod $\ddot{U}_2^0$, we can compute σ_s, considering that

$$\dot{U}_2^0 = 2\dot{U}_2.$$

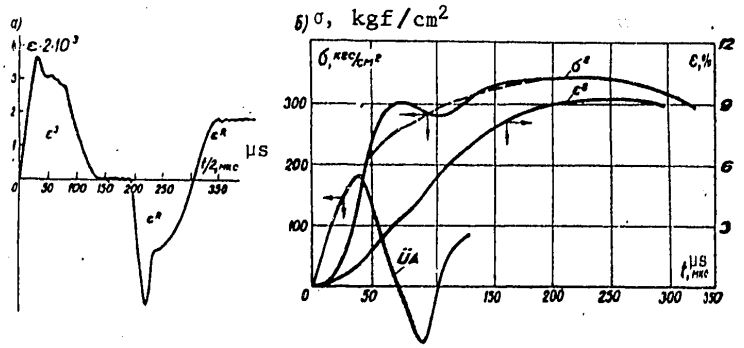

Fig. 3.11. Typical results found in compression testing Teflon by the HSB method (see Fig. 3.2, a): a--plots of ε^J, ε^R as functions of t; b--curves for σ_s-t, ÜA-t and ε_s-t (calculated from (3.9)), $A = L\rho_s$, $L/D = 0.5$.

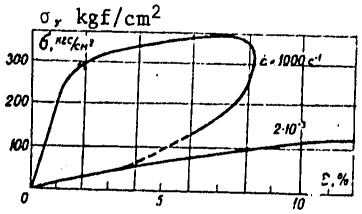

Fig. 3.12. Static and dynamic stress-strain diagrams for Teflon (compression testing); ---- assumed behavior of the diagram

Fig. 3.11 shows experimental curves for $\varepsilon^{J,R}$-t (Fig. 3.11, a), ε_s, U and σ_s (Fig. 3.11, b), and Fig. 3.12 shows the stress-strain diagram for Teflon under compression with an average strain rate of $\dot{\varepsilon} \approx 10^3$ s^{-1}. The inertial component of the stress $\rho_s LU/2$ according to (3.23) in the given case is about 13% of σ^T, and therefore we can take a strain rate of $\dot{\varepsilon} \approx 10^3$ s^{-1} as the limiting value for Teflon, defining the applicability of relation (3.11) for computing σ_s.

When a tensile variant of the Hopkinson split bar is used for tests (Fig. 3.4), registration of acceleration is impossible for purely technical reasons. In the given instance, direct measurements of strain on the specimen are advisable. Short-base strain gages have recently come into use that enable registration of considerable relative deformations. The use of such sensors enables us to repeat Bell's experiments.

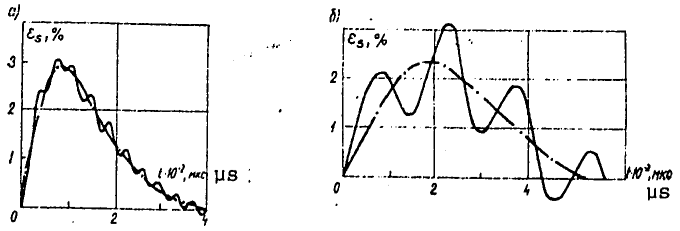

Fig. 3.13. Curves of ε_s-t plotted in accordance with (3.9) (-·-) and from direct registration (——): a--tensile testing of an epoxy resin specimen in accordance with the diagram of Fig. 3.4, b; b--the same for a polycarbonate specimen with tensile testing according to the diagram of Fig. 3.4, a

Fig. 3.13 shows oscillograms obtained by direct registration of strain on a specimen subjected to tension. The measurements were made with strain gages having a base of 5 mm. As shown in Fig. 3.13, the quasistatic nature of deformation can be validated on the basis of strain recordings.

The conditions of the quasistatic approach to deformation of a specimen when the HSB method is used are formulated as follows: the period of the oscillations superimposed on the curve of ε_s-t must be at least an order of magnitude less than the load duration. Measurements of strains directly on the specimens for tensile variants of the HSB method are

illustrated by Fig. 3.13, showing that: 1) the specimen shaped like a cup with a massive bottom is not applicable to tests of polymer materials; 2) a miniature bar specimen with threaded section can be used up to a strain rate of 10^3 s^{-1}, necessarily accompanied by registration of the deformation of the specimen to validate its quasistatic behavior.

Matching of functions σ_s *and* ε_s. Diagrams based on oscillograms for ε^R as well as ε^T are constructed by the HSB method by eliminating time from relations σ_s-t and ε_s-t. Accurate plotting requires that these functions be strictly matched in time, i. e. we must know the times of arrival of the functions ε_s and σ^T. The time of arrival of the ε^R wave can be seen on oscillograms (including ours) quite clearly. It would be difficult to pin down the arrival of the σ^T wave from the oscillogram shown in Fig. 3.11, a because of the viscosity properties of the material of the specimen, i. e. ordinary measurements are inadequate for plotting stress-strain diagrams because of the lack of matching of the functions σ and ε in time. To find the time of arrival of the stress pulse, a supplementary recording is made of the acceleration of the free end of the anvil since according to one-dimenisonal theory the deformation recorded by the strain gage is $\varepsilon^T = -\dot{U}_2/c_0$, whereas the measured acceleration is $2\partial\dot{U}_2/\partial t$. The time of arrival of pulse ε^T is clearly determined when the function is compared with its time derivative (see Fig. 3.11, b). It should be noted that for more exact determination of the time of arrival of a signal, the function must be compared with its higher-order derivative. However, unfortunately at present we still have not developed methods of measuring such quantities.

Reliable stress-strain diagrams can be plotted by combining conventional HSB methods with additional registration of acceleration.

Chapter 4

METHODS OF TESTING POLYMERS WITH DYNAMIC BENDING

Mechanical tests of polymer materials, and particularly of laminated composites, cannot be exhaustive without studying their resistance to shearing loads. This study reduces to investigation of transverse impact.

An examination of bending in accordance with the three-dimensional problem leads to the Poghammer-Chree theory [see Ref. 22, 24]. Simplifications of the Poghammer-Chree theory are: the elementary theory, theory of the Timoshenko type, two-dimensional problem of the plane stressed state and so on. The accuracy of such approximations is usually evaluated by comparing wavelength dependences of the phase and group velocities with their corresponding dependences plotted according to the Poghammer-Chree theory. Numerous problems on dynamic bending of beams have been solved on the basis of simple theories. The elementary theory is based on an equation of a type (parabolic) that has led to a number of

contradictions. Complications are introduced into the simplest theory on the basis of the Timoshenko model. Applicability of the theory to analysis of transient processes is demonstrated in Ref. 1, 73, 102. It is established in Ref. 1, 73 that the theory is not applicable in the region that extends from the compression wavefront to the conventional front of Rayleigh surface waves, or in the immediate vicinity of this region. Ref. 1 gives a number of numerical data on the accuracy of the theory in the region where it can be considered applicable. Neither the elementary nor the Timoshenko theory of beam bending considers transient processes at the point of load application, which considerably complicate the problem since they must be considered on the basis of a three-dimensional theory. It has been experimentally shown that the influence of these transient processes on the nature of wave propagation in the beam is slight, and in most cases they can be disregarded (including in the cases to be considered herein).

Elementary theory of beam bending. Solution of the Euler-Bernoulli beam bending problem reduces to solution of the equation

$$\frac{\partial^2 M}{\partial x^2} + \rho \frac{\partial^2 y}{\partial t^2} = 0, \tag{4.1}$$

where M, y are the moment and flexure of the beam, t is time, ρ is the density of the beam material. Equation (4.1) has been solved [Ref. 22] for an infinite beam under the action of a concentrated force Q that causes motion of the cross section of the beam under the force at constant velocity V_0.

The initial condition of the problem is: at $t = 0$, $y(x,t) = 0$. The velocity of displacement of all cross sections of the beam except that in which the load is applied is also taken as zero. As shown by Boussinesq [see Ref. 22], the problem can be solved by assuming that the ratio y/t is a function of the parameter $\eta = x^2/4t$.

For a transverse force, the elementary theory of bending leads to an invalid result. The relation $Q = \partial M/\partial x$ causes an infinite force in cross sections where M undergoes a discontinuity. This is not physically substantiated. The reasons for such a discrepancy are as follows. In the given problem the intial conditions are discontinuous: at $t = 0$

$$V = 0 \text{ when } x \neq 0; \quad V = V_0 \text{ when } x = 0.$$

At the same time, initial equation (4.1) is an equation of parabolic type that does not permit wave propagation at infinite velocity, and consequently does not allow velocity discontinuities. The latter contradicts the initial conditions. Despite the disadvantages, the elementary theory of bending gives satisfactory results far from the shear wavefront.

Use of the Timoshenko theory. The differential equations of motion of the beam that correspond to the Timoshenko theory [Ref. 22, 98]:

$$\frac{\partial^2 y}{\partial x^2} - \frac{\rho}{k'G}\frac{\partial^2 y}{\partial t^2} = \frac{\partial \Theta}{\partial x};$$
$$\frac{\partial^2 \Theta}{\partial x^2} - \frac{\rho}{E}\frac{\partial^2 \Theta}{\partial t^2} = -\frac{k'GF}{EI}\left(\frac{\partial y}{\partial x} - \Theta\right), \tag{4.2}$$

where y is flexure of the beam, Θ is the angle of turn of an element of cross section of the beam under the action of bending forces alone, E and G are the elastic and shear moduli, and k' is a coefficient that depends on the shape of the beam cross section. Ref. 125, 139 survey research on determining k' according to a set of distributions of tangential stresses. This chapter gives the results of experiments investigating the influence that the shape of the cross section of beams (and hence the coefficient k') has on the velocities of shear wave propagation. System of equations (4.2) is of hyperbolic type with four families of characteristics:

(4.3)
(4.4)

where
$$dx_1 = \pm a\,d\tau; \quad d\varphi \mp dV = \varkappa dx_1;$$
$$dx = \pm d\tau; \quad d\varkappa \mp d\omega = -a^2(\varphi - \Theta)\,dx,$$

$$x_1 = \frac{x}{L}; \quad i = \sqrt{\frac{I}{F}}; \quad \tau = \frac{c_0 t}{i}; \quad c_0 = \sqrt{\frac{E}{\rho_0}};$$
$$\omega = \frac{\partial \Theta}{\partial \tau}; \quad \varkappa = \frac{i}{c_0}\cdot\frac{\partial \Theta}{\partial x}; \quad a^2 = \frac{k'G}{E}; \tag{4.5}$$
$$V = \frac{1}{ac_0}\cdot\frac{\partial y}{\partial t}; \quad \varphi = \frac{\partial y}{\partial x}; \quad L \text{ is the length of the beam.}$$

According to (4.4) the moments (and consequently the deformations as well) propagate along the beam at velocity $c_0 = \sqrt{E/\rho_0}$. The curves for the transverse forces are discontinuous, and the discontinuity moves at the velocity of the shear waves:

$$ac_0 = \sqrt{\frac{k'G}{\rho_0}} = c_G. \tag{4.6}$$

A number of problems on impulse loading of Timoshenko beams have been solved in Ref. 57, 61, 75, 81, 85, 98, 103, 118, 119, 153 and 160.

4.1. Transverse Impact of a Freely Thrown Mass

Local deformations that arise in the vicinity of the contact zone of colliding bodies have an appreciable influence on the process of impact: they lead to softening of the blow, an increase in its duration and a reduction of maximum contact forces. As noted in Ref. 81, the phenomena observed upon bending impact can be explained in general only when local deformations are taken into consideration.

Shtayerman [see Ref. 81] found a solution for the contact problem in accordance with which the contact force P is related to the corresponding approach δ of the bodies by the expression

$$P=[k^{-1}_{*}\delta]^{\frac{2n+1}{n}}, \tag{4.7}$$

where k_* is a coefficient that depends on the curvature of the bodies at the point of contact and on the properties of the material, n = const. In a special case, (4.7) is taken in the form of Hertz law: $\delta = k_* P^{2/3}$. For the case where a sphere of radius R is thrown against a plate, k_* is determined from the formula

$$k_*=\sqrt[3]{\frac{9}{16R}\left(\frac{1-\nu_1^2}{E_1}-\frac{1-\nu_2^2}{E_2}\right)^2}, \tag{4.8}$$

where E_1, E_2, ν_1, ν_2 are the moduli of elasticity and the Poisson ratios of the contacting bodies. The values of k_* for different cases of contact deformations are given in Ref. 81.

To solve mechanical problems with consideration of local deformations, we must have information on the relation between P and δ in the vicinity of contact in addition to the law of deformation of the investigated beam. In this regard, as a rule the projectile is taken as rigid or elastic. Thus to solve the problem of dynamic bending with consideration of local deformations, it is necessary to know the dependence of contact force on the approach δ of the pressing bodies in addition to the law of deformation of the investigated object. To approach the actual conditions of the problem, this dependence must be experimentally determined at loading rates as close as possible to those that are realized in impact loading of a beam.

The problem of bending impact with consideration of local deformations. In Ref. 61 a solution is found for the problem of bending of an elastic Timoshenko beam by an incident mass M with velocity V_0 at the instant of contact. With consideration of local deformations, the boundary conditions of the problem in cross section $x = x_1$ are written in the form

$$V_0 t+\frac{gt^2}{2}-\frac{1}{M}\int_0^t dt_1\int_0^{t_1} P dt_2=\delta+y\ (x_1,\ t), \tag{4.9}$$

where y(x,t) is flexure of the cross section of the beam that is under contact force P, g is acceleration of free fall. The initial condition of the problem:

$$t=0, \frac{\partial y}{\partial t}=y=0. \tag{4.10}$$

Contact force and approach δ at t = 0:

$$P=0; \quad \delta=0. \tag{4.11}$$

The value of dP/dt = 0 at t = 0 if the relation between P and δ is chosen in a form similar to Hertz law, according to which

$$\left.\frac{dP}{d\delta}\right|_{P,\delta\to 0}=0.$$

Thus $\frac{dP}{dt}=\frac{dP}{d\delta}\frac{d\delta}{dt}=0$. The boundary condition at y = 0

$$\frac{\partial y\,(x_1, t)}{\partial t}=V_0-\frac{d\delta}{dt}. \tag{4.12}$$

If $\partial y/\partial t$ is understood to mean the velocity of the center of gravity of the beam at $x = x_1$, then at t = 0

$$\frac{\partial y\,(x_1, t)}{\partial t}\equiv 0,$$

whence

$$\left.\frac{d\delta}{dt}\right|_{t=0}\equiv V_0. \tag{4.13}$$

Thus (4.10)-(4.13) imply that when local deformations are considered the sudden application of a load does not cause a discontinuity of the transverse force and its derivative with respect to t if the law for P vs. δ is taken in the form of a Hertz law or in some other form that gives $\left.\frac{dP}{dt}\right|_{\delta\to 0}=0$; does not cause discontinuities of the velocities of flexures of cross sections of the beam; the discontinuity of function $d\delta/dt$ is taken as rapidly damped in the vicinity of contact.

Softening of the impact by local deformations that eliminate discontinuities considerably simplifies solution of the problem, which can be found by using the method of Laplace transformation. According to Ref. 75, the solution of the formulated problem takes the form:

$$y_k=\frac{2b_3}{lF\rho^2L}\sum_{n=1}^{\infty}\left\{\frac{P_k}{S_{1n}^2S_{2n}^2}\left(1+\frac{\alpha^2b_4}{b_3}\right)+\right.$$

$$\left.+\frac{1}{S_{2n}^2-S_{1n}^2}\left[\left(\frac{1}{S_{1n}}+\frac{b_5}{b_3}S_{1n}+\frac{\alpha^2b_4}{b_3S_{1n}}\right)\times\right.\right.$$

$$\times \left(\sin S_{1n} k\tau \sum_{i=1}^{k} I_{in}{}^{1} + \cos S_{1n} k\tau \sum_{i=1}^{k} I_{in}{}^{1}\right) -$$

$$-\left(\frac{1}{S_{2n}} + \frac{b_5 S_{2n}}{b_3} + \frac{b_4 \alpha^2}{b_3 S_{2n}}\right)\left(\sin S_{2n} k\tau \sum_{i=1}^{k} I_{in}{}^{2} + \right.$$

$$\left. + \cos S_{2n} k\tau \sum_{i=1}^{k} I_{in}{}^{2}\right)\Bigg]\Bigg\} \sin \alpha x_1 \sin \alpha x; \tag{4.14}$$

$$\Theta_k = \frac{2b_3}{lF\rho_0{}^2 L} \sum_{n=1}^{\infty} \alpha \left\{\frac{P_k}{S_{1n}{}^2 S_{2n}{}^2} + \frac{1}{S_{2n}{}^2 S_{1n}{}^2}\left[\frac{1}{S_{1n}}\left(\sin S_{1n} k\tau \sum_{i=1}^{k} I_{in}{}^{1} + \right.\right.\right.$$

$$\left. + \cos S_{1n} k\tau \sum_{i=1}^{k} I_{in}{}^{1}\right) - \frac{1}{S_{2n}}\left(\sin S_{2n} k\tau \sum_{i=1}^{k} I_{in}{}^{2} + \right.$$

$$\left.\left.\left. + \cos S_{2n} k\tau \sum_{i=1}^{k} I_{in}{}^{2}\right)\right]\right\} \sin \alpha x_1 \sin \alpha x, \tag{4.15}$$

where

$$b_3 = k'FG; \quad b_4 = EI; \quad b_5 = \rho_0 I; \quad \alpha = \frac{\pi n}{L};$$

$$I_{in}{}^{r} = \frac{P_{i-1} - P_i}{S_{rn}{}^2 \tau}\left[\sin S_{rn}\, i\tau - \sin S_{rn}\,(i-1)\tau\right]; \tag{4.16}$$

$$J_{in}{}^{r} = \frac{P_i - P_{i-1}}{S_{rn}{}^2 \tau}\left[\cos S_{rn}\, i\tau - \cos S_{rn}\,(i-1)\tau\right];$$

S_{1n}, S_{2n} are two sets of natural frequencies that correspond to equation (4.3); τ is a time segment on which a linear approximation is taken for the contact force

$$P = P_{k-1} + \frac{1}{\tau}(P_k - P_{k-1})\,[t - (k-1)\tau]; \quad k-1 \leqslant \frac{t}{\tau} \leqslant k;$$

P_i is the contact force at time $i\tau$; Q and M are expressed in terms of Θ and y.

The forces of interaction between the striker and beam are found in accordance with (4.12) and (4.10), calculation of the double integral $S = \int\int P\, dt\, d\tau$ reducing to the recurrent relation

$$S_k = S_{k-1} + \left[\sum_{i=0}^{k-1} P_i + \frac{1}{6}(P_k - P_{k-1})\right]\tau^2,$$

while the approach δ is related to the contact force by some expression $\delta = kP^m$. As we have already pointed out, the use of (4.9) makes it necessary to study the relation between contact force P and approach δ. Experimental determination of the relation $P-\delta$ (Fig. 4.1) consisted in recording P vs. t and δ vs. t with impact of a massive body against a fixed plate. The initial impact velocity $V_0 \approx 1.5$ m/s.

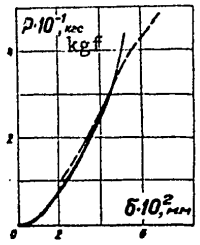

Fig. 4.1. P vs. δ for a sphere (R = 3 mm) striking a glass textolite plate:
—— Hertz law
---- experiment

In computer calculations of series (4.14) and (4.15) we retained 160 terms. The problem was solved for the case where a body weighing 590 g was dropped on the center of a beam from heights of 5, 10 and 15 cm. Studies on dynamic bending were done for beams 300 mm long, 10 mm wide and 9 mm high. Density of the glass textolite is $\rho_0 = 1.8$ g/cm^3, $E = 2.5 \cdot 10^5$ kgf/cm^2, $G = 0.43 \cdot 10^5$ kgf/cm^3. The calculations assumed $\tau = 2.5$ μs. Fig. 4.2 shows the results of numerical solution of the problem of bending of a beam with consideration of local deformations, shears and rotational inertia.

Force of contact upon transverse impact. As shown by Timoshenko [Ref. 98], the phenomenon of elastic impact against a beam is considerably more complicated than the phenomenon of inelastic impact considered by St. Venant. In the cited paper, Timoshenko gives calculations for contact force without consideration of displacements or rotational inertia. The relation P vs. δ is taken in the form of Hertz law. The boundary conditions and initial conditions of the problem are the same as in the previously considered problem. The equation from which force P is calculated takes the form [Ref. 98]

$$V_0 t - \int_0^t \frac{dt_1}{M} \int_0^{t_1} P dt_1 = kP^{2/3} + \sum_{i=1,3,5,\ldots}^{\infty} \frac{1}{i^2} \frac{L^2}{\pi^2 c_0^2} \frac{2}{\rho F L} \int_0^t P \sin \frac{i^2 \pi^2 c_0 (t-\tau)}{L^2} d\tau, \tag{4.17}$$

where M is the mass of the incident body. The problem was solved for the case where the force is applied in the middle of the span of the beam. Ref. 98 gives solutions for two cases of the ratio of masses of the striker and the beam. In the first case a beam with cross section of 1 x 1 cm, length of 15.35 cm was struck by a steel ball with radius of 1 cm and initial velocity of 1 cm/s, and in the second case the length

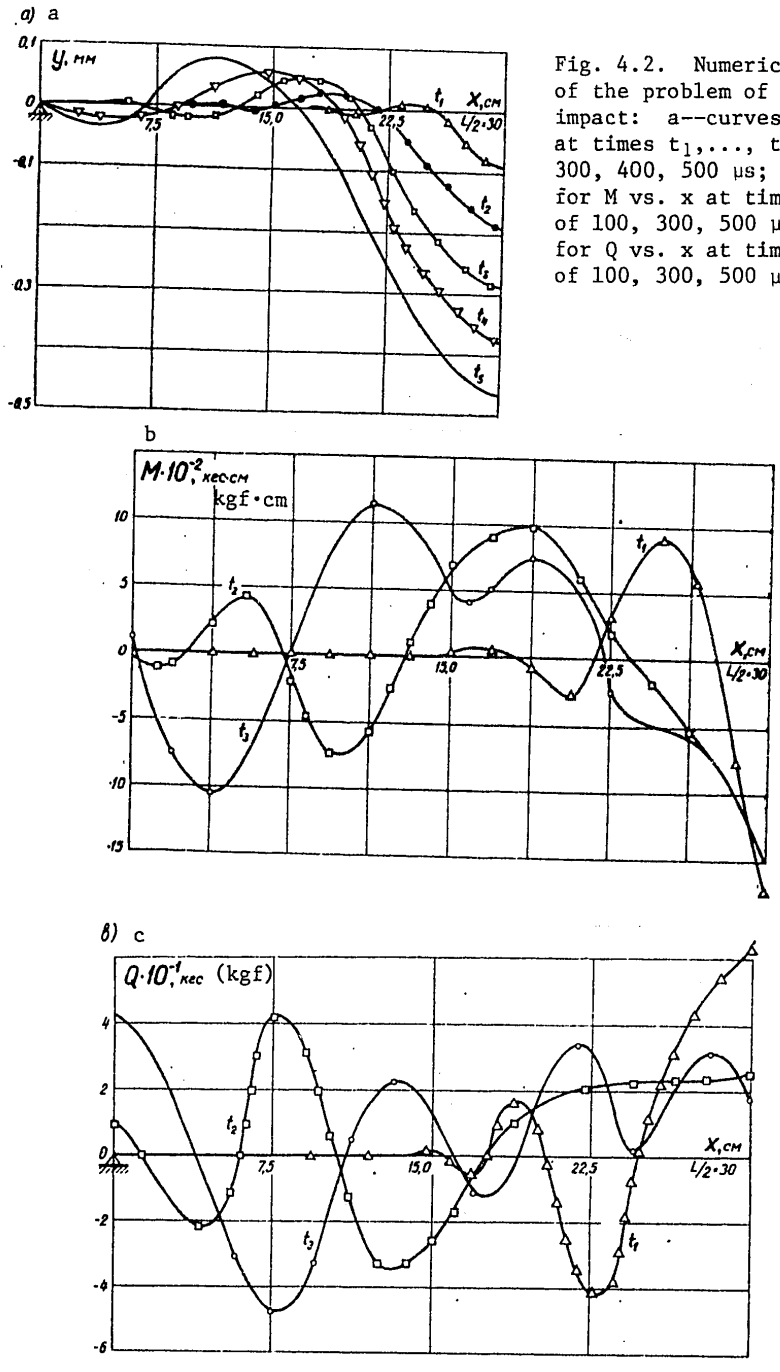

Fig. 4.2. Numerical solutions of the problem of transverse impact: a--curves for y vs. x at times $t_1, \ldots, t_5 = 100$, 200, 300, 400, 500 μs; b--curves for M vs. x at times $t_{1, 2, 3}$ of 100, 300, 500 μs; c--curves for Q vs. x at times $t_{1, 2, 3}$ of 100, 300, 500 μs

of the beam and the radius of the ball were doubled. The modulus of elasticity of the beam was $E = 2.2 \cdot 10^6$ kgf/cm^2, and density was $\rho_0 = 7.96$ g/cm^3. The period of the fundamental mode of oscillations $\tau = 10^{-3}$ s in the numerical calculations was divided into $1/\delta = 180$ parts.

Timoshenko showed that when the ratio of the mass of the beam to the mass of the ball $m/M > 1$, a single impact occurs. In the given example the duration of the contact $t^* \approx \frac{1}{6}\ \tau$. When $m/M < 1$, repeated collisions occur. The first collision terminates at time 19.5 $\delta\tau$; the beginning and end of the second collision correspond to 60 $\delta\tau$ and 80 $\delta\tau$, respectively. As the stiffness of the beam increases, there is an increase in the amplitude of the contact force.

For a complete study of the phenomenon of repeated collisions of a beam and ball discovered by Timoshenko, we give here the numerical calculations of contact force with consideration of shears, rotational inertia and the ratio m/M. The graphs presented in Fig. 4.3, 4.4 show that as

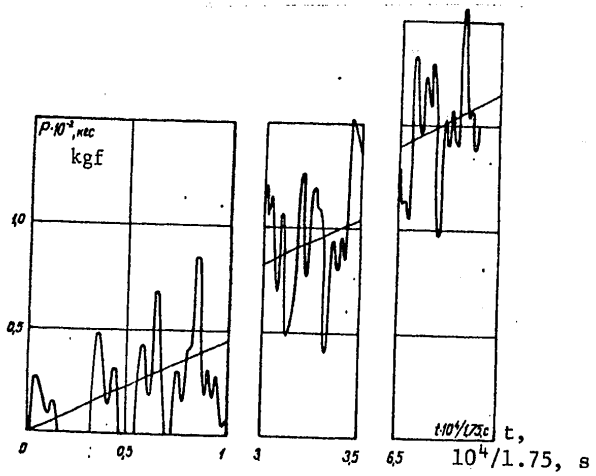

Fig. 4.3. Results of numerical calculation of a beam 33 cm long loaded by an infinite mass, $V_0 = 1.4$ m/s

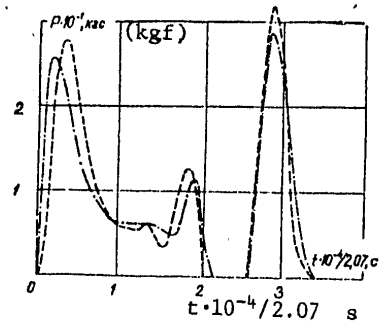

Fig. 4.4. Curves for P vs. t at $E/G = 5$ (-·-) and 10 (---), $m/M = 20$

m/M increases, there is a corresponding increase in the number of collisions; for $m/M \to 0$ the time intervals between collisions decrease rapidly; after 4-5 collisions the striker moves into uninterrupted contact with the beam. The contact force is comprised of polyharmonic oscillations (the sum of the odd harmonics of the beam) around the straight line $P = A_0 t$, where $A_0 = 48EIV_0/L^3$. The influence of shears and rotational inertia shows up as a small change in amplitude and in delay of the onset of the repeat collision (see Fig. 4.4).

4.2. Experimental Studies of Transverse Impact

Experiments [Ref. 61] on recording reactive forces, deformations of the outside line and contact force in dynamic bending of a beam were done with impact by a mass of 590 g in the form of a rod freely dropped from a height of 5, 10 and 15 cm.

A method of determining the static modulus of interlaminar shear from tests of bending of a beam by a concentrated load P is proposed in Ref. 96, 98. G is calculated from the formula

$$y = \frac{PL^3}{48EJ}\left[1 + \frac{3}{2}\left(\frac{H}{L}\right)^2 \frac{E}{G}\right], \qquad (4.18)$$

where E/G is the ratio of the elastic modulus to the shear modulus; H/L is the ratio of the cross section of the beam to the length of the span. Numerous experiments done under static conditions as well as with transverse impact have shown that using (4.18) for calculating the shear modulus leads to considerable errors and scatter of results as a consequence of the fact that the order of magnitude of quantities $\frac{3}{2}\left(\frac{H}{L}\right)^2 \frac{E}{G}$ is commensurate with the accuracy of the experiment. We consider below a method of calculating the dynamic shear modulus with high accuracy from data of registration of shear wave propagation.

Reactive forces and bending moments in the case of dynamic bending. The propagation of bending moments was studied in Ref. 61 from data of registration of the deformation of the outside line of a beam by strain gages with a base of 10 mm. The results of numerical calculations according to (4.1) and also experimental data are given in Fig. 4.5, which shows in particular that the main portion of the signal M vs. t propagates at the velocity of the shear wave; the part of the pulse that propagates at velocity c_0 is recorded in the form of a forerunner.

The reactive force was determined from a dynamometer combined with a support (Fig. 4.6). It was established by preliminary experiments that the form of the support fasteners has a noticeable effect on the study results in the case of dynamic bending. It was found that the reaction of the support is most sensitive to the form of the support fastener.

Development of a support design (see Fig. 4.6) that produces supporting conditions fairly close to hinge support is dictated by the need for comparing data of experiments with the results of numerical calculations for the case of bending of a hinged beam. Two piezoceramic pellets are placed in the opening of the support and compressed by a screw. Signals from the piezoelectric elements are sent through an amplifier to the input of an oscilloscope. The arrangement permits static calibration. Triggering of the oscilloscope was synchronized with the beginning of contact of the striker and the beam. Fig. 4.7 shows typical oscillograms of R vs. t recorded during impact. We can see from Fig. 4.7, a, that preceding the registered force pulse is an oscillating forerunner that propagates at velocity c_0. The oscillograms can be used in particular to determine the rate of shear wave propagation c_G. The results of numerical calculation according to (4.1) and experimental data are given in Fig. 4.8. Steel and fiberglass beams were tested to check out the method. The problem was posed of calculating the values of c_G and G from propagation of the transverse force, and also experimentally confirming the influence that the shape of the beam cross section has on the velocity of shear wave propagation stemming from the relation $c_G = \sqrt{k'G/\rho}$, where k' is a coefficient that accounts for the shape of the cross section [Ref. 125]. Data on the shape and dimensions of specimens are summarized in Table 4.1. The values of $G_э$, c_{GT} given in the Table were calculated from the expressions

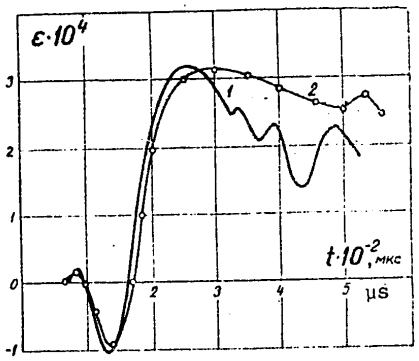

Fig. 4.5. Theoretical (1) and experimental (2) curves for ε vs. t for cross section x = 18.8 cm. Length of the beam 60 cm

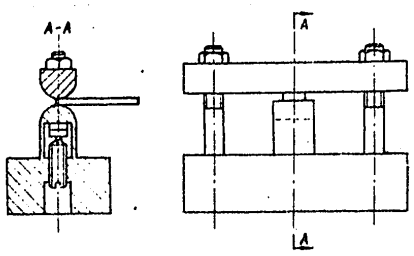

Fig. 4.6. Design of the support for studying dynamic bending of beams

$$G_э = \frac{\rho (c_G)^2}{k'}, \quad c_{G,T} = \sqrt{\frac{k'E}{2\rho(1+\nu)}}, \tag{4.19}$$

where ν is the Poisson ratio equal to 0.3. It can be concluded from a comparison of the data given in the Table that the proposed method of

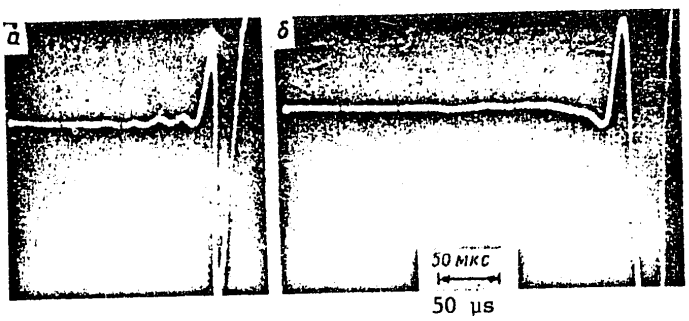

Fig. 4.7. Typical oscillograms of R vs. t with dynamic bending of steel (a) and fiberglass (b) beams 88.8 cm long

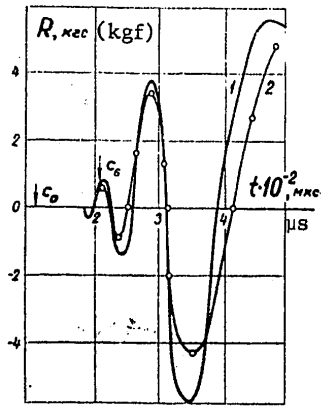

Fig. 4.8. Theoretical (1) and experimental (2) curves for R vs. t for a beam 60 cm long. The arrows indicate times of arrival of waves c_0 and c_G

determining the velocity of shear waves is reliable. The theoretical position on the influence that the shape of the beam has on the velocity of shear waves can be taken as theoretically proved. Registration of the velocity of shear waves enables determination of the shear modulus for glass-textolite where the reinforcing layers are perpendicular or parallel to the acting force. In the former case the given characteristic is termed the interlaminar shear modulus. For glass-textolite the computed value of the ratio E/G was 5.80. The static ratio of these quantities is about 10.

Registration of contact forces. One paper on studying contact force [see Ref. 22] describes a method of recording it. A steel ball fell on top of a steel hemisphere fastened on the upper surface of a beam. A barium titanate pellet secured to the beam measured the contact force. However, such a beam cannot be used to record repeated collisions.

At the Institute of Mechanics of Polymers, Lithuanian SSR Academy of Sciences, a special dynamometer (Fig. 4.9) has been made for studying contact force. The device consists of a long (750 mm) cylinder 10 mm in diameter terminating in a short thicker cylinder in which an opening has been cut to accommodate two piezoelecttric ceramic pellets. The thick part of the dynamometer is tipped with a hemisphere 3 cm in radius.

TABLE 4.1

Material and shape	k'	$c_{G,\ni}$, km/s	c_0, km/s	$E \cdot 10^{-6}$, kgf/cm^2	$c_{G,T}$, km/s	$G_\ni \cdot 10^{-6}$, kgf/cm^2	E/G
Steel							
circle, D = 10 mm	0.887	3.14	5.0	2.0	2.9	0.830	2.25
ring, D_1 = 10 mm, D_2 = 7.5 mm	0.548	2.51	5.0	2.0	2.3	0.920	2.17
Glass-textolite							
reinforcing layers perpendicular to the acting force:			4.3 along the base	0.25 along the base	-	0.043	5.80
rectangle b = 12 mm, h = 8 mm	0.833	1.40	4.3	0.25	-	0.056	4.5
reinforcing layers parallel to the acting force:							
rectangle b = 8 mm, h = 12 mm	0.833	1.60	along the base	along the base			
Polymethyl methacrylate square 10x10 mm	0.833	1.30	2.0	0.046	1.3	0.023	2.0
Graphite-reinforced plastic (monodirectional)							
rectangle b = 18 mm, h = 5 mm	0.833	2.06	10.8	1.85		0.066	28

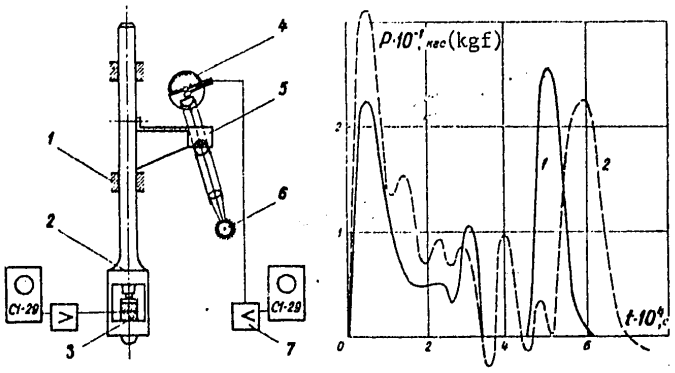

Fig. 4.9. Diagram of registration of dynamic forces and displacements: 1--journal bearing; 2--dynamometer; 3--piezoelectric crystal; 4--photocell; 5--indicator element (flag); 6--light source; 7--amplifier

Fig. 4.10. Theoretical (1) and experimental (2) [time] dependences of contact force with impact on a beam [of length] L = 60 cm

The piezoelectric elements were compressed by a bolt. Signals from the piezoelectric elements were sent through an amplifier to an oscilloscope. The force sensor was claibrated by loading the dynamometer with calibrated weights. The dynamometer design shown in Fig. 4.9 enables use as a striker in studying dynamic bending of beams. The dynamometer was placed in a vertical position, and horizontal movements were prevented by Teflon sleeves secured to a stationary stand. The experiments consisted in rgistration of the contact force with free fall of the dynamometer onto the beam from a height of 5, 10 and 15 cm. The force was electronically recorded. The system permitted static calibration directly on the facility. The time dependence of the contact force was recorded by an oscilloscope. A typical oscillogram of P vs. t is shown in Fig. 4.10.

4.3. Wave Phenomena in the Striker upon Transverse Impact

In solving the problem given in section 4.1, the influence of wave effects in the striker with beam bending was disregarded since the solution was found for cases in which the time of collision is much longer than the time of wave propagation through the striker, in which the stressed state can be considered quasistatic.

Accounting for wave phenomena in the striker is simplest in the case where a striker of very simple shape is used. Therefore the striker shape used in Ref. 98 (a ball) is rejected due to the necessity in this case of solving a complex three-dimensional problem. Wave phenomena are most simply accounted for in a striker that is a thin rod. While waves in a striker rod were taken into consideration in Ref. 85, the influence of

local deformations on interaction between the striker and beam was disregarded, which is an impediment to an in-depth understanding of the phenomenon.

Transverse impact with consideration of wave motions in the striker. A program for computer calculations was compiled on the basis of the solution described in section 4.1. The refinement of the problem amounted to consideration of one-dimensional wave phenomena in the striker. The problem is solved for the loading arrangement shown in Fig. 4.11 used in conducting the experiment described below. The equations of motion of the beam are given in section 4.1. The boundary conditions (the usual ones for hinged support): $y = 0$, $y'' = 0$. The equation of motion of the rod (Fig. 4.11):

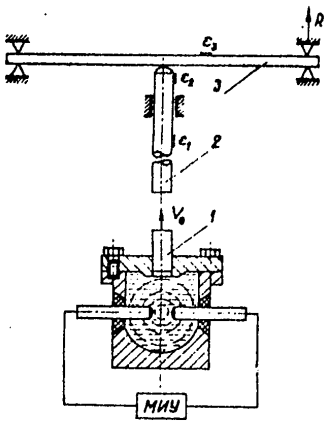

Fig. 4.11. Diagram of beam testing for transverse impact by means of a waveguide: 1--striker; 2--waveguide rod; 3--test beam; МИУ--magnetic-pulse facility

$$\frac{\partial^2 U}{\partial t^2} = c_0^2 \frac{\partial^2 U}{\partial y^2} \tag{4.20}$$

with initial conditions

$$U\left(y, -\frac{L}{c_0}\right) = \frac{\partial U\left(y, -\frac{L}{c_0}\right)}{\partial t} = 0. \tag{4.21}$$

The solution of the equation of motion of the rod for displacements $U(y,t)$ takes the form

$$U(y, t) = \sum_{n=0}^{\infty} \left[\Phi\left(t - \frac{L(2n+1)+y}{c_0}\right) + \Phi\left(t - \frac{L(2n+1)-y}{c_0}\right) - \right.$$
$$\left. - \Phi_1\left(t - \frac{2Ln-y}{c_0}\right) - \Phi_1\left(t - \frac{L(2n+1)+y}{c_0}\right) \right];$$

$$\Phi(z) = \begin{cases} -\int_{-L/c_0}^{z} e^{J}(\xi)\, d\xi, & z > -L/c_0, \\ 0, & z \leqslant -L/c_0; \end{cases}$$

$$\Phi_1(z)=\begin{cases}\dfrac{1}{EF}\displaystyle\int_0^z P(\xi)\,d\xi, & z>0,\\ 0, & z\leqslant 0;\end{cases}$$

$$\frac{\partial U(0,t)}{\partial y}=-\frac{P(t)}{EF}, \qquad \frac{\partial U(-L,t)}{\partial y}=\varepsilon^J(t). \tag{4.22}$$

The function $\varepsilon^J(t)$ is a predetermined boundary condition; P(t) is determined by simultaneous solution of the problem for the beam and rod at the contact point with fulfillment of the condition

$$U(0,t)-y(x_1,t)=\delta[P(t)], \tag{4.23}$$

where $y(x_1, t)$ is flexure of the cross section of the beam with coordinate $x = x_1$; $\delta[P(t)]$ is the relation between the contact force and the size of the approach; U(0,t) is displacement of the end of the rod in contact with the beam.

The algorithm for computer calculations was compiled for different forms of the dependence $\delta(P)$ determined experimentally for the selected form of the end of the rod striking the beam. The problem was solved with consideration of the elastic dependence $\delta(P)$ for which crumpling totally vanishes as the load is removed, and also with consideration of the dependence $\delta(P)$ for which crumpling is irreversible upon removal of the load.

Experimental plotting of the dynamic dependence between P *and* δ. The relations between P and δ necessary for solving the formulated problem were experimentally found in tests with a Hopkinson bar. The pressure-transmitting rod in the HSB method (see Fig. 3.1) was replaced by a long striker rod with a specially shaped end face. Disregarding deformation of the specimen as compared with buckling deformation, by analogy with classical relations of the HSB method we get

$$\delta=-2c_0\int_0^t \varepsilon^R dt'. \tag{4.24}$$

The force is determined in accordance with the relation

$$P=\sigma^T, \quad F=\varepsilon^T EF, \tag{4.25}$$

where E is the modulus of elasticity of the pressure-transmitting rod; F is the cross sectional area of the specimen (specimen with flat end faces; end of the rod cylindrical, R = 30 mm, with axis perpendicular to the axis of the rod).

A number of theoretical and empirical relations have been proposed [Ref. 42] that describe curves of P vs. δ for a given geometry of the contacting bodies. Let us note that for further calculations the analytical description of the graph (Fig. 4.12) is unnecessary since the problem was solved on a computer. To show how relations between P and δ affect the quantitative characteristics of beam bending in the contact zone, the problem of studying bending of isolated beams was posed. Such a condition is realized in experiments using beams with and without a spacing liner in the contact zone.

Experimental study of dynamic bending (a diagram of the experiment is shown in Fig. 4.11). The rod was loaded by a striker block shot from the discharge chamber with free electric discharge. The block was a Duralumin cylinder 20 mm in diameter; the length was varied to change the duration of the loading pulse. The necessary measurements for comparison with the results of numerical solution are as follows: 1) deformation $\varepsilon^{J,R}$ in the striker rod cross section $y = y_1$; 2) bending moments M recorded by strain gages in several cross sections of the beam ($x_1 = 0$; $x_2 = L/2$); 3) the reactive force R of the beam. Contact force P_k is calculated from the $\varepsilon^J(t)$ and $\varepsilon^R(t)$ obtained by a strain gage cemented to the rod (Fig. 4.11). A typical oscillogram of ε^J, ε^R vs. t (Fig. 4.13) enables us to calculate the contact force:

$$P = FE\left[\varepsilon^J(t) - \varepsilon^R\left(t - \frac{y_1 + L}{c_0}\right)\right], \tag{4.26}$$

where F, E are the cross sectional area and modulus of elasticity of the striker rod, ε^J and ε^R are deformations for rod coordinate $y = -y_1$ in the

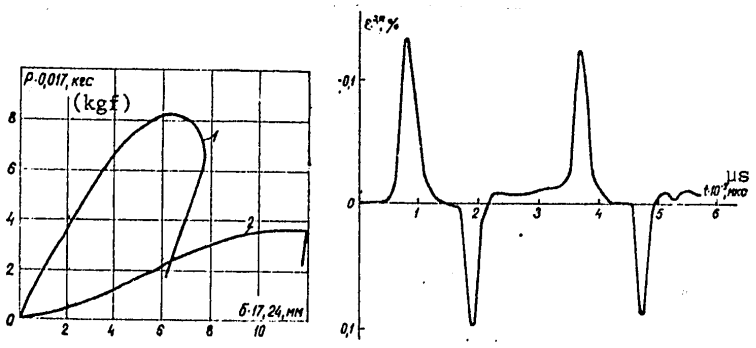

Fig. 4.12. Dynamic relations of P vs. δ for fiberglass-reinforced (1) and kerovinyl-coated glass-textolite (2) specimens

Fig. 4.13. Typical oscillogram of $\varepsilon^{J,R}$ vs. t found in an experiment according to the arrangement on Fig. 4.11

incident and reflected waves. In addition to these recordings, direct measurements were made of the contact force P_k by strain gages close to the contact point $y = 0$ (strain gage ε_2 in Fig. 4.11). Despite the fact that the resultant data are somewhat distorted by dispersion, the values of P_k found in our experiments were not very different from those calculated by formula (4.26). The tests were done on glass-textolite beams (ASTT glass cloth -- 50%, EDT resin -- 50%).

To study the influence that the relation between P and δ has on transverse bending, the force was transmitted to the beam from a long rod through an intermediate spacing liner and also without such a liner. This spacer was a plate (10 x 10 x 3 mm) cemented to the surface of the beam in the middle of its span. First the relation between P and δ was studied by a previously described method for the spacer. Fig. 4.14-4.16 show graphs plotted on the basis of numerical calculations and experimental data. In both cases the striker rod was subjected to the same input pulse ε^J. Fig. 4.16 shows some results of solution of the problem for the case where impact is by a striker rod with a conical tip having a vertex angle of 90° and round-off radius of 1 mm. As we can see from Fig. 4.14-4.16, the relation between P and δ in the contact zone of the striker has a considerable effect on all bending parameters.

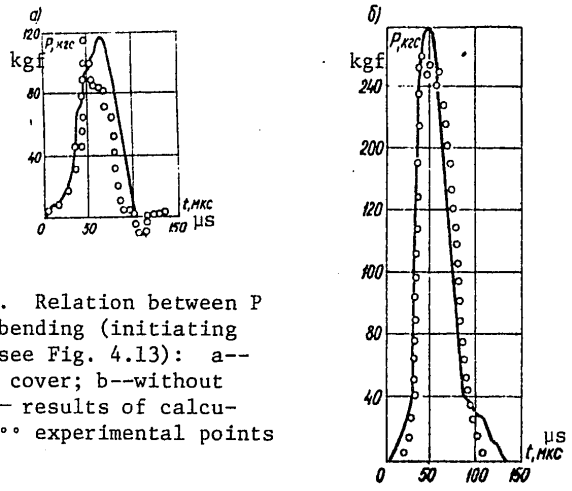

Fig. 4.14. Relation between P and t in bending (initiating pulse ε^J see Fig. 4.13): a--beam with cover; b--without cover; —— results of calculation; ◦◦◦ experimental points

Let us note that repeat collisions occur in the given loading scheme as well; however, the condition of their occurrence cannot be formulated with consideration of the relation m/M as was done in the case of low-speed impact of a massive body against the beam (see section 4.1) since the repetition of collisions depends on the length of the rod and the natural frequencies of the beam, and may be infinitely varied.

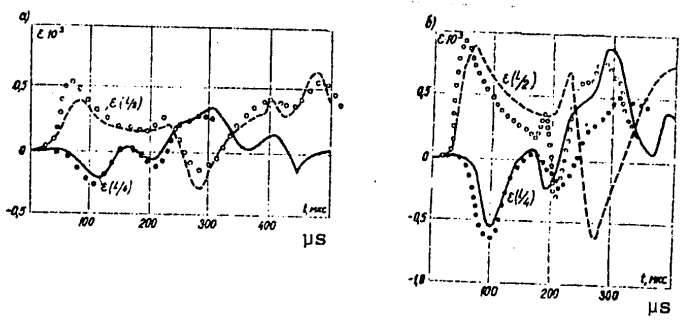

Fig. 4.15. Curves for deformations in the mid-span of a beam L/2 and at a distance of L/4 from the support (see Fig. 4.13 for initiating pulse): a--covered beam; b--uncovered beam; —— results of calculation; °°° experimental points

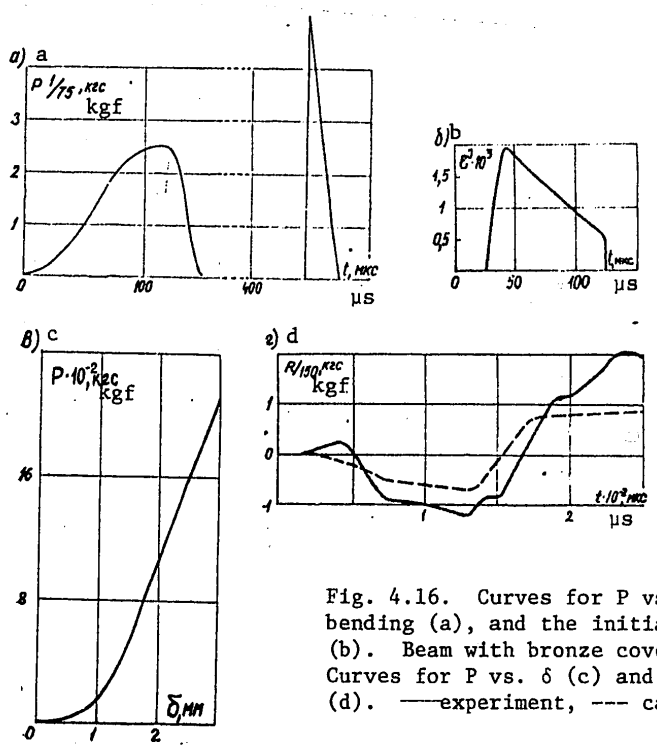

Fig. 4.16. Curves for P vs. t in bending (a), and the initiating pulse (b). Beam with bronze covering. Curves for P vs. δ (c) and R vs. t (d). ——experiment, --- calculated

4.4. Pulse Loading by Electromagnetic Fields

Not much research has been done on experimental investigation of the bending of beams by distributed pulse loads, although we feel that the method has indisputable advantages over methods of beam bending (see sections 4.1-4.3). These advantages are shown mainly by the absence of local deformations during loading, which appreciably facilitates theoretical studies. Up until now, a strip of explosive material placed on the surface of the beam and detonated from both sides (from the supports toward the center) has been used to produce a distributed load [Ref. 104]. Recording is done by high-speed photography of the beam outline. The disadvantage of the method is the low accuracy of determining comparatively small flexures.

Numerical solution of the problem of beam bending. A solution was found for the same problem as in section 4.1 with the following difference: external loading was taken as uniformly distributed over the beam. The problem was solved for a function arbitrarily assigned in time for a hinged beam. Following Ref. 75, we get the solution in the form

$$y_k=\frac{4k'G}{\pi I\rho^2}\sum\left\{\frac{q_k}{S_{1n}^2S_{2n}^2}\left(1+\frac{\alpha^2b_4}{b_3}\right)+\right.$$

$$+\frac{1}{S_{2n}^2-S_{1n}^2}\left[\left(\frac{1}{S_{1n}}+\frac{b_5}{b_3}S_{1n}+\frac{b_4\alpha^2}{b_3S_{1n}}\right)\sin S_{1n}k\tau\sum_{i=1}^{k}I_{in}^1+\right.$$

$$+\cos S_{1n}k\tau\sum_{i=1}^{k}I_{in}^1\Big)-\left(\frac{1}{S_{2n}}+\frac{b_5}{b_3}S_{2n}+\frac{b_4\alpha^2}{b_3S_{2n}}\right)\times$$

$$\left.\left.\times\sin S_{2n}k\tau\sum_{i=1}^{k}I_{in}^2+\cos S_{2n}k\tau\sum_{i=1}^{k}I_{in}^2\right]\right\}\frac{\sin\alpha x}{n}; \qquad (4.27)$$

$$\Theta_k=\frac{4k'G}{\pi I\rho^2}\sum_{n=1}^{\infty}\alpha\left\{\frac{q_k}{S_{1n}^2S_{2n}^2}+\frac{1}{S_{2n}^2-S_{1n}^2}\left[\left(\sin S_{1n}k\tau\sum_{i=1}^{k}I_{in}^1+\right.\right.\right.$$

$$+\cos S_{1n}k\tau\sum_{i=1}^{k}I_{in}^1\Big)-\frac{1}{S_{2n}}\Big(\sin S_{2n}k\tau\sum_{i=1}^{k}I_{in}^2+$$

$$\left.\left.\left.+\cos S_{2n}k\tau\sum_{i=1}^{k}I_{in}^2\right)\right]\right\}\frac{\cos\alpha x}{n}; \qquad (4.28)$$

$$b_3=k'FG;\quad b_4=EI;\quad b_5=I\rho;\quad \alpha=\frac{\pi n}{L};$$

$$I_{in}^r=\frac{q_i-q_{i-1}}{S_{rn}^2\tau}[\cos\tau iS_{rn}-\cos(i-1)\tau S_{rn}];$$

$$I_{in}^r=\frac{q_{i-1}-q_i}{S_{rn}^2\tau}[\sin\tau iS_{rn}-\sin(i-1)\tau S_{rn}]; \qquad (4.29)$$

S_{1n}, S_{2n} are two sets of natural frequencies corresponding to the Timoshenko equation.

We compiled a program for computer calculation of series (4.27), (4.28) with retention of 160 harmonics. The numerical calculations were done at values of the elastic constants of the beam material given in section 4.1. The moments M and transverse forces Q arising in the beam are functions in time independently of the form of q(t) considered in the calculations, the results of which for the case of impulse bending of a beam with hinged fastening and loaded by a uniformly distributed impulse force q are given in Fig. 4.17. With impulse loading of a beam by a

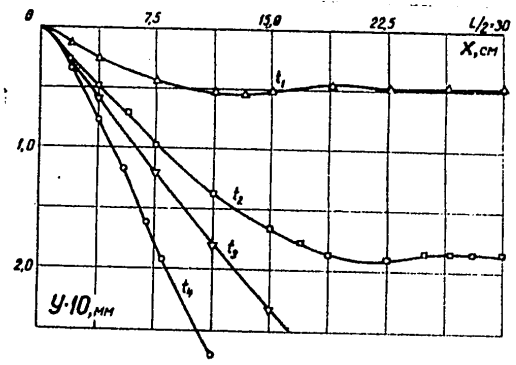

Fig. 4.17. Numerical solutions of the problem of bending of a beam by a distributed impulse load. Dependence of y vs. x at times $t_1, \ldots, t_4$ = 100, 200, 300, 400 μs.

uniformly distributed load, the main part of the waves propagates at a velocity close to the shear wave propagation velocity c_G. The portion of the corresponding pulse that propagates at the longitudinal wave velocity c_0 takes the form of a forerunner. As a consequence, on the initial stage of bending (at $t_0 \leqslant L/2c_G$), a practically undeformed section of the beam appears that shifts along the line of action of the force as a rigid body changing lengthwise at a rate of c_G; noticeable values of M in the cross section L/2 of the beam show up at time $t_0 = L/2c_G$.

Experimental investigation of impulse loading of beams. Tests were done on beams (10 x 10 x 250 mm) made of glass-textolite (ASTT glass cloth, EDT resin -- 50%). The method of impulse bending of beams by electromagnetic forces is described in Ref. 57. The beam was loaded by using a single-turn inductor -- a flexible foil strip 10 mm wide and 0.2 mm thick. The inductor was thoroughly insulated. A diagram of tests for impulse bending of beams is shown in Fig. 4.18. The electrodynamic force that arises upon discharge of the capacitors through the inductor is transmitted to the beam as a distributed load. It has been found that the distance from the end of the inductor loop to the support must be at

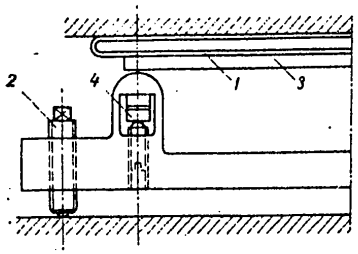

Fig. 4.18. Diagram of transmission of impulse pressure to a beam: 1--inductor; 2--screw; 3--specimen; 4--piezoelectric element

least 20 mm for uniform distribution of the load. To create conditions close to hinged support (see Fig. 4.18) the bolts were put under a certain tension, and the end of the beam extended beyond the axis of the support no more than 5 mm.

For purposes of adequately complete investigation of the phenomenon of dynamic bending of beams, simultaneous recordings were made by three oscilloscopes of the pressure pulse q, the reactive force R on one of the supports, and the deformation of cross section $x = L/2$. The difficulties of recording pulse pressure are well known. They are due to the electromagnetic interference that accompanies discharge of the capacitors. Since direct measurements of mechanical pressure are impossible, electrical quantities are recorded: I(t) -- the current strength in the inductor circuit, and the pulse pressure is then calculated by the formula

$$q = \frac{\mu}{2b^2} I^2(t), \qquad (4.30)$$

where b is the width of the inductor, μ is the coefficient of magnetic induction. Expression (4.30) is applicable when $\delta/b \ll 1$, where δ is the width of the aperture of the inductor loop. This condition was satisfied in the formulated experiments, which was verified by high-speed photography.

The current strength at discharge of the capacitors was measured by a shunt. The relation between I and t is satisfactorily approximated by two parabolas. The function q(t) found from formula (4.30) was taken into consideration in the numerical calculations.

The reactive forces were recorded by a dynamometer combined with the support (see Fig. 4.18). Two piezoceramic pellets (8 mm in diameter and 5 mm thick) were placed in the opening of the support, and a silver plate connected to a cable was placed between them. The pellets were compressed by a screw. The amplifier was an East German PM-1. As a result of shielding of the piezoelectric elements and the connecting parts of the circuit, oscillograms were obtained that are not distorted by the electromagnetic wave that arises upon discharge of the capacitors.

Deformations of the outer line of the beam were recorded by strain gages with a 5 mm base cemented to the mid-span of the beam. The oscilloscopes

were triggered from the electromagnetic wave accompanying discharge of the capacitors. With consideration of the conclusion that the outside fibers of the beam at mid span begin to stretch at time $t_0 = L/2c_G$, by varying L we can realize the condition $t_0 > t_{dis}$, where t_{dis} is the time of existence of pickups. The amount of deformation of a beam fiber in cross section L/2 will not be distorted by electromagnetic pickups upon discharge of the capacitors if the corresponding length of the beam is selected from the condition $L \geqslant 2c_G t_{dis} = 2(1250 - 1400) \cdot 10^{-4} = 0.25\text{-}0.28$ m. The chosen length of the beam (250 mm) is minimum for discharge duration up to 100 μs. At this value of L the shear wave reaches cross section L/2 simultaneously with cessation of the action q(t) and electromagnetic pickups.

The proposed recording method enabled us to check the correctness of formulation of the experiment. It was shown that with transmission of force to the beam, the mass of the moving part of the single-turn inductor has a considerable effect on the deformation in cross section L/2 and on the reaction of the supports. With a change in thickness of the inductor from 2 to 0.2 mm, the value of ε increases by 60-80%, which is apparently due to the distribution of momentum between the beam and the inductor. Accounting for the inertia of the inductor in theoretical solution of the problem of beam bending makes it more complicated to get the final results, and therefore to compare theory with experiment we need to work with inductors of minimum mass. We feel that such a requirement is completely satisfied by the thin foil inductor that we have used.

To check the uniformity of pressure distribution along the beam, additional experiments have been done based on the use of strain gages that are symmetrically cemented relative to the cross section of the beam. It has been established that comparatively uniform pressure distribution occurs when the inductor loop (see Fig. 4.18) projects beyond the axis of the support by no more than 20 mm. To set up conditions on the end of the beam that are sufficiently close to hinged support, it is necessary to press the beam against the support with a static force in a range of 10-20 kgf. Under higher compressive forces, the conditions of support become close to those that occur when the ends of the beam are clamped. Slight compression was sufficient to prevent repeated collisions of the beam ends against the supports; such repeat collisions are unavoidable in the case of a simply supported beam. At the same time, slight compression allowed turning of the cross sections of the beam resting on the supports.

Fig. 4.19 compares the data of numerical calculation and experiment. Some discrepancies between experimental data and the results of solution may be due to viscosity effects in the beam material.

Thus the velocity of shear wave propagation c_G can be fairly accurately recorded from the time of noticeable deformation in cross section L/2 of

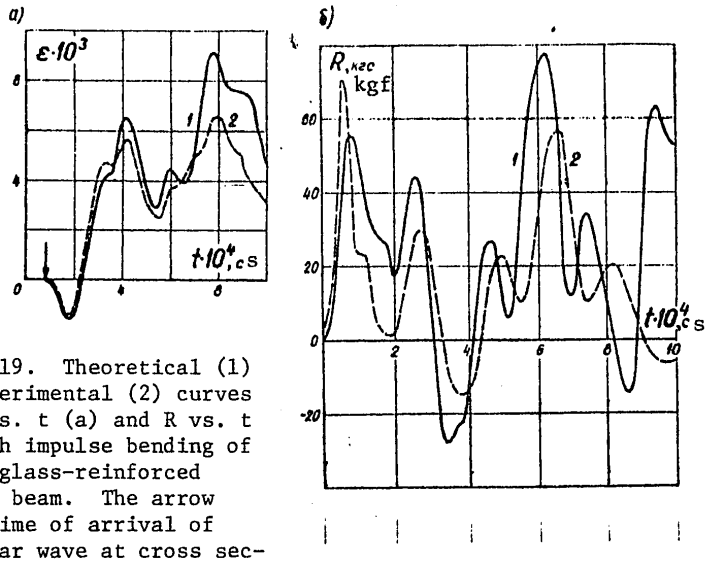

Fig. 4.19. Theoretical (1) and experimental (2) curves for δ vs. t (a) and R vs. t (b) with impulse bending of a fiberglass-reinforced plastic beam. The arrow shows time of arrival of the shear wave at cross section x = L/2

a beam (see Fig. 4.19). The parameter calculated from the relation $G = \rho c_G^2/k'$ can be called the modulus of interlaminar shear, and is an important characteristic of laminar materials. A series of experiments showed that for the investigated material $c_G = 1.3 \pm 0.1$ km/s, and the ratio E/G is about 5.7-5.8, which agrees with the data given in section 4.2.

4.5. Standard Methods

Standard test methods to a great extent are used to work out recommendations on choosing material in accordance with measurements of the absorbed energy to fracture. Tests for impact toughness, despite a number of disadvantages, are still a satisfactory means of material quality control. The results of standard tests can be used only for comparative characterization of the properties of polymer materials. The data found in testing by a standard procedure cannot serve as characteristics of the material in strength calculations.

The necessity for fairly exact quantitative values of the characteristics of materials that are used as the basis of strength calculations has brought about improvement of standard testing methods, and the development of new methods. The improvement of standard test methods is based on using oscillographic studies, examining the shape and dimensions of specimens, and changing to tests with new loading devices. Research has been started to develop dynamic methods of the mechanics of fracture for the purpose of exact determination of the energy of destruction.

In 1909, Charpy suggested evaluating the inclination of materials to brittle fracturing from the energy expended on destruction of specimens under impact bending. Since that time, impact toughness testing has been considered a simple means of determining the qualitative differences of absorbed energy in fracture of materials being compared.

Existing GOST State Standards propose the following definitions: the impact toughness of unnotched specimens (a_n, kgf·cm^2) characterizes the work expended on fracture of an unnotched specimen with reference to its cross sectional area; impact toughness of notched specimens (a_k, kgf·cm/cm^2) characterizes the work expended on destruction of a notched specimen with reference to its cross sectional area at the place where it is notched; the coefficient of weakening of impact toughness by a notch is the ratio of the impact toughness of a notched specimen to that of an unnotched specimen.

The energy expended on destruction of a specimen in biaxial bending on pendulum hammers is determined in accordance with GOST 4647-69 (Plastics. Method of tests for two-support impact bending) from the difference of pendulum energies in the initial and final positions.

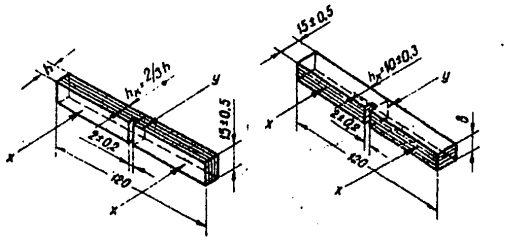

Fig. 4.20. Standard specimens made of laminar materials

The test specimens are made by pressing, molding, casting and so on. They must correspond to the requirements of GOST 14359-69 (Plastics. Methods of mechanical tests. General requirements). The shape, size and placement of the notch must also meet GOST specifications. The depth of the notch must be such that the remaining area of the cross section of the specimen is 2/3 of the area of the unnotched specimen. The specimens used for testing are in the form of notched and unnotched bars (Fig. 4.20). The round-off radius of the notch is no more than 0.2 mm. In testing, the notched specimens are installed on the pendulum hammer so that impact occurs on the side opposite the notch, and the knife of the pendulum faces the notch. Pendulum velocity at the instant of impact is 2.9 ± 0.1 m/s and 3.8 ± 0.1 m/s at maximum energy of impact of less than and more than 0.5 kgf·m respectively. Tests for impact toughness begin with raising of the hammer to the upper starting position where it is held by an arresting device. Then the scale pointer is set at the end position and the pendulum is released, giving it free fall. After destruction of the specimen, the pendulum is stopped, and the scale reading

gives the work expended on breaking the specimen with accuracy to half a scale division for the corresponding hammer. If the hammer scale is graduated in degrees, the reading is taken with accuracy down to 1°, and the amount of work expended is calculated from the formula

$$A = GL\left[(\cos\beta - \cos\alpha) - (\cos\gamma - \cos\alpha)\ \frac{\alpha+\beta}{\alpha+\gamma}\right], \tag{4.31}$$

where G is the weight of the pendulum, kgf; L is the length of the pendulum, cm (distance from the axis of the suspension to the center of gravity); α is the loading angle of the pendulum, deg; β is the angle of rise of the pendulum after breaking the specimen, deg; γ is the angle of rise of the pendulum in free travel, deg.

The impact toughness of an unnotched specimen (a_n, kgf·cm/cm^2) is calculated from the formula

$$a_n = \frac{A_n}{bh}, \tag{4.32}$$

where A_n is the work expended on breaking the specimen, kgf·cm; b is the width of the specimen at the middle, cm; h is the thickness of the specimen at the middle, cm. The specific toughness of a notched specimen (a_k, kgf·cm/cm^2) is calculated from the formula

$$a_k = \frac{A_k}{bh_k}; \tag{4.33}$$

A_k is the work expended on breaking the specimen, kgf·cm; h_k is the thickness of the specimen at the middle of the notch, cm. The specific work of impact fracture

$$z = \frac{GA}{bh^2}; \tag{4.34}$$

bh^2/G is the moment of resistance of the cross section of the specimen, cm^3. The test result is taken as the arithmetical mean of all parallel determinations and (if provided by the standard or technical specifications for the material) the characteristic of data scatter evaluated from the standard deviation.

The coefficient of weakening is calculated from the average values of a_n and a_k by the formula

$$k_z = \frac{a_k}{a_n} \cdot 100\%. \tag{4.35}$$

Tests for impact bending of a cantilevered specimen are provided by GOST 19109-73 (Plastics. Method for Izod impact testing of a cantilevered specimen) and GOST 14235-69 (Plastics. Method of determining impact toughness on a Dinstat type device). Izod tests for cantilever bending are done with notched specimens. Geometric dimensions of specimens: length 63.5 mm; width 3.2-12.7 mm; height 12.7 ± 0.15 mm. A V notch with vertex angle of 45 ± 1° is milled in the middle of the beam. The radius of the notch is 0.25 ± 0.025 mm, and depth is 2.54 mm.

The essence of the Izod testing method is in bending of the cantilever specimen fastened in the device so that the central line of the notch is on the level of the upper clamping surface, and the notch faces the pendulum held by an arresting device in the extreme upper position. The scale pointer is set at the zero position, and the pendulum is released. The velocity of fall of the pendulum at the instant of impact is 3.35 ± 0.05 m/s. After breaking the specimen, the pendulum is stopped, and the work expended in breaking is read out from the scale.

The standard provides for tests that are done with consideration of the energy of recoil of the broken part of the specimen. For this purpose, the energy found in supplementary tests is subtracted from the energy determined with fracture of the whole specimen. The part of the specimen that breaks off is put back (refit into the second half of the specimen clamped in the device), and the test is repeated. The energy expended on recoil of the specimen is determined from the scale reading. If the impact toughness is less than 2.75 kgf·cm/cm^2, the recoil energy is not considered.

United States Standard D 256-72a (Standard Methods of Testing Impact Resistance of Plastics and Electrical Insulation Materials) provides for the following types of tests: method A (Izod), method B (Charpy), method C (Izod method with determination of the additional energy of recoil of the unfastened part of the test specimen), method D (Izod method with determination of the influence that the radius at the tip of the notch has on impact toughness), method E (Izod method using a specimen with notch facing the direction of working motion of the pendulum). Geometric dimensions of specimens:

Izod -- length 63.5 and 60.3 mm;
Charpy -- length 127.0 mm and 124.5 mm; height 12.7 ± 0.15 mm; width 3.17-12.7 mm.

Angle at the tip of the V notch 22.5 ± 0.5°. Notch depth 2.54 mm. Distance between hammer supports 101.6 ± 0.3 mm (95.3 ± 0.3 mm for Izod tests). Round-off radius of hammer supports 3.17 ± 0.12 mm; round-off radius of pendulum knife 3.17 ± 0.12 mm. Vertex angle of knife 43-47°.

In principle, methods A, B, C and D are no different from the test methods provided by GOST State Standards. Method D calls for testing two batches

of specimens with two types of notches (with radii of 1.012 and 0.254 mm at the tip). The test results reduce to computing the quantity that characterizes the influence of notch sharpness:

$$b = E_A - \frac{E_B}{R_2 - R_1},$$

where E_A, E_B are the energies of fracture of the specimens with radii of 1.012 and 0.254 respectively at the notch tip.

Method E is used for specimens with notch radius of 0.25 mm to determine the energy of fracture of a beam, excluding the influence of the notch on crack formation. Here the notch is needed so that compared specimens will have the same stiffness. In tests, the specimen is fastened so that the notch faces the same way as the pendulum.

The Soviet Union has a standard for testing miniature cantilever specimens on a Dinstat machine (GOST 14235-69. Plastics. Method of determining impact toughness on a device of Dinstat type). Dynamic tests are done similarly to the Izod method. In addition to dynamic tests, static tests are done on the Dinstat hammer for bending in accordance with GOST 17036-71, which enables comparison of dynamic and static characteristics of the material as determined on a single device. The Dinstat is a miniature pendulum hammer with energy capacity of 20 kgf·cm and pendulum velocity of 2.2-0.05 m/s. Test specimens are in the shape of notched and unnotched bars. Unnotched specimens: length 15 ± 1 mm, width 10 ± 0.5 mm, thickness 1.5-4.5 mm. A notch 0.8 ± 0.1 mm in width is milled at a distance of 5.5 ± 0.1 mm from the edge of the specimen. The rounding radius of the edges of the notch is 0.1 mm.

Testing of plastics and electrical insulation materials under impact stretching is standardized in the United States (D 1822-68). The need for determining tensile impact toughness is dictated by the fact that some plastics cannot be tested by an impact bending method since they are not broken in testing even when notched. The method according to standard D 1822-68 has a number of disadvantages, and elimination of these shortcomings forces re-examination of a considerable part of the method.

Testing to determine tensile impact toughness consists in breaking the specimen, which is fastened at one end to the pendulum; the other end is fastened to a washer. The pendulum with the specimen is deflected through a certain angle and held by an arresting device. The released pendulum travels through the massive supports of the machine that prevent motion of the washer. Since the pendulum continues to move by inertia, the specimen is stretched. The washer fastened to the specimen is broken away from the supports of the specimen. A formula and table are provided in standard D 1822-68 for determining the recoil energy of the washer, which has a mass determined by the standard. The breaking energy is calculated from the relation

$$X = E - Y + e,$$

where E is the energy calculated from the scale readings of the machine; Y is the energy expended on air resistance and friction (determined in the conventional way from the free oscillations of the pendulum); e is the additional tensile energy due to the recoil of the washer.

The test specimens are in the form of a double blade 63.5 mm long with a working section 3.18 wide (the thickness of the specimen is not standardized). The standard gives three types of specimens including holes for fastening. The disadvantages of the method are: 1) bending of the specimen is unavoidable; 2) recoil of the washer is not recorded (use of high-speed photography for this purpose puts the method into the research laboratory class, and obviates the major requirement of standard methods -- maximum simplicity of doing tests); 3) the work of friction at the points of fastening of the specimen may lead to a considerable error in computation of the breaking energy.

Dimensions and shape of specimens in Charpy tests. The question of the influence that the dimensions of the specimen have on the reliability of Charpy and Izod tests has been the topic of numerous studies. The cross section of standard specimens has not been sufficient to guarantee that a large part of the break is flat. To eliminate containment of deformation, it has been necessary to make side notches, which has been expressed in the draft of a standard for static breaking toughness tests [Ref. 12]. Dynamic tests of glass-reinforced and boron-reinforced plastic specimens in accordance with this draft are described in Ref. 159. The elimination of contained deformation (and implementation of planar deformation) leads to the necessity of testing specimens with considerable dimensions by loading devices with large energy capacity. A change to large beam heights leads to independence of the calculated breaking energy [Ref. 25].

The ASTM plan (1969) gives a specimen for dynamic bending tests by a falling weight. The specimen is a beam 354 mm long and 76 mm high; depth of the V notch is 5 mm. The width of the beam is not standardized. Ref. 106 gives the dimensions of a metal beam designed for dynamic bending (length 406 mm, height 121 mm, width 25.4 mm). The change to outsized specimens has led to development of hammers with considerable energy capacity. Ref. 106 describes a two-pendulum hammer with energy capacity of 280 kg m, and gigantic hammers with energy of 830 kg·m and 110,000 kg·m.

4.6. Oscillographic Methods

While standard impact toughness tests are excellent for qualitative comparison of the energy absorption of different materials, because of inherent disadvantages they do not give exact qualitative [sic] data needed for strength calculations. Therefore over the last decade intensive work has been done on developing methods to eliminate the shortcomings of integral evaluation of breaking energy. These methods amount

essentially to enlargement of standard methods. For example the enlargement of Charpy tests was begun in the late twenties. Subsequently many works have appeared [Ref. 15, 97, 131] that substantiate the use of recording facilities in Charpy tests. The simplest enlargement of the Charpy test is to measure the reaction of one of the supports. The design of a support with piezoelectric sensor for recording reactive forces was discussed earlier (see page 63). Ref. 89 gives a design in which a strain gage is placed on the pendulum of a hammer to measure contact force. Registration of displacement of the cross section of a beam under an external force reduces to measurement of pendulum displacement by a flag and photocell system. Instrumentation of the Charpy method has revealed a number of peculiarities in bending tests of short beams.

The kinetic energy of the specimen is not taken into consideration in conventional calculation of the energy of destruction of standard specimens by the Charpy and Izod methods. Oscillographic registration of the force on the pendulum and its displacement in dynamic bending of a standard specimen enables calculation of the integral value of the energy of deformation and fracture when the work of the mass forces acting on the beam is disregarded. The graph given in Fig. 4.3 shows that a load on the beam, even at a velocity of 1.4 m/s makes it impossible to consider bending quasistatic. Relations for P vs. t were calculated by the method given in section 4.1 for impact of an infinite mass on a beam of variable length. The calculations showed that in bending of short elastic beams conforming to the standard, quasistatic interpretation is invalid. As the length of the beam decreases, the relation between P and t takes a form close to a harmonic function with the frequency of the fundamental mode of beam vibrations.

Existing methods of calculating quasistatic bending specify bending of freely supported beams. The condition of support is disrupted in dynamic loading where the ends of the beams move away from the supports and repeatedly collide with them. Viscosity effects that accompny beam bending lead to the result that the described phenomena (collision of the beam with the pendulum and the supports) become transient processes. If the viscosity effects are sufficiently strong, the condition of quasistatic bending of beams can be expressed in the form generally accepted for quasistatic tests: testing time must be at least an order of magnitude greater than the period of natural oscillations of the beam. The correctness of quasistatic interpretations in bending tests of brittle notched specimens has not been substantiated up to the present due to the complexity of the problem.

Noncorrespondence of the load on the hammer and the support in testing of standard specimens that has been experimentally observed [Ref. 15] is an indication of considerable inertial loads, and consequently considerable accelerations. The latter introduce a slight measurement error if damped oscillations can be noticed on the force versus time

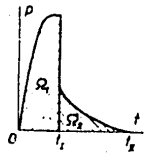

Fig. 4.21. Typical force-time dependence corresponding to quasi-brittle fracture in Charpy tests

oscillogram with period at least an order of magnitude shorter than the testing time. When this requirement is not met (in the case where the quasistatic approach to bending is impossible), a transition must be made to impact velocities lower than the recommended standard.

Force vs. time oscillograms in Charpy tests. The impact toughnesses found from standard tests are frequently identified with the breaking energy. This is incorrect since the balance of recorded impact toughness includes the energy of beam unloading as a consequence of the change in stiffness that accompanies crack propagation, in addition to quantities that can be accounted for in separate experiments (losses of energy to air resistance, the energy of dispersed fragments and so on). Practice in the use of oscillographic registration by the Charpy method has shown that the force-time oscillogram for bending of polymer beams has three types. Fig. 4.21 shows the relation between P and t in quasi-brittle fracture. In the case of brittle fracture, section Ω_2 in Fig. 4.21 is missing. The third type of oscillogram occurs in the absence of a jump in force P versus t (viscous fracture). The discontinuity on the P-t curve is caused by rapid crack propagation, which leads to a considerable reduction in beam stiffness. The oscillogram does not show the oscillations that occur as transient processes at the beginning of regions Ω_1 and Ω_2.

Depending on the test velocity and the viscous properties of the material, the amplitude and frequency of the oscillations associated with the inertia of the beam may be different. Let us consider the case where both transient processes can be disregarded.

Consider an oscillogram of P vs. t in the case of quasi-brittle fracture (see Fig. 4.21). We separate it into two parts as shown in the figure. The shaded (left) part of the oscillogram corresponds to deformation of the beam and onset of fracture; the right part corresponds to final breaking of the beam. The energy corresponding to deformation of the left part of the oscillogram is determined from the law of conservation of momentum [Ref. 89]:

$$A_I = \left[V_0 - \frac{1}{2m} \int_0^{t_I} P(t)\,dt \right] \int_0^{t_I} P(t)\,dt, \qquad (4.36)$$

where V_0 is the initial velocity of impact, m is the mass of the striker, and t_I is the duration of deformation of the section designated by the letter Ω_1 on Fig. 4.21.

The energy corresponding to the further course of the process is

$$A_{II}=\left[V_{II}-\frac{1}{2m}\int_{t_I}^{t_{II}}P(t)\,dt\right]\int_{t_I}^{t_{II}}P(t)\,dt, \tag{4.37}$$

where $V_{II}=V_0-\frac{1}{m}\int_0^{t_{II}}P(t)\,dt$ is the velocity of the hammer pendulum at $t=t_I$.

Denoting $\Omega_I=\int_0^{t_I}P\,dt$; $\Omega_2=\int_0^{t_{II}}P\,dt$, we get

$$A_I=\left(V_0-\frac{\Omega_1}{2m}\right)\Omega_1;\quad A_{II}=\left(V_0-\frac{\Omega_1}{m}-\frac{\Omega_2}{2m}\right)\Omega_2. \tag{4.38}$$

With consideration of the energy A_p of beam unloading when a crack appears, the energy of crack onset $A_э$ and the energy of final fracture $A_д$ are determined from the relation

$$A_э=A_I-A_p;\quad A_д=A_{II}+A_p. \tag{4.39}$$

The sum $A=A_I+A_{II}$ expresses the impact toughness. It has not been possible to single out the energy of formation of the fracture surface.

Specimens with a ready-made crack (e. g. a fatigue crack) have been used to facilitate separation of the impact toughness into components. However, even in this case most polymers show an oscillogram analogous to that of Fig. 4.21, i. e. the crack does not start immediately after the load is applied. Thus it can be concluded that additional studies are needed to get information on advancement of the crack and the change that it produces in stiffness of the specimen. The mentioned methods of registration are utilized in instrumentation of the method of determining energy of destruction by dynamic splitting of beams. Here the crack propagates lengthwise of the beam rather than transversely as is the case in the Charpy test, and therefore measurements associated with crack motion are simplified.

Determining the surface energy of fracture in beam splitting. The impossibility of exact calculation of the energy of destruction according to the oscillogram shown in Fig. 4.21 and obtained in Charpy tests shows up in the lack of experimental data on the change in stiffness of a specimen with the onset and propagation of a crack. Berry [Ref. 8] demonstrated the relation between the surface energy of fracture on the one hand the stiffness (or pliability) of a specimen and the length of a crack on the other. He also worked out a static method of splitting a

cantilever beam in which the crack propagates along the middle surface under the action of the force. The cross section of the beam is reduced to impart a strict direction to the cracking. The upper end of the beam can be immobilized, while the lower end is secured to the drive of a standard testing machine. According to Ref. 8, the energy of destruction is calculated from the relation

$$A_p = -\frac{1}{4} P^2 \frac{\partial l/K}{\partial F}, \qquad (4.40)$$

where F is the cross section of the crack ($F - Wl$, W is the thickness of the specimen, l is the length of the crack), P is the applied force that causes advancement of the crack, K is the stiffness of the specimen.

Ref. 120 proposes a dynamic method for splitting beams loaded by a hydraulic device with constant velocity up to 7.5 m/s. To facilitate calculation of energy in accordance with (4.40) beams of polymethyl methacrylate and polystyrene of the same shape were tested, leading to $\frac{\partial l/K}{\partial F} = \text{const}$. In this case, after the crack starts, P = const.

The shape of the beam was determined as follows. For the cantilever $\frac{1}{K} = \frac{2}{3}\frac{l^3}{EI}$. Disregarding flexure of the unsplit part of the beam, we can assume

$$\frac{\partial l/K}{\partial F} = \frac{2}{3EW}\frac{\partial}{\partial l}\left(\frac{l^3}{I}\right).$$

The condition $\frac{\partial I/K}{\partial F} = \text{const}$ is satisfied by dependence of I on the coordinate l: $I = Wh^3(l)/24$; $h = \alpha l^{2/3}$, where $\alpha = \text{const}$. Then

$$\frac{\partial l/K}{\partial F} = \frac{16}{\alpha^2 EW^2} = \text{const}.$$

For a beam with variable height $h = \alpha l^{2/3}$ force P does not depend on time during crack propagation [Ref. 120].

The dynamic method of splitting beams has advantages over the Charpy method expressed in the capability for testing beams with a shape such that the tested system is stable during displacement of the crack. The main advantage of the method is the capability of calculating energy γ from the equilibrium values of $\frac{\partial I/K}{\partial F}$ and P. Since the quasistatic nature of bending of a specimen with dynamic splitting has not been theoretically validated up to the present, tests under conditions of velocities of clamp displacement exceeding 1-3 m/s cannot be recommended.

The dependence of the surface energy of fracture γ on strain rate and temperature, although now clear in overall features, has as yet not been finally formulated due to lack of experimental material. According to Ref. 120, the energy of destruction increases faster than the modulus of elasticity as temperature decreases. It is shown in Ref. 120 that the surface energy of destruction depends on the velocity of crack propagation $\dot{l}$, and consequently on the strain rate. The relation between γ and $\dot{l}$ for polymethyl methacrylate is due to the nature of the deformation that takes place in the fracture zone. Corresponding to the α-relaxation transition is weak dependence of γ on $\dot{l}$, while the dependence is much stronger for β-transition. Analogous results were found previously in Ref. 130.

Chapter 5

METHODS OF TESTING ANNULAR AND TUBULAR SPECIMENS

The necessity for eliminating stress concentration and the influence of wave processes on measurands in dynamic testing has led to a re-examination of the shape of the test specimen. One of the simplest testing methods in which the influence of waves can be disregarded is the method of testing thin rings. At present developments have already begun on methods of testing rings subjected to uniform stretching and compression.

In testing for the complex-stressed state under static conditions, tube specimens are traditionally used which, thanks to the capability of application of internal pressure, torque and axial force, have also been used in the initial stages of development of dynamic methods.

The purpose of testing tubular specimens is to establish the principles that govern the way that the strength of the material depends on strain rate and the ratio of stress components.

5.1. Testing Thin Rings

The most important advantages that distinguish the method of testing rings from methods of testing rod specimens are as follows: 1) the possibility of disregarding wave processes; 2) minimization of the effect of cut fibers in testing specimens of reinforced plastics; 3) the capability of setting up uniformly distributed pressure, and hence uniformly distributed stress; 4) the load is registered by a device that is not mechanically fastened to the specimen.

The capability of attaining uniform stress distribution in a ring specimen is due to the absence of wave phenomena in testing a thin ring, and uniform transmission of pressure to the specimen, including through an intermediate medium. An appreciable disadvantage of using rod specimens is wave phenomena, as well as nonuniformity of stresses caused by

the concentrations of necking sections necessary for fastening the specimens to clamps. Pressure registration in testing of an annular specimen has an advantage over force measurement in testing rod specimens in that the pressure sensor is not mechanically fastened to the specimen. This is a very important design peculiarity of measurement, enabling an appreciable increase in the natural frequency of the dynamometer. We will use the term quasistatic for tests of ring specimens in which the duration of the external load is at least an order of magnitude longer than the period of the lower mode of oscillations of the ring (with the attached mass of liquid, if it is a medium that transmits pressure to the specimen.

5.1.1. Use of Mechanical Loading Devices, Explosives and Magnetic-Pulse Facilities

The simplest facility for quasistatic tests of rings [Ref. 82] includes a vertical hammer with falling weight and reverser (Fig. 5.1) consisting of a massive steel housing with a plunger that slides in a central channel. The ring specimen is placed between upper and lower plates. Axial compression of the specimen during setup is prevented by a ring stop block that is 0.01 mm higher than the height of the specimen. The working liquid fills the cavity of the specimen and the central channel of the housing. A special orifice is provided for removal of air during deformation of the specimen. A replaceable lead shock absorber protects the reverser housing from damage by taking the excess energy of the weight. When the falling weight strikes the plunger, a hydraulic pressure wave stretches the specimen. The liquid pressure is recorded by a hollow cylinder with strain gages; the deformation of the specimen is recorded by a strain gage. The stress was calculated from the relation $\sigma = PR/\delta$, where R and δ are the radius and thickness of the ring.

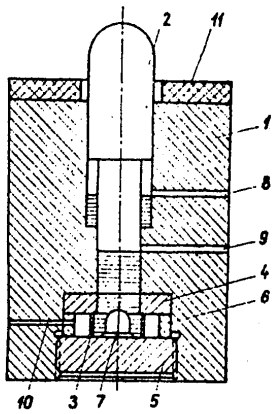

Fig. 5.1. Facility for quasistatic stretching of rings [Ref. 82]: 1--steel housing; 2--plunger; 3--specimen; 4--set collar; 5--stopper; 6--spacer; 7--dynamometer; 8-10--channels for removal of air; 11--shock absorber

Tests of rigid high-strength ring specimens require drives for transmitting more energy to the specimen. Use of the method described above is limited to impact velocities such that the process of ring stretching can be considered actually quasistatic, and therefore the use of the formula $\sigma = PR/\delta$ must be validated, and tests of the rings must be limited to velocities of 20 s^{-1}. The need for evaluating the inertial forces in testing a ring by hydraulic impact obviates quasistatic formulation of the problem and necessitates the dynamic method.

Use of explosives for dynamic testing. Dynamic tests of rings were first described in 1939 [Ref. 137]. A ring specimen without tension is placed over a thin-walled steel cylinder in which an explosive is detonated. The ring, receiving the acceleration, is displaced axisymmetrically with respect to inertia. Radial displacements of the ring were recorded by high-speed photography. The stress was calculated by double differentiation of the experimental curve. In doing this, it was assumed that the ring is stretched only by inertial forces. In Ref. 158 a description is given of a repeat of this same experiment. The strain rates found in the experiments range in limits of $10^3 \leqslant \dot{\varepsilon} \leqslant 10^4$ s^{-1}. Analogous experiments on stretching of rings at $100 < \dot{\varepsilon} \leqslant 2000$ s^{-1} are described in Ref. 90.

Among the disadvantages of the method are the impossibility of evaluating the nonuniformity of pressure on the ring, the low accuracy of determining displacements and considerable errors caused by double differentiation in stress calculation, and absence of data on the initiating pulse.

Use of magnetic-pulse facilities. Single-turn inductors are used for loading rings with magnetic-pulse facilities. This method can be used to transmit considerable energy to the inner (stretching) and outer (compression) surfaces of the ring. The method of testing rings by a single-turn inductor is described in Ref. 101, 105, 170. A diagram of the experiment of Ref. 101 is shown in Fig. 5.2. The device for stretching the polymer rings consists of a split ring (inductor) with leads made of a copper strip 10 mm wide and up to 5 mm thick. A one-piece ring is placed over the inductor. In testing polymer materials, the ring is called a "satellite." The specimen is placed on the "satellite" without tension. A variant is possible in which the stiffness of the tested polymer material in the radial direction of the ring is an order of magnitude greater than that of the "satellite," which may be made for example of thin foil. The "satellite" may be cemented to the inside of the ring. The method of compression testing rings [Ref. 101, 105] differs from that described only in the placement of the specimen relative to the inductor. Pulse current from the magnetic-pulse facility is fed to the inductor ring. The current I_1 induced in the "satellite" flows in the direction opposite to that of current I_2. These currents lead to development of electromagnetic pressure

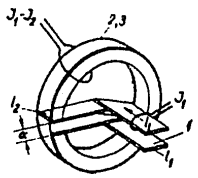

Fig. 5.2.
Diagram of testing of polymer rings by the action of electrodynamic forces [Ref. 101]: 1--inductor; 2--"satellite"; 3--specimen

$$p = \mu \frac{I_1 I_2}{2b^2}, \tag{5.1}$$

where μ is the permeability of the ambient medium, b is the width of the ring.

In the experiments of Ref. 101, 105, recordings were made of the current I_1 and the difference $I_1 - I_2$. This difference depends on the gap between the satellite and inductor. When the specimen is placed without tension, this quantity may amount to 10% of I_1. Current I_1 can be measured by a shunt, but the current difference $I_1 - I_2$ can be recorded only by a Rogowski loop.

Oscillograms of deformations of the ring in tests with the magnetic-pulse facility are complicated by pickups that distort the oscillograms for as long as pickups continue to exist. Ref. 101, 105 give oscillograms obtained by strain gages cemented to the ring in the peripheral direction. The recordings were made for times exceeding the time of cpapcitor discharge (20 μs).

The disadvantages of the method are as follows: 1) because of design features, the inductor is a split ring, and therefore the load acting on the test ring is distributed nonuniformly; there is no load on the gap of the ring; 2) the applicability of formula (5.1) is limited to fairly small displacements; 3) in the case of intense discharge the magnetic field induces an electric current in the strain gage wire that is recorded by an oscilloscope; as a result of interaction of magnetic fields, the strain gage may be subjected to considerable mechanical stresses that may either destroy it or strain it beyond the yield point; 4) necessity of recording signals of I_1 and $I_1 - I_2$ to calculate pressure.

A commom disadvantage of the methods described in this section is the impossibility of correct determination of stresses for plotting stress-strain diagrams.

5.1.2. Loading by Electric Discharge in a Liquid

The advantages of testing rings by the electrohydraulic effect as compared with the method described above based on using explosives and single-turn inductors are associated with the capability of making adequately correct recordings while totally eliminating interference caused by capacitor discharge. The advantage that the magnetic-pulse facility has over a hammer with a falling weight as a drive for a testing machine is the capability of transmitting more energy to the test specimen, doing tests over a wider range of strain rates, and also the capability of widely varying the duration of the loading pulse.

The facility for quasi-static and dynamic tests (Fig. 5.3) consists of a discharge chamber held in the stand of the magnetic-pulse facility, a waveguide, an upper plate, and fastening bolts. The specimen is placed between the waveguide and the plate. The waveguide is a pipe with one end threaded into the discharge chamber. The other end of the pipe is

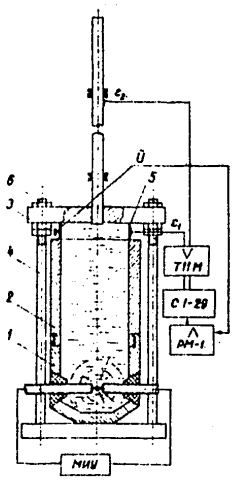

Fig. 5.3. Diagram of a facility for stretching rings: 1--discharge chamber; 2--tubular waveguide; 3--plate; 4--pins; 5--specimen; 6--nuts; Ü--accelerometer; ε_1--radial deformation of the specimen; ε_2--longitudinal deformation of waveguide rod; МИУ--magnetic-pulse facility

polished to reduce friction with movement of the specimen. When placing the specimen between the plate and the waveguide, a special feeler gage sets a clearance of at least 0.01 mm that is fixed by nuts.

Measurements made during tests included: 1) current strength in the capacitor discharge circuit of the magnetic-pulse unit; 2) liquid pressure; 3) peripheral deformation of the specimen; 4) radial acceleration of the specimen.

Measurement of current strength by a Rogowski loop is done to check the reproducibility of the experiments. After a certain number of experiments (30-40) the breakdown gap between electrodes increases, the electrode surface corrodes, causing a change in the shape of the registered curve of I vs. t as compared with the initial shape. When there is a noticeable change in the shape of the curve, the electrodes are replaced by new ones for purposes of reproducibility of the experiments.

Pressure registration is done by a waveguide rod with lower end touching the liquid. The rod is vertically fastened in Teflon bearings. It is established by preliminary experiments that the optimum waveguide for reliable measurements is a duralumin rod 20 mm in diameter and 500 mm long. Measurement of pressure in the liquid by the rod reduces to measurement of deformations by strain gages cemented in the middle of the rod. To eliminate the influence of flexural modes, the sensors are connected in a differential circuit. Signals from the strain gages go through an amplifier to the input of an oscilloscope. By selecting the length of the waveguide, a time delay was obtained sufficient for getting oscillograms undistorted by pickups caused by capacitor discharge. The time delay to the beginning of recordings was enough for the oscilloscope beam to settle to a stable zero line. Deformation of the ring in the peripheral direction was measured by a strain gage with a base of 5 mm.

Calculation of peripheral stress in the ring with dynamic stretching. Considering loading of a ring according to the arrangement shown in Fig. 5.3, let us pose the problem of deriving an equation of equilibrium of a ring with attached mass of liquid. The Hamilton principle is used:

$$\dot{K}+\dot{\Pi}=Q\dot{U}, \tag{5.?}$$

where $\dot{K}$ is the kinetic energy of the system, Q, $\dot{U}$ are generalized force and velocity, $\dot{\Pi}=\int_{\Omega}\sigma\dot{e}d\Omega$ is the power of the energy of deformation in volume Ω.

Taking the liquid as incompressible, it is assumed that the value of $\dot{\Pi}$ depends on the energy of simple stretching of the ring:

$$\dot{\Pi}=2\sigma(t)\frac{\dot{U}_{\text{к}}(t)}{R}\pi R\delta h, \tag{5.3}$$

where σ is the peripheral stress of a ring of radius R, thickness δ, and height h; $\frac{\dot{U}_{\text{К}}(t)}{R}$ is the peripheral deformation of the ring; $\dot{U}_{\text{К}}$ is the reduced velocity.

For the product $Q\dot{U}$ we have

$$Q\dot{U}=2\pi Rhp(t)\dot{U}_{\text{к}}(t); \tag{5.4}$$

p(t) is pressure in the liquid. The kinetic energy of the system K consists of the energies of the ring $K_{\text{К}}$ and the attached liquid $K_{\text{Ж}}$. The kinetic energy of the ring is

$$K_{\text{к}}=\rho_{\text{к}}\pi Rh\delta\dot{U}_{\text{к}}^2(t); \tag{5.5}$$

$\rho_{\text{К}}$ is the density of the ring material. To calculate $K_{\text{Ж}}$, we assume that the attached mass of liquid is included in volume πR^2h. We will consider the case where the height of the ring h is fairly small compared with a pressure wavelength, i. e. $h<c_0t^*$, where c_0 is the velocity of propagation of longitudinal hydraulic waves, t^* is the duration of a pressure pulse. In the following it is convenient to use a cylindrical coordinate system r, θ, z (coordinate origin -- the center of the upper face of the specimen). Let us assume that for z>>h the solution of the problem of hydraulic impact has the form

$$p(t)=-\rho c_0\dot{U}_z, \tag{5.6}$$

where p, $\dot{U}_z$ are the pressure and longitudinal velocity in the liquid, ρ_0, c_0 are the density of the liquid and the velocity of propagation of longitudinal waves in the liquid. At z = 0, the pressure in the hydraulic wave is doubled, and velocity $\dot{U}_z=0$. With distance from the end face (z = 0), the velocity $\dot{U}_z$ is determined by the difference between the direct and reflected waves:

$$\dot{U}_z=\frac{1}{\rho_0c_0}\left[p(t)-p\left(t-\frac{z}{c_0}\right)\right]. \tag{5.7}$$

Assuming that the hydraulic wave is not distorted during reflection, we can set for small z

$$\dot{U}_z = -f(t)\,z, \tag{5.8}$$

since pressure is independent of the coordinate r. For large values of z ($z > h$), $\dot{U}_z$ is determined by superposing the direct and reflected waves (5.7). The unknown function f(t) is determined from the condition of incompressibility of the liquid:

$$\frac{\dot{U}_r}{r} + \frac{\partial \dot{U}_r}{\partial r} = -\frac{\partial \dot{U}_z}{\partial z}, \tag{5.9}$$

where $\dot{U}_r$ is the radial velocity of the liquid. Since the second member of (5.9) is independent of r, and the first member is independent of z,

$$\frac{\dot{U}_r}{r} + \frac{\partial \dot{U}_r}{\partial r} = f(t); \quad \frac{\partial \dot{U}_z}{\partial z} = -f(t). \tag{5.10}$$

The unknown f(t) is determined from the conditions of continuity of the velocity on the interface between the liquid and the test ring, i. e. at $r = R$; $\dot{U}_R(t) = \dot{U}_K(t)$. Hence $f(t) = \frac{2\dot{U}_K(t)}{R}$, and

$$\dot{U}_r = \frac{r}{R}\,\dot{U}_к(t); \quad \dot{U}_z = \frac{2z\dot{U}_к(t)}{R}. \tag{5.11}$$

Considering the kinetic energy of an annular element of the liquid with coordinates z, r, thickness dr and height dz, we have

$$dK_ж = \pi\rho_0(\dot{U}_r^2 + \dot{U}_z^2)\,dz\,dr. \tag{5.12}$$

With consideration of (5.11), and after integration with respect to r and z, we get

$$K_ж = \dot{U}_к^2(t)\frac{\pi}{4}\rho_0 R^2 h\left(1 + \frac{3}{8}\,\frac{h^2}{R^2}\right); \tag{5.13}$$

$$K = 2\dot{U}_к(t)\,\dot{U}_к(t)\rho_к \pi R h\delta\left[1 + \frac{\rho_0}{4\rho_к}\,\frac{R}{\delta}\left(1 + \frac{8}{3}\,\frac{h^2}{R^2}\right)\right]. \tag{5.14}$$

With consideration of (5.3), (5.4) and (5.14), the Hamilton equation takes the form

$$2\sigma(t)\,\dot{U}_к(t)\,\pi\delta h + 2\dot{U}_к(t)\,\dot{U}_к(t)\,\frac{\rho_к}{\alpha^2}\pi R h\delta = 2\pi R h p(t)\,\dot{U}_к(t). \tag{5.15}$$

Expression (5.15) reduces the the following equation:

$$\sigma(t) = \frac{p(t)R}{\delta} - \ddot{U}_{\text{ж}}(t)\frac{\rho_{\text{ж}}R}{\alpha^2}, \tag{5.16}$$

where

$$\alpha^2 = \left[1 + \frac{\rho_0}{4\rho_{\text{ж}}}\frac{R}{\delta}\left(1 + \frac{8}{3}\frac{h^2}{R^2}\right)\right]^{-1} \tag{5.17}$$

Let us rewrite (5.16) in the form

$$\sigma = \frac{p(t)R}{\delta} - \ddot{U}_{\text{ж}}(t)\frac{E_{\text{к}}}{\omega_*^2 R}, \tag{5.18}$$

where E_K is the modulus of elasticity of the ring material; $\omega_0 = c_K/R$; $\omega_* = \alpha\omega_0$ are respectively the frequencies of the free oscillations of the ring in a void and in the liquid.

Let us note that when $\ddot{U} = 0$ (5.17) coincides with the known relation for statics. Accounting for the inertia of the ring without the attached mass of the liquid leads to $\alpha = 1$; accounting for the radial inertia of the liquid gives $\alpha^2 = \left[1 + \frac{\rho_0}{4\rho_{\text{ж}}}\frac{R}{\delta}\right]^{-1}$. Accounting for axial acceleration of the liquid leads to an increase in the value of α^{-2} by

$$\frac{2}{3}\frac{\rho_0}{\rho_{\text{ж}}}\frac{R}{\delta}\frac{h^2}{R^2}.$$

To calculate peripheral stress in the ring in accordance with (5.18), the experimental measurements of pressure p(t) must be supplemented by experimental data on acceleration of the ring. The coefficient σ according to (5.17) depends on the geometric dimensions of the ring. Since simplifying assumptions have been used in deriving the expression for α, formula (5.17) must be experimentally validated.

Registration of accelerations. Radial acceleration of the ring was measured by a sensor consisting of a light aluminum frame into which a quartz pellet was pressed, and two inertial masses. The sensor was cemented to the ring. The mass of the sensor did not exceed 2 g. The natural frequency of the sensor is about 100 kHz. The PM-1 amplifier produced in East Germany was used to record the signals from the sensor. The acceleration sensor was made as light as possible since considerable accelerations (up to $1\text{-}2\cdot10^4$ g) caused a force q distributed over the supporting surface of the sensor ($S = 1$ cm^2). This load does not cause noticeable asymmetric forms of deformations of the ring since in our experiments

$$q = \frac{2\cdot10^{-3}(1\text{-}2)\cdot10^3 g}{g} = 20\text{-}40 \ [\text{kg/cm}^2]$$

is an order of magnitude less than the pressure of the liquid. Measurements of peripheral deformations of the ring by strain gages placed in different sections of the specimen showed differences of no more than 2-3%, which is evidence of symmetric loading of the ring.

Processing of the experimental results included plotting of experimental curves in coordinates of $\frac{pR}{\delta}$ vs. t and $\frac{E_K\ddot{U}_K}{\omega_*^2 R}$ vs. t (Fig. 5.4, b) and ε vs. t (Fig. 5.4, a). According to (5.15), stress σ is determined by the difference $\frac{pR}{\delta} - \frac{E_K\ddot{U}_K}{\omega_*^2 R}$ (vertical shading on Fig. 5.4, b). The diagrams of stress versus strain (Fig. 5.4,c) were plotted by eliminating time from relations of σ vs. t and ε vs. t. Specimens of glass-textolite (ASTT glass cloth, EDT resin -- 50%) and of epoxy resin were tested.

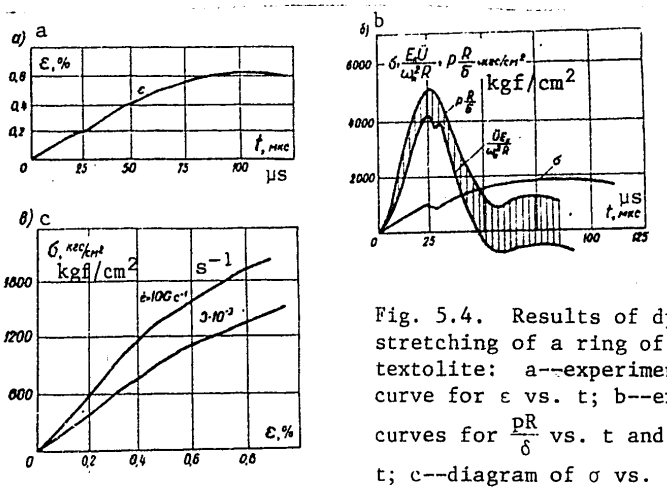

Fig. 5.4. Results of dynamic stretching of a ring of glass-textolite: a--experimental curve for ε vs. t; b--experimental curves for $\frac{pR}{\delta}$ vs. t and $\frac{E\ddot{U}}{\omega_*^2 R}$ vs. t; c--diagram of σ vs. ε

Relative reliabilities of plotted diagrams for stress versus strain. In conclusion let us give the results of additional experiments that validate the proposed method of testing ring specimens. Fig. 5.5 shows stress-strain diagrams for epoxy resin obtained by the method of stretching rings and by using the tensile variant of the HSB method. The advantage of this method shows up at high strain rates where the wave process in the specimen used in the HSB method obviates the use of classical relations for calculating σ and ε.

To validate the coefficient α in accordance with (5.17) a series of supplementary experiments was done, consisting in calculation of the frequency of natural oscillations of the ring and the liquid according to the scheme shown in Fig. 5.4 [sic]. Explosion of a wire in a liquid set up a short-term intense pressure pulse, after which the ring was set into free damped oscillation registered by strain gage ε. As a result of

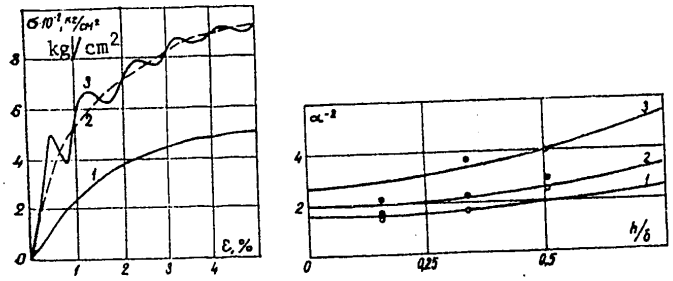

Fig. 5.5. Stress-strain diagrams for epoxy resin at $\dot{\varepsilon}$, s^{-1} of: 1--10^{-3}, 2, 3--300 (2--tests in accordance with the diagram of Fig. 5.3; 3-- the same according to Fig. 3.4, b)

Fig. 5.6. Curve for α^{-2} as a function of h/R for ratios δ/R of: 1--0.21, 2--0.14, 3--0.07

testing specimens with different geometric dimensions, graphs were plotted (Fig. 5.6) that validate the use of (5.17).

Quasistatic testing of rings on the facility shown in Fig. 5.3 is done by exploding a wire in a liquid. The recording procedure does not differ from that described. Just as in dynamic tests, the accelerations of the ring must be recorded, which in the given case is done to make sure that the experiments are really quasistatic, and that inertial forces are negligible. Without such a check, the test results could be doubtful.

5.2. Tests for the Complex-Stressed State

In addition to the difficulties inherent in uniaxial tests, tests in the complex-stressed state are accompanied by additional difficulties due to synchronization of specimen loading by the components of the load. This difficulty is purely technical, and in many cases can be overcome. Another barrier in the complex-stressed state is the necessity for validating the limits of applicability of quasistatic approaches to deformation as a consequence of the necessity for using the solution of the problem of propagation of combined waves. Despite the fact that the latter difficulty is irremovable, we give here a number of techniques for tests in the complex-stressed state as first steps in solution of the problem.

5.2.1. Use of Mechanical Loading Devices

One of the first works on dynamic tests under conditions of the plane stressed state was published in 1957 [Ref. 129]. An investigation was made of deformation and destruction of circular diaphragms in a shock tube under conditions of uniform bilateral stretching. The strain rate was up to about 10 s^{-1}. The next paper [Ref. 133] was published in 1966,

dealing with investigation of the plane stressed state $\sigma_2/\sigma_1 = 0.455$. Experiments were done on thin-walled tubular specimens with strain rates of $\dot{\varepsilon} = 2$, 19 and 35 s^{-1}. The tubular specimen was loaded by liquid pressure with impact against a piston. The stresses in the wall of the specimen were determined from the pressure measured in the liquid. The ratio of axial to tangential stress in all experiments was constant, i. e. the study was done on only one kind of plane stressed state at three strain rates.

More extensive studies of the influence that the kind of stressed state has on the mechanical properties under impact were done in Ref. 146. The authors designed and made a pneumatic device that enabled loading of a thin-walled tubular specimen with an axial pulse force and a torque with different ratios between them. The strain rates in the tests were quantities ensuring destruction of the specimen within $(40\text{-}100)\cdot10^{-3}$ s, which corresponded to a longitudinal relative strain rate of $\dot{\varepsilon} = 1\text{-}1.5$ s^{-1}. The form of the stressed state in the elements of the wall of the specimen was varied from simple stretching to pure shear with 4-5 intermediate forms of stressed state.

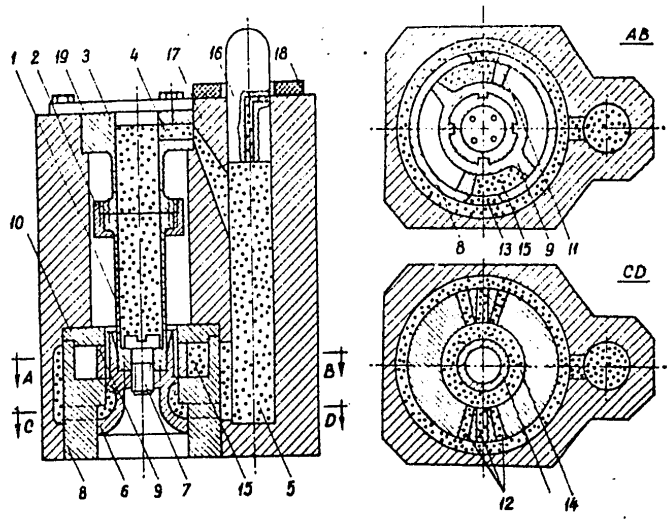

Fig. 5.7. Quasistatic testing facility for the complex-stressed state [Ref. 83]. See text for explanation.

A description is given in Ref. 82, 83 of a device (Fig. 5.7) based on a design proposed in Ref. 146 (distinguished by the capability of producing hydraulic pressure inside a tubular specimen). The facility for quasistatic tests of materials that is shown in Fig. 5.7 enables loading

of a thin-walled tubular specimen with internal fluid pressure, axial force and torque in different proportions. A vertical hammer with a falling weight was used to create hydraulic pressure. The thin-walled tubular specimen was fastened by a locknut at the upper end to an elastic dynamometer with a channel through the thickened part connecting the hydraulic cylinder to the dynamometer cavity. A stepped piston connected by a screw to the lower end of the specimen can move reciprocally and rotationally in the cylinder. Annular grooves that act as a labyrinth seal are cut into the outer surfaces of the piston. A vaned wheel in a recess of the cylinder is splined to the piston. The working fluid was compressed by a plunger with maximum travel selected so that the volume of liquid displaced is sufficient to strain the specimen to the breaking point.

The pressure of the working fluid is transmitted through apertures to the piston and the vaned wheel. The pressure taken by the piston sets up an axial force with magnitude and direction that depend on the ratio between the lower and upper diameters of the piston. The pressure in the cavities between the vanes of the wheel and the stationary set edges of the cylinder cover sets up a torque with magnitude determined by the height of the vaned wheel. Thus the piston, being splined to the vaned wheel transmits an axial force and a torque to the specimen. Pins are used in the connections between the specimen and the piston and between the specimen and dynamometer to prevent mutual rotations. The pressure of the liquid transmitted through the channel and dynamometer to the inner cavity of the specimen sets up longitudinal and tangential tensile stresses there.

As a result of the application of force factors, the wall of the specimen is subjected to bilateral stretching and shear. The relations between stresses may be varied over a wide range by using a set of interchangeable parts of different dimensions. To get the simplest kinds of stressed state, the channel and the apertures in the cylinder are made to overlap. The action of internal pressure on the specimen is eliminated when the channel is covered, which is achieved by rotating the dynamometer through a certain angle. The apertures must be stopped to prevent the action of axial force or torque. Thus the reverser can be used to test materials at stresses ranging from uniform biaxial stretching to pure shear, and the direction of the principal stress vectors can occupy any position in the plane tangential to the surface of the specimen, which is especially important for testing anisotropic materials. It should be noted that obtaining each kind of stressed state involves making interchangeable parts; however, for studying the influence that the form of stressed state has on the mechanical properties of materials, it is quite sufficient to do tests where the ratio of the principal stresses changes in steps. For example, if eight interchangeable pairs of pistons and cylinders, and four pairs of vaned wheels and cylinder covers are available, tests can be done with 52 forms of plane stressed state. For isotropic materials it is sufficient to do tests in the first

nine forms of stressed state, which can be done with five pairs of pistons and cylinders, and three pairs of vaned wheels and cylinder covers.

Measurements of forces and deformations. In Ref. 83, forces were measured from the deformation of an elastic steel dynamometer by resistance strain gages. Strain gages with base of 5 mm and resistance of 100 ohms were cemented to the outside of the dynamometer. Deformation of the specimen was measured by resistance strain gages with base of 20 mm and resistance of 100 ohms cemented to the outside of the specimen in the direction of the principal stresses. In cases where the specimen was subjected to torque, deformation was measured by strain gages. Since the described device is based on transmission of forces through a liquid, and since accelerations were not recorded, quasistatic treatment of the results of the experiments has not been proved. The described technique can be used at strain rates of no more than 5-10 s^{-1}.

5.2.2. Use of the Magnetic-Pulse Facility

An installation for testing in the biaxial stressed state using the electrodynamic forces generated by a magnetic-pulse facility was first described in Ref. 156. When the capacitors are discharged, the magnetic-pulse facility induces a strong magnetic field in the primary coil. Since this field changes rapidly in time, it produces eddy currents in nearby conductors. Located close to one of the ends of the primary coil is a secondary coil placed in an aluminum disk that is coaxially coupled to the moving clamp of the device. The principle of a unipolar electric machine was used to produce torque in Ref. 156. The secondary coil was designed in such a way that the discharge current passing through it flowed from the center toward the periphery along radii. Interaction of the magnetic fields of the primary and secondary coils produces forces of repulsion and torque. By adjusting the current flowing in the secondary coil, it is possible to get different ratios between σ and τ. The force F_z of repulsion of the coils that stretches the specimen depends on the axial component of the vector B of magnetic field induction [Ref. 156]:

$$F_z = \text{const} \frac{\partial B_z}{\partial z} \cdot \frac{\partial B_t}{\partial t},$$

and the torque acting on the specimen is

$$M = \text{const}\, B_z \frac{\partial B_z}{\partial t}.$$

For the greatest effect in tests, the inductance of the primary coil should be equal to the inductance of the discharge circuit of the magnetic-pulse facility.

In short-term dynamic biaxial loading of the specimen, tests are complicated by the necessity of synchronizing the action of the axial load with

torque. In Ref. 156 this synchronization was effected by setting up conditions on the clamp of the facility such that the dilatational-compression wave traveled a greater distance to the working cross section of the specimen than the torsional wave. Synchronization was adjusted by selecting the width of the hub of the moving clamp. To do tests in a pure wave (to avoid reflection of the waves from the clamps) the length of the specimen is calculated in accordance with loading duration. Four time-dependent parameters were measured: axial force, torque, strain and angle of twist of the specimen. All measurements were made photoelectrically.

Biaxial variant of the Hopkinson bar. Testing of a tubular specimen for the combined action of synchronous compression and torque by the HSB method was first described in Ref. 67, 157. In the device described in Ref. 67, the tubular specimen was placed between two loading rods. Torsional and compressional waves propagating along the rods from opposite directions reach the specimen nearly simultaneously, within a time of a few microseconds. For the biaxial bar, longitudinal compression was produced by a pneumatic facility, and twisting was produced by the release of stored torque. The torque in the accumulator rod was maintained by a cemented flange joint containing a thin metal foil that was exploded by discharging capacitors. Simultaneous arrival of a longitudinal compressional wave and a torsional wave was accomplished by triggering the torsional wave at the instant of onset of the compressional wave. The dimensions of the accumulator rod and the pressure transmitter were matched so that the torsional and compressional waves, propagating at different velocities in these rods, reached the specimen at the same time. Deformation of the specimen was measured by strain gages directly on the specimen.

Biaxial tests enabled determination of torsional and compressional strain, and also the transmitted torque and the force of compression. Typical oscillograms for Q-t, M-t, γ-t and ε-t are shown in Fig. 5.8. Deformation of the specimen was measured by a single axial strain gage. The stresses of the specimens were calculated by a standard technique of data processing for a unit with Hopkinson bar.

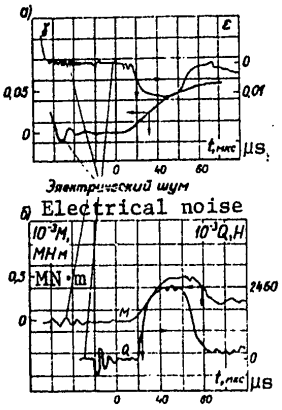

Fig. 5.8. Typical oscillograms obtained in testing a tubular specimen by a biaxial HSB [Ref. 67]: a-- γ vs. t and ε vs t; b--Q vs. t and M vs. t

* * *

The Hopkinson split bar (HSB) method is based on a very simple technique for transmitting forces to a specimen, and therefore there are no particular difficulties in precise mathematical formulation of dynamic loading of the system,

which is a considerable advantage of the method. The problem of wave propagation in the split bar (including the specimen) must be solved to validate experimental results and find the reasonable limits of applicability of the method. At mean strain rates that go beyond the limits of applicability, the inadmissability of using classical relations for calculating stresses and strains in the specimen is due to slow waves associated with nonlinearity of the stress-strain diagram. At these strain rates it is necessary to account for the influence of inertia of radial motions. Such a procedure will enable finding optimum relations for the geometric dimensions of the test specimens.

Use of the HSB method for studying the mechanical properties of polymers involves difficulties in plotting stress-strain diagrams due to the uncertainty of the time of arrival of the function σ^T at the cross section of the anvil rod where the recording is made. For precise determination of the time of arrival of pulse σ^T the method is supplemented by measuring acceleration of the free end of the anvil rod. The time of arrival of signal σ^T is fairly precisely determined by comparing the function σ^T and its first time derivative. Direct measurement of deformations on the specimen permits experimental validation of the quasistatic interpretation of straining of the specimen. Tests of nonlinear materials by the HSB method must be supplemented by direct measurement of deformations.

At the present time, transverse dynamic bending of beams is one of the most correct methods of studying the resistance of reinforced materials to interlaminar shear. The selected model of beam motion and quasistatic treatment of an experiment are validated by studying transverse impact. Transverse bending when beams are loaded by distributed intense loads has an advantage over transverse impact by a massive body in that there are no localized strains. Local deformations at the contact zone of an impacting body and a beam have a considerable effect on all functions that characterize bending. The repeated collisions between a beam and impacting body with mass ratio $m/M > 1$ observed by Timoshenko have been experimentally confirmed. Accounting for wave propagation in an impacting body in the form of a long rod leads to some possible collisions that depend on the length of the rod and the corresponding frequencies of the beam. Inertia of the specimen, repeated collisions, local deformations are an incomplete list of the effects that are an impediment to the quasistatic experiment on beam bending, including that specified by a standard.

Evaluation of the inclination of materials to brittle fracture from the energy expended on destruction is done in accordance with standard test methods. The data of standard tests are used for comparative characteristics of the properties of polymer materials. Standard methods based on the simplest loading method and uncomplicated measurements are carried out under the conditions of plant laboratories. Theoretical substantiation of standard tests leads to the necessity of changing the geometric shape and dimensions of the specimen, and accounting for inertial forces. To get quantitative data that are used as the basis of strength

calculations, the instrumentation of standard tests is inadequate. Development has begun on dynamic methods of the mechanics of destruction. Tests on dynamic splitting of beams are the most promising thanks to the capability of precise recordings needed for experimental determination of the surface fracture energy.

The advantage of using annular specimens is the capability of disregarding wave effects when a ring is loaded by uniformly distributed pressure. When pressure is transmitted to the ring through an intermediate medium, it is necessary to consider the inertia of the ring and the inertia of the attached mass of liquid. Acceleration measurements are necessary for quantitative determination of the inertial force. The previously considered method of testing rings by the electrohydraulic effect can be recommended for studying reinforced polymer materials in connection with the fact that using specimens of a different shape leads to concentration of stresses and weakening of the carrying capacity of the specimen when filaments are cut.

Methods of testing materials in the complex-stressed state are just beginning to be developed. Correct theoretical validation of these methods is difficult due to a lack of developed theories of propagation of combined waves, including in nonlinear media. The most promising direction in development of testing methods in the complex-stressed state is the search for appropriate versions of the Hopkinson split-bar method.

PART III
GENERALIZING THE RESULTS OF DYNAMIC TESTS OF RIGID POLYMERS

The material of this division reflects the results of tests of polymer materials at different strain rates. The reference material of the book includes data on the influence of strain rates on the mechanical properties of amorphous and crystalline polymers, as well as reinforced materials. In some cases the results of tests have been systematized and are presented in the form of rigorous patterns of mechanical behavior. This applies primarily to dependence of the elastic modulus and limiting stresses (E, σ_s) on strain rate.

The description of mechanical behavior of polymers is based on models that are in turn based on the results of tests with wide variation of $\dot{\varepsilon}$. It is suggested that an investigation of wave propagation be invoked to verify and validate the reliability of the model. A model that has passed such a test can be recommended as a starting point for calculating polymer components that work under conditions of dynamic loads.

Mechanical tests of polymers cannot be considered complete without studying the influence of temperature, since for most of the materials studied

inelasticity is not exhausted in the attainable range of $\dot{\varepsilon}$. The experimental results found in a wide range of variation of T and $\dot{\varepsilon}$ lead to the possibility of finding generalizing patterns in the temperature-time dependence of mechanical behavior of materials that are deformed in time.

Chapter 6

INFLUENCE OF STRAIN RATE ON THE MECHANICAL PROPERTIES OF POLYMER MATERIALS

This chapter examines the results of an investigation of the mechanical properties of polymers over a wide range of strain rates. The mechanical properties of these materials are fairly completely reflected by stress-strain diagrams plotted over a wide range of strain rates and temperatures. The stress-strain diagrams are the basis for constructing dependences of mechanical characteristics on $\lg\dot{\varepsilon}$ and T. The patterns of mechanical behavior of polymers considered below show appreciable dependence of all mechanical characteristics of polymers on strain rate.

6.1. Amorphous Polymers

Depending on temperature, amorphous polymers may be in the viscofluid, viscoelastic or vitreous state. The point of transition of a polymer to a given state can be determined from the way that the damping constant or the tangent of the angle of phase shift ($\mathrm{tg}\delta$) depends on temperature at a fixed frequency of harmonic waveforms.

The mechanical behavior of amorphous polymers is determined by testing conditions, i. e. by one of the relaxation processes termed α and β. The principal relaxation process (α-transition) is related to segmental mobility of polymers [Ref. 10, 27]; the secondary transition of vitreous polymers (β-transition) is attributable to local mobility in polymers, i. e. to the motion of side groups and small segments of the principal chain [Ref. 2, 27, 99, 134, 148].

Shifting of the curve of the elastic modulus as a function of strain rate (E-$\lg\dot{\varepsilon}$) takes place as the temperature changes without distortion of the curve. Thus the Williams-Landel-Furry (WLF) formula can be used to plot a generalized curve in coordinates of E vs. $\lg a_T\dot{\varepsilon}$. The coefficient a_T is given the meaning of the ratio of characteristic relaxation times of the chain of the macromolecules at temperatures of T and T_0, where T_0 is the reference temperature. At low stresses, these relaxation times are assumed to conform to the relation [Ref. 2, 87, 99]

$$a_T = \frac{\tau_T}{\tau_{T_0}} = e^{\frac{U_0}{RT}}, \qquad (6.1)$$

where U_0 is a constant of the material (it is assumed that U_0 is the activation energy of the relaxation process); R and T are Boltzmann's constant and absolute temperature respectively.

The empirical WLF formula is written in the form [Ref. 99]

$$\lg a_T = \frac{C_1 T - T_0}{C_2 + T - T_0}, \tag{6.2}$$

where C_1 and C_2 are constants. The glass point T_g is frequently taken as T_0. The validity of temperature-velocity superposition must be checked by the requirement of constancy of U throughout the investigated region. A single relaxation process corresponds to the value of U = const. In this case, (6.1) implies

$$\frac{R d \lg a_T}{d \frac{1}{T}} = U = \text{const.} \tag{6.3}$$

The mechanical behavior of most polymers at limited stresses is in the most complete accord with temperature-time superposition. For high stresses formula (6.1) becomes inapplicable. A refinement is the relation [Ref. 2, 87]

$$\frac{\tau_T}{\tau_{T_a}} = e^{\frac{U_0 - \gamma\sigma}{RT}}. \tag{6.4}$$

The limiting stress σ_s is used instead of the instantaneous value of σ, and (6.4) in this case is rewritten as

$$a_T' = e^{\frac{U_0 - \gamma\sigma_s}{RT}}, \tag{6.5}$$

where U and γ are constants of the material, σ_s is the limit of forced elasticity of the material (this characteristic is called the yield stress in non-Soviet literature).

Two methods have been suggested for determining the σ_s of polymers. The first is based on finding σ_s as the point of intersection of straight lines that approximate the stress-strain diagram. According to the second method the value of σ is determined from the intersection of the stress-strain diagram with a straight line parallel to the initial slope of the diagram and starting from the point $\varepsilon = 2\%$. Both methods of determining σ_s give approximately the same numerical results (in what follows we take σ_s to be the characteristic determined by the second method). According to GOST 11262-68 (Plastics. Method of tensile testing), the convenional yield is the stress calculated from the ratio of the load to the initial cross section of the specimen. The load must correspond to the point of intersection of the curve on the load-elongation graph with a straight line drawn parallel to the initial straight segment of the curve that cuts off a certain elongation on the strain axis.

Experimental data are examined below on the mechanical behavior of a number of amorphous polymers.

Polymethyl methacrylate (PMMA) is the most widely studied polymer [Ref. 134, 142, 148, 161]. According to the temperature dependence of Ref. 27 for the damping constant δ at a frequency of harmonic oscillations of 1 Hz, temperatures T_g and T_β have values of approximately 100 and 200°C respectively (Fig. 6.1). Stress-strain curves over a wide range of

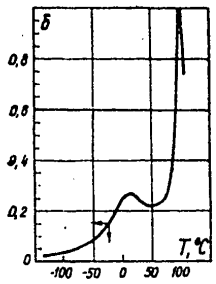

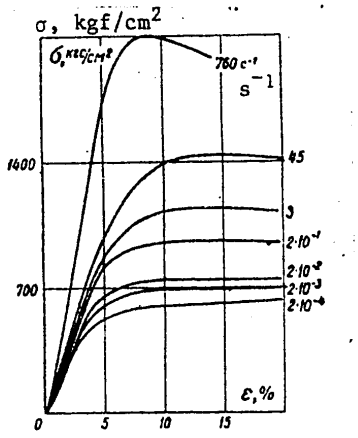

Fig. 6.1. Dependence of the angle of phase shift δ on temperature at a fixed frequency of oscillations of 1 Hz [Ref. 27]

Fig. 6.2. Stress-strain diagrams for PMMA under compression over a wide range of strain rates. Test temperature 20°C [Ref. 123]

strain rates at fixed temperature are shown in Fig. 6.2. Curves for stresses $\sigma_{\varepsilon\%}$ corresponding to fixed deformation, as well as σ_s as a function of $\lg\dot{\varepsilon}$ at room temperature T = 20°C are shown in Fig. 6.3. The dependence $\varepsilon_{2\%}$ vs. $\lg\dot{\varepsilon}$ has the S-shape typical of amorphous polymers in the state of the β-transition. As temperature changes, the curve shifts parallel to itself, which enables construction of a generalized curve (Fig. 6.4). The relation $\lg a_T$ vs. $1/T$ that corresponds to the curve of Fig. 6.5 is linear, which is evidence of the constancy of the activation energy.

In the region of the β-transition the curves for $\sigma_{\varepsilon\%}$ vs. $\lg\dot{\varepsilon}$ deviate further and further from the S-shape as ε increases, and there is a transition to the linear dependence of σ_s vs. $\lg\dot{\varepsilon}$ (see Fig. 6.3). A deformation of 8-10% corresponds to stress σ_s for PMMA. Variance of the temperature above T_β and strain rates in a range of 10^{-5}-10^{1} s^{-1} led to the possibility of studying [Ref. 161] the dependence of σ_s vs. $\lg\dot{\varepsilon}$ in regions of the α- and β-transitions (Fig. 6.6). It was found that the function σ_s/T vs. $\lg\dot{\varepsilon}$ can be treated as consisting of two straight lines with a smooth transition of the sections between them. Relations of

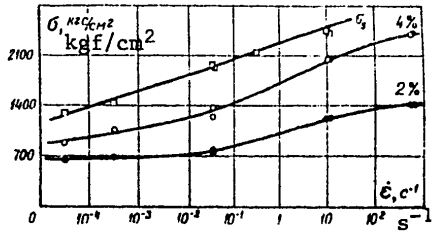

Fig. 6.3. Yield point and stresses at fixed deformations as functions of the strain rate for PMMA [Ref. 134]

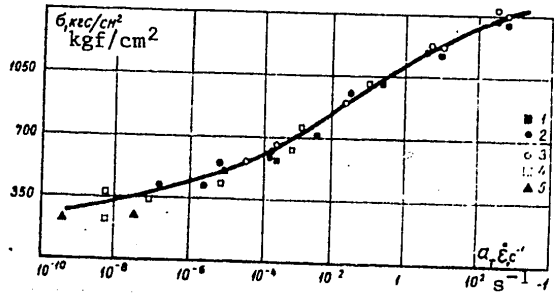

Fig. 6.4. Generalized curve for stress at a fixed deformation of 2%. The points show data obtained at T in °C of: 1--0; 2--22; 3--50; 4--82; 5--115. T_{ref} = 22°C. Material PMMA

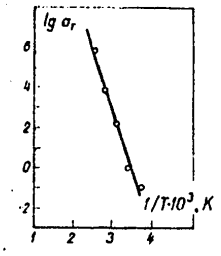

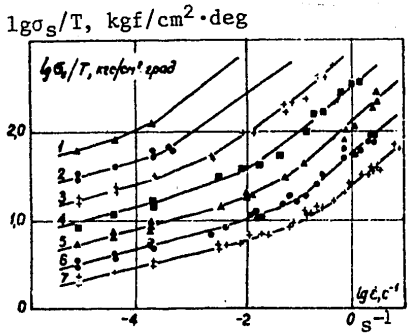

Fig. 6.5. Dependence of $\lg a_T$ vs. 1/T. The solid line corresponds to the WLF formula; the points are experimental data found in accordance with Fig. 6.4 [Ref. 134]

Fig. 6.6. Dependence of σ_s/T vs. $\lg\dot{\varepsilon}$ for PMMA [Ref. 161] at different testing temperatures, °C: 1--30; 2--40; 3--50; 4--60; 5--70; 6--80; 7--90

σ_s/T vs. $\lg\dot{\varepsilon}$ are described by the Eyring formula that accounts for the influence of two relaxation phenomena occurring simultaneously [Ref. 161],

$$\frac{\sigma_s}{T} = \frac{1}{2}\sum_i \frac{1}{A_i} \lg\left(\frac{C_i\dot{\varepsilon}}{T} e^{\frac{U_i}{RT}}\right), \qquad (6.6)$$

where $i = 1, 2$, since we are restricting ourselves to consideration of two processes (α and β); C_i, A_i, U_i are the constants for the respective processes. The values of constants calculated according to experimental data (see Fig. 6.6) are summarized in Table 6.1 [Ref. 161].

TABLE 6.1

Process	U, $\frac{\text{kcal}}{\text{mole}}$	lnC, $\frac{\text{s}}{\text{K}}$	A, $\frac{\text{K}\cdot\text{cm}^2}{\text{dyne}} \cdot 10^{-6}$
α	81	-90	15
β	24	-25	7.2

The graphs given in Fig. 6.6 show good agreement between experiment and formula (6.6).

Polyethyl methacrylate (PEMA) has mechanical properties similar to those described for PMMA. The dependence of δ vs. T for PEMA is the same in nature as for PMMA, but shifted 10-15°C toward lower temperatures. This causes analogous mechanical behavior. Constants calculated in accordance with experimental data and (6.6) are summarized in Table 6.2 [Ref. 162].

TABLE 6.2

Process	U, $\frac{\text{kcal}}{\text{mole}}$	lnC, $\frac{\text{s}}{\text{K}}$	A, $\frac{\text{K cm}^2}{\text{dyne}} \cdot 10^{-6}$
α	38	-127	23.0
β	32	-38	9.2

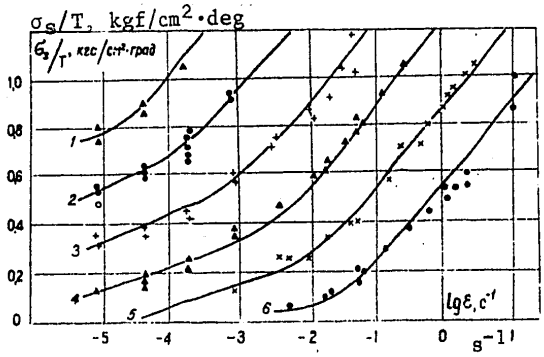

Fig. 6.7. Dependence of σ_s/T vs. $\lg\dot{\varepsilon}$ for polyethyl methacrylate [Ref. 162] at different testing temperatures, °C: 1--30; 2--40; 3--50; 4--60; 5--70; 6--80

Polyvinyl chloride (PVC). The curves of tgδ vs. T are similar for PVC, PMMA and PEMA. The glass point of PVC is about 75°C. The secondary transition point of PVC is about -50°C [Ref. 27]. Fig. 6.8 shows the generalized curve for σ_s vs. $\lg a_T\dot{\varepsilon}$ in the temperature range from 70 to -37°C. Correspondence between the coefficient a_T and temperature is shown in Table 6.3.

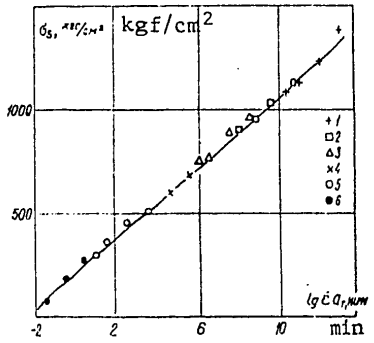

Fig. 6.8. Generalized curve for σ_s vs. $\lg a_T\dot{\varepsilon}$ for polyvinyl chloride [Ref. 148] at different testing temperatures, °C: 1-- -37; 2-- -16; 3--10; 4--50; 5--60; 6--70

Amorphous polycarbonate (PC) is characterized by a wider range of T_α-T_β than the materials considered above. For polycarbonate this range is 270°C (T_g = 150°C, T_β = -120°C). A generalized curve for σ_s vs. $\lg a_T\dot{\varepsilon}$ in the regions of α- and β-transitions of PC is shown in Fig. 6.9. The points on the two straight lines on the graph correspond to these two processes. The relation for σ_s vs. $\lg a_T\dot{\varepsilon}$ shown on the left part of the graph corresponds to the viscofluid state of the polymer, which is not discussed here.

Polystyrene (PS) shows a single clear transition (α). The glass point is about 100°C. No noticeable secondary transitions have been observed in isotactic polystyrene. The presence of an ataxic phase leads to two secondary transitions

TABLE 6.3

Material	T_{ref}, °C	Coefficient a_T at different temperatures													Fig.
		-100	-75	-50	-10	-25	-20	0	20	40	50	75	100	125	150	
PVC	60				12	11	10	8.6	8.0	5.2	3.1	-4.1				6.8
PC	25	9.83	7.44	5.73		3.60			1.92		-2.23	-4.33	-6.09	-7.60	-11.44	6.9
PS	82				9.10		7.80	7.10	5.50	4.02		1.05				6.11
FT	25	10.27	7.64	6.11		4.71		3.32			-2.30	-3.34	-4.52	-5.80	-7.02	6.20
PF	25	14.17	10.93	7.73		5.17		2.15			-2.41	-5.58	-7.56	-9.51	-11.34	6.21

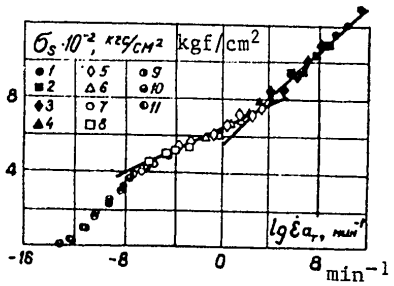

Fig. 6.9. Generalized dependence of σ_s vs. $\lg a_T \dot{\varepsilon}$ for polycarbonate [Ref. 148] at different testing temperatures, °C: 1-- -100; 2-- -75; 3-- -50; 4-- -25; 5--0; 6--25; 7--50; 8--75; 9--100; 10--150; 11--140

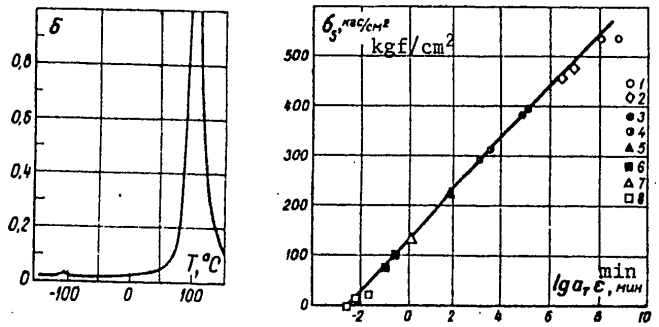

Fig. 6.10. Curve of δ vs. T for polystyrene. Testing frequency 1 Hz [Ref. 27]

Fig. 6.11. Generalized relation of σ_s vs. $\lg a_T \dot{\varepsilon}$ for polystyrene [Ref. 148] at different testing temperatures, °C: 1-- -40; 2-- -20; 3--0; 4--20; 5--40; 6--75; 7--100; 8--125

(Fig. 6.10), but they are so faint that their effect on the mechanical properties of PS can be disregarded. As a result, the experimental relation for σ_s vs. $\lg a_T \dot{\varepsilon}$ is a straight line. The experimental points found over wide ranges of strain rates and deformations of PS fit well on a generalized straight line (Fig. 6.11). Stress-strain diagrams [Ref. 123] with changing strain rate are shown in Fig. 6.12. PS is an example of an amorphous polymer with the simplest mechanical properties.

Time dependence of the strength of amorphous polymers. The tensile strength (breaking stress) is a most important characteristic of materials. Experimental data on the time and temperature dependence of breaking stress are taken as a basis in strength calculations. Generalization of the results of experiments and representation as principles governing strength are the physical basis of theories of mechanical destruction.

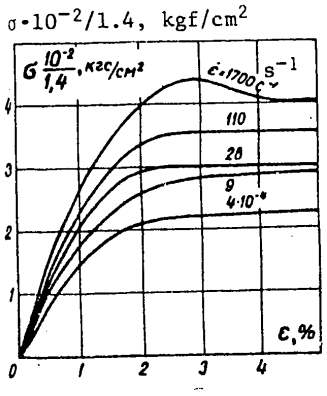

Fig. 6.12. Stress-strain diagram for polystyrene. Compression testing at T = 20°C [Ref. 123]

Comments on methods of determining the time dependence of polymer strength. Quantitative data on the true breaking stresses σ_b obtained as a result of quasistatic tests at a constant strain rate can be reduced to the relation σ_b vs. $\lg\dot{\varepsilon}$, or to the relation between durability τ and σ_b. The dependence between σ_b and τ can be obtained by durability tests that consist in determining the times of destruction of a specimen by a stepwise applied load. Large durabilities and the corresponding σ_b are obtained by the standard methods of creep testing. As we move to durability measured in units of the order of $1\text{-}10^{-3}$ s, it becomes necessary to use special loading devices. Loading with a stepped pulse is comparatively easy to do in tests with low strain rates. As the strain rate increases (more than 100 s^{-1}), such loading is not feasible. In this case the time dependence of strength can be plotted on the basis of the principle of linear superposition of fractures, which is written as the Bailey formula

$$\int_0^{t_p} \frac{dt}{\tau[\sigma(t)]} = 1, \qquad (6.7)$$

where t_p is the time of onset of fracture of a specimen loaded by a force $\sigma(t)$ that varies in time; $\tau[\sigma(t)]$ is the law of durability of the material determined under condition $\sigma = \text{const}$. The possibility of scaling the results of measurements with respect to σ_b and τ under different loading conditions is demonstrated in Ref. 17, 87.

Quasistatic methods combined with static methods enable determination of the time dependence of strength in ranges of the order of 10^{-3}-10^{7} s. Tests with duration measured in fractions of a microsecond are needed for a complete understanding of the time behavior of strength. The only known method that can be used for testing solids at such brief load durations is a technique based on cleavage [Ref. 11, 32, 33, 113]. The method essentially reduces to the following. An impulse load applied to the surface of the body propagates along it, and, reaching the opposite surface, is reflected from it with the reverse sign. As a result of superposition of the incident and reflected waves, the material close to the free surface is under the action of tensile forces. In the case where an intensive pulse loads materials for which the compression strength is greater than the tensile strength, a layer close to the free surface is split off. The distance from the surface of the split to the free surface is determined by the shape of the pulse.

To make quantitative estimates of the breaking stress in tests based on cleavage phenomena, a rod is taken as the object of study. The essence of the method of determining stress and durability under intense short-term loading leading to cleavage phenomena consists in recording the velocity of the free surface and calculating the stress and its duration in the cross section that is split as the sum of the direct and reflected waves. In doing this, it is assumed that the rod is elastic and fairly slender. The value of the stresses acting in the split is

$$\sigma = \rho c_0 \frac{\Delta V}{2};$$

here ΔV is the difference of the ordinates of the time dependence of the velocity of the free end V(t) and the same dependence shifted relative to the first by the segment $2t^* = x/c_0$, where t^* is the time of travel of the perturbation through the thickness of the split-off layer. It is assumed that the shape of the perturbation wave is not changed upon reflection. Velocity is measured by one of the methods described in Chapter two. When impulse duration is a fraction of a microsecond, laser interferometry can meet the requirements that are now made for accuracy in velocity registration [Ref. 11, 32, 33].

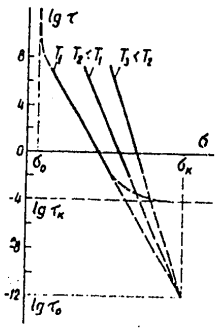

Fig. 6.13. Typical curves for lgτ vs. σ [Ref. 26]

Relations for lgτ vs. σ_b of most amorphous polymers are linear, which agrees with the current concepts of the kinetic nature of the strength of solids. The strength behavior expressed as the dependence of durability on breaking stress for most amorphous polymers has the form of the graphs of Fig. 6.13. The transition to brittle fracture when the time of crack propagation through the cross section of the specimen is commensurate with the durability leads to a considerable increase in the stress that can be taken as the breaking stress (Fig. 6.13). The longitudinal extension of the specimen also increases in this case. On the durability curve, stress ceases to depend on τ, or is weakly dependent, which is a common feature of most materials [Ref. 11, 32, 33]. An intensive impulse load that does not exceed the theoretical tensile strength of the material will not separate the specimen into halves until the inception of a crack.

For many materials the interrelation between strain and fracture is complicated by effects that accompany large deformations. The relation between fracture and strain is most obvious in glassy amorphous polymers, which is confirmed for example by the curves shown in Fig. 6.14 and 6.15. The feasibility of reducing the relation between σ_b and lgε̇ to a single generalized curve was first demonstrated by Smith [Ref. 165, 166] for elastomers. As implied by the results of Ref. 138, there is also a generalized curve of σ_s vs. $\lg a_T \dot{\varepsilon}$ for amorphous polymers, and in particular for epoxy resin. Curves for $\lg a_T$ vs. T plotted from data of the elastic

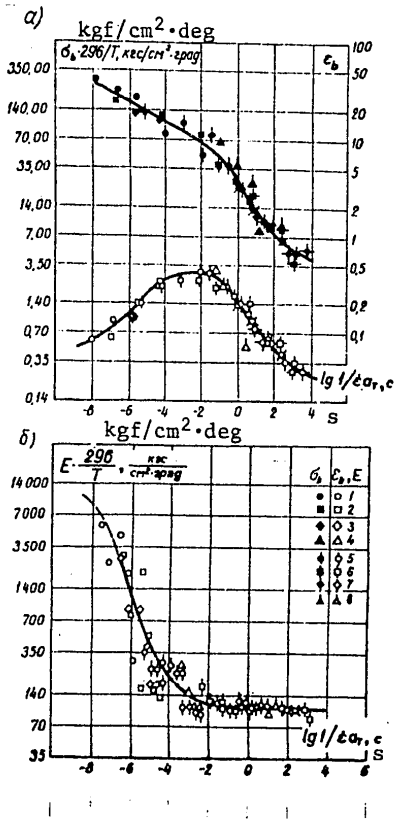

Fig. 6.14. Generalized relations for σ_b/T vs. $\lg^1/\dot{\varepsilon}a_T$, ε_b vs. $\lg^1/\dot{\varepsilon}a_T$ (a) and E/T vs. $\lg^1/\dot{\varepsilon}a_T$ (b) for epoxy resin [Ref. 138] at different test temperatures, °C: 1--36; 2--45; 3--55; 4--65; 5--75; 6--85; 7--96; 8--115

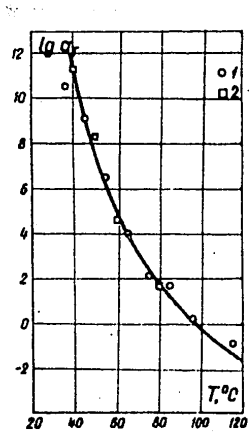

Fig. 6.15. Relation for $\lg a_T$ vs. T. The solid line shows calculations by the WLF formula [Ref. 138]: 1--calculation from σ_b and ε_b; 2--calculation from E

modulus and from data of the tensile strength show satisfactory agreement (see Fig. 6.15).

6.2 Crystalline Polymers

The mechanical behavior of crystalline polymers is due to the supermolecular structure that arises prior to testing. The presence of crystalline and amorphous phases leads to development of several mechanisms of relaxation phenomena with the influence of one of them prevailing if optimum conditions of its occurrence are brought about, i. e. with a certain combination of $\dot{\varepsilon}$ and T. Semicrystalline polymers show a complex set of relaxation phenomena that lead to a multiplicity of transitions, and display transitions inherent in the amorphous phase, as well as processes associated with: 1) transition from one crystal modification to another (phase transition); 2) motion of side groups within crystalline regions; 3) interaction of amorphous and crystalline regions; 4) motion within crystalline regions [Ref. 10].

The rather complicated combination of these processes leads to a multiplicity of relaxation mechanisms of deformation. However, only a few of the enumerated processes have any appreciable effect on the mechanical behavior of the polymer. Experiments show that curves for δ vs. T have pronounced peaks and slight inflections indicating the predominant influence of the corresponding mechanism of deformation. Experimental data are considered below on the mechanical behavior of some semicrystalline polymers.

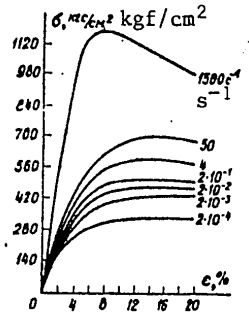

Fig. 6.16. Stress-strain diagrams for polypropylene. Compression testing at T = 20°C [Ref. 123]

Polypropylene (PP) has three peaks on the δ vs. T curve [Ref. 26, 123, 135, 162]. Corresponding to the peak at 60°C is a phase transition, i. e. a rearrangement of the crystalline phase (α-transition). The second peak occurs at a temperature of about 5°C. The corresponding relaxation process is caused by an increase in segmental mobility (glass transition) of the amorphous phase (β-transition). The greater the amount of amorphous phase in the polymer, the more pronounced will be the peak. The third relaxation process (γ) is due to the glass transition of the polymer, and can be attributed to motion of crystals in the amorphous phase [Ref. 10]. It can be noted on the δ vs. T curve from a broad peak at the glass point $T_g = -70°C$, the height of this peak decreasing with increasing degree of crystallinity. Fig. 6.16 and 6.17 show stress-strain diagrams and strain-rate

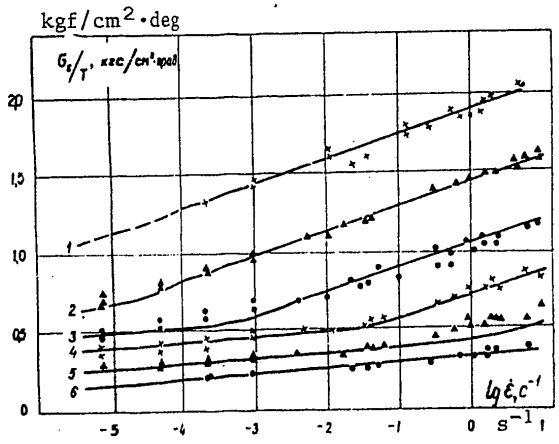

Fig. 6.17. Curves of σ_s/T vs. lg$\dot{\varepsilon}$ for polypropylene [Ref. 162] at different test temperatures, °C: 1--10; 2--30; 3--50; 4--70; 5--90; 6--110

dependences of σ_s for semicrystalline polypropylene. The behavior of σ_s/T vs. $\lg\dot{\varepsilon}$ over a wide temperature range for the α- and β-regions (Fig. 6.17) has a form analogous to that of the same function for amorphous polymers (see Fig. 6.6 and 6.7). Formal description of the relations by formula (6.6) yielded the constants in Table 6.4 [Ref. 162].

TABLE 6.4

Process	U, $\frac{\text{kcal}}{\text{mole}}$	A, $\frac{\text{K cm}^2}{\text{dyne}} \cdot 10^{-6}$	lnC, $\frac{\text{s}}{\text{K}}$
α	88.6	62	-90.4
β	45.6	19	-58.8

The fact that curves for σ_s/T vs. $\lg\dot{\varepsilon}$ are displaced parallel as temperature changes means that temperature-time superposition can be used.

Semicrystalline *oriented polypropylene* [Ref. 135] shows more pronounced differentiation of behavior in the corresponding regions. Fig. 6.18 gives strain-rate dependences of $\sigma_{2\%}$, $\sigma_{5\%}$, $\sigma_{10\%}$, $\sigma_{15\%}$ and σ_s. In the region of the β-transition the intensity of the change in dependence of $\sigma_{2\%}$ on increasing $\lg\dot{\varepsilon}$ is strongly reduced by preliminary orientation. The region of glass transition of the polymer (γ-transition) is characterized by a secondary increase in dependences of $\sigma_{\varepsilon\%}$ and σ_s on $\lg\dot{\varepsilon}$.

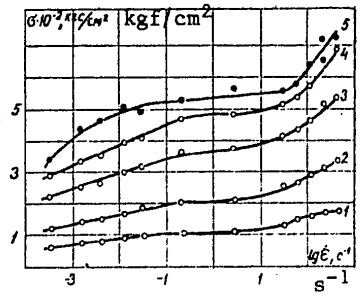

Fig. 6.18. Dependence of the yield stress σ_s and the stresses that correspond to different deformations (%) on $\lg\varepsilon$ for oriented polypropylene [Ref. 135]: 1--2%; 2--5%; 3--10%; 4--15%; 5--σ_s

Fluorocarbon (FT). A maximum is observed on the curve for δ vs. T at $T_g = -87°C$, attributed to glass transition of the polymer (γ-process). The height of the maximum decreases with increasing crystallinity. The maximum at 30°C increases with an increase in the degree of crystallinity. A phase transition occurs in the corresponding region in the vicinity of the peak. The transition to the glassy state in fluorocarbon plastic involves a sharp increase in longitudinal extension of the specimen during tensile tests [Ref. 48, 55], and a considerable change in the shape of stress-strain diagrams (Fig. 6.19). Fig. 6.20 shows the behavior of σ_s vs. $\lg a_T\dot{\varepsilon}$.

Polyformaldehyde (PF). As a consequence of the fact that PF is a strictly linear high-crystalline polymer, any relaxation processes will involve movement of the main chain, its segments, or end groups. Glass point is at $T_g = -70°C$ (γ-transition), and phase transition is at $T_\alpha = 120°C$

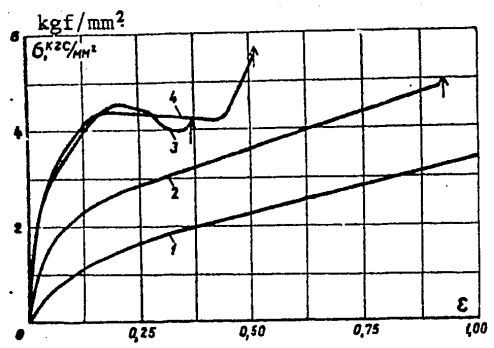

Fig. 6.19. Stress-strain diagram for Teflon in tensile tests at 20°C. strain rates, s^{-1}: 1--10^{-3}; 2--11.2; 3--700; 4--2000. The time of fracture is shown by an arrow

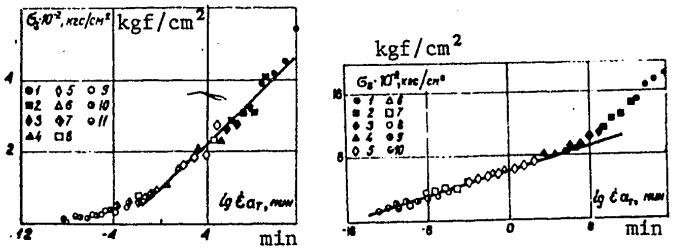

Fig. 6.20. Generalized behavior of σ_s vs. $\lg a_T\dot{\varepsilon}$ for fluorocarbon [Ref. 148]. The points show experimental data found at T (°C) of: 1-- -100; 2-- -75; 3-- -50; 4-- -25; 5--0; 6--25; 7--50; 8--75; 9--100; 10--125; 11--150. See Table 7.3 for values of a_T.

Fig. 6.21. Generalized curve of σ_s vs. $\lg a_T\dot{\varepsilon}$ [Ref. 148] for polyformaldehyde. Notation the same as on Fig. 6.20. For values of a_T see Table 7.3.

(α-transition). No intermediate relaxation processes are observed. To judge from the generalized curve of σ_s vs. $\lg a_T\dot{\varepsilon}$, the transition from the α- to the γ-process is quite clear. On Fig. 6.21, the curve corresponding to the α-process is shown by a straight line. The upper part of the curve corresponds to the γ-process.

Polyethylene (PE). The phase transition (α) and glass transition (γ) are characterized by peaks on the δ vs. T curve at 50°C and -120°C respectively. Branching of the polymer leads to the observed inflection of the behavior of δ vs. T at -10°C, which corresponds to glass transition of the amorphous phase of the polymer. The mechanical properties of PE are analogous to those of fluorocarbon. in the γ region of the relaxation process abrupt elongation of the specimen is observed [Ref. 48, 59] as well as a change in behavior of the stress-strain diagrams (Fig. 6.22).

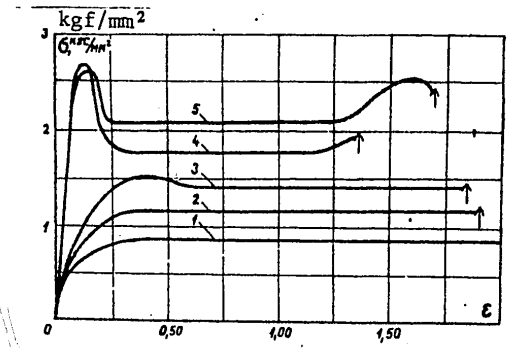

Fig. 6.22. Stress-strain diagrams for polyethylene in tensile tests. Strain rates $\dot{\varepsilon}$, s^{-1}: 1--10^{-3}; 2--10^{-1}; 3--16; 4--700; 5--3000. The arrows indicate fracture times. T = 20°C.

Influence of strain rate on the strength of crystalline polymers. The mechanical properties of crystalline polymers are determined mainly by the properties of the supermolecular structure formed prior to deformation. Ref. 26 investigates the influence that supermolecular structure has on the strength of crystalline polymers. Tests were done on polypropylene specimens with different aggregations of the crystal phase, but with about the same degree of crystallinity (approximately 50%). It has been shown (Fig. 6.23) that at comparatively low stretching rates where highly elastic deformation develops and the material is oriented in the drawing process, an increase in breaking stress is observed for three kinds of polypropylene. A further increase in strain rate is accompanied by a reduction in the degree of orientation of the material. However, in this region, as previously in the region of fracture, the material is oriented, although the orientation is the less, the greater the velocity, which causes a reduction in the σ_b.

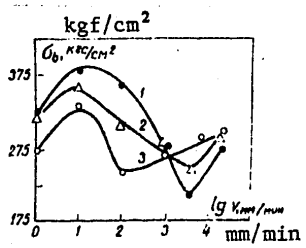

Fig. 6.23. Dependence of breaking stress of polypropylene of various structures on the velocity of clamp displacement: 1--quenching; 2--molding; 3--annealing [Ref. 26]. T = 25°C.

According to Ref. 25, the degree of orientation depends on the type of supermolecular structure. At low strain rates, orientation is most readily attained in tests of microcrystalline material (quenched specimen) and least readily in the case of testing of a material that consists of coarse spherolites (annealed specimen). At high strain rates the structure of quenched specimens is fractured more readily than that of annealed specimens. Preliminary drawing of polypropylene [Ref. 135] leads to a change in the form of the curve for σ_b vs. lg$\dot{\varepsilon}$ (Fig. 6.24). Analogous patterns for breaking stress and strain rate are

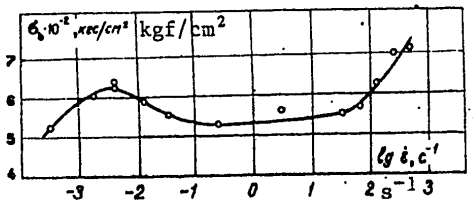

Fig. 6.24. Breaking stress as a function of strain rate for oriented polypropylene [Ref. 135]. T = 20°C.

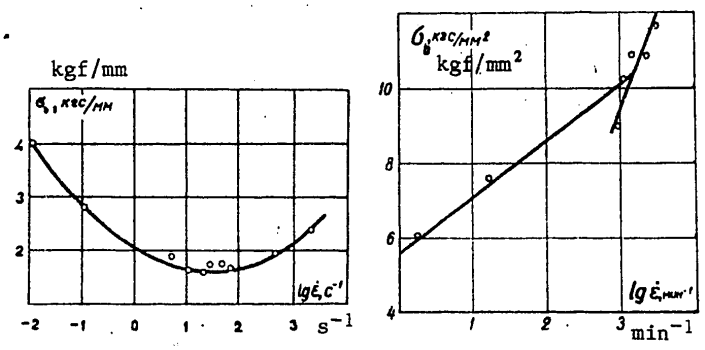

Fig. 6.25. Breaking stress of Teflon as a function of strain rate. Tensile testing. T = 20°C.

Fig. 6.26. Breaking stress of polyformaldehyde as a function of strain rate. Tensile testing. T = 20°C.

observed for fluorocarbon plastic [Ref. 48, 59] (Fig. 6.25). Fig. 6.26 shows curves for σ_b vs. lgė for a high-crystallinity polymer -- polyformaldehyde [Ref. 58].

6.3. Reinforced Materials

The mechanical properties of reinforced materials over a wide range of strain rates have been studied in a number of papers [Ref. 17, 19, 52, 53, 57-62, 113, 128, 131, 151, 152]. Shown in Fig. 6.27-6.30 are relations typical of reinforced materials, one of their most pronounced features being anisotropy of mechanical properties. The influence of strain rate on the degree of anisotropy is reflected by Fig. 6.27. An increase in strain rate reduces the degree of anisotropy.

Commom features of the mechanical behavior of reinforced materials are: 1) the stress-strain diagrams for dynamic loading (Fig. 6.28) are higher than the static diagrams at all points; 2) E is a linear function of lgė; 3) the stress corresponding to the salient point of the stress-strain diagram increases with increasing ε; increasing the strain rate does not eliminate the salient point; 4) maximum deformation at fracture is practically independent of strain rate.

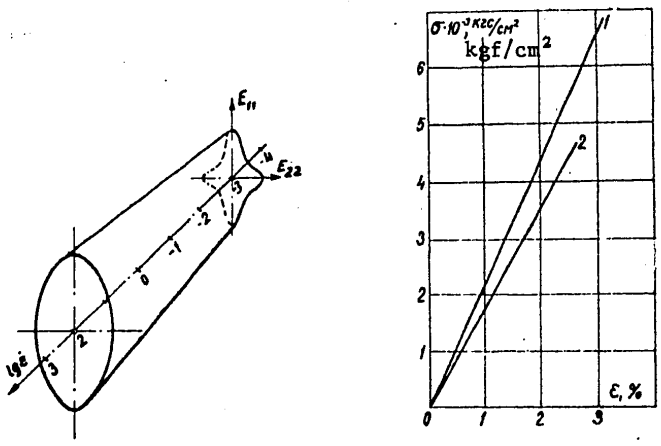

Fig. 6.27. Diagram illustrating the influence of strain rate on the degree of anisotropy of glass-textolite (ASTT cloth--50%, EDT resin--50%). T = 20°C

Fig. 6.28. Stress-strain diagram for woven glass-textolite. Binder was epoxy resin [Ref. 113]. Time to fracture: 1--0.014 s; 2--80 s.

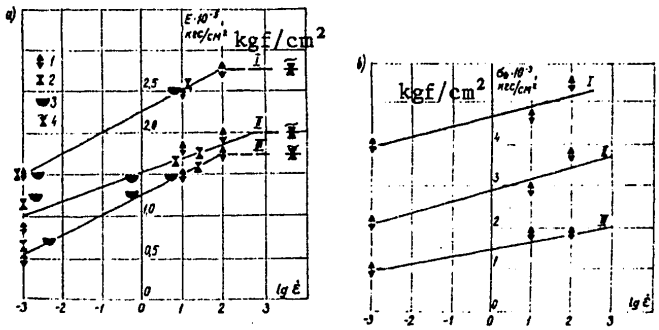

Fig. 6.29. [Strain-rate] dependences of transverse elastic modulus on a deformation base of 0.2% (a), and breaking stress (b) for glass textolite (ASTT fabric--50%, EDT resin--50%). Symbols for types of tests used in getting the data: 1--tensile; 2--compression; 3--bending; 4--wave propagation; I--on the warp; II--on the weft; III--on the bias at 45°

Curves for E vs. lgė, and also σ_b vs. lgė for a number of fiberglass plastics under conditions of non-brittle fracture are shown in Fig. 6.29. Time dependences of strength of fiberglass plastics [Ref. 17] are shown on Fig. 6.30.

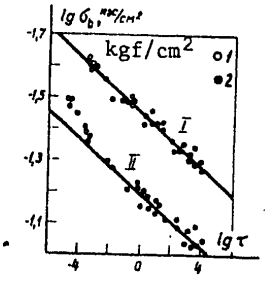

Fig. 6.30. Time dependences of strength for polyester fiberglass plastic [Ref. 17]: 1--calculation by (6.7); 2--tests under condition σ = const; I--stretching along the warp; II--stretching along the weft

Chapter 7

MODELS OF MECHANICAL BEHAVIOR OF POLYMERS

The results of experiments form the basis of models of mechanical behavior of polymers. A model that describes the linear behavior of a material at rather low deformations can be constructed from the frequency dependences of the real and imaginary parts of the elastic modulus $E'(\omega)$ and $E''(\omega)$ based on test results for harmonic oscillations. The order of magnitude of the deformation increases with use of the results of experiments for uniform stretching-compression.

1.1. Calculation of Relaxation Spectra

The technique for constructing a model of mechanical behavior of polymers is based on the results of experiments on uniform stretching over a wide range of strain rates [Ref. 60]. Construction of the model uses experimental relations for the transverse elastic modulus E_a on some fixed deformation base ε. We will show that results on measurement of the transverse modulus over a wide range of strain rates enable calculation of the spectra of relaxation times -- the most important of the viscoelastic characteristics that completely defines the deformational properties of a linear viscoelastic body at small deformations, enabling construction of a model of the material.

Let us consider a model of a linear viscoelastic body consisting of n Maxwell elements connected in parallel (Fig. 7.1). For the i-th element of the model, the strain law takes the form

$$\frac{1}{\eta_i}\sigma_i+\frac{\dot{\sigma}_i}{E_i}=\dot{\varepsilon}_i. \qquad (7.1)$$

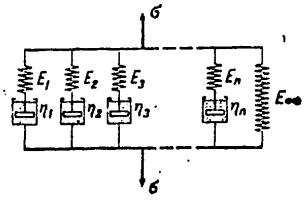

Fig. 7.1. Model of a viscoelastic body

In the case of uniform strain at a rate of $\dot{\varepsilon}_0 = \text{const}$

$$\sigma_i = E_i \dot{\varepsilon}_0 \tau_i \left(1 - e^{-\frac{t}{\tau_i}}\right), \tag{7.2}$$

where $\tau_i = \eta_i / E_i$ is the relaxation time of the i-th element of the model, and the stress σ is the sum of the stresses σ_i in the individual elements:

$$\sigma = \sum_{i=1}^{n} \sigma_i = \dot{\varepsilon}_0 \sum_{i=1}^{n} E_i \tau_i \left(1 - e^{-\frac{t}{\tau_i}}\right). \tag{7.3}$$

Let us replace the continuous relaxation spectrum with a discrete spectrum. We characterize the relaxation spectrum in the i-th interval by the quantity H_i. For each element of the discrete model we determine E_i:

$$E_i = \frac{H_i}{\tau_i} \Delta\tau; \tag{7.4}$$

Note that E_i is a quantity of the same order of magnitude as $\Delta\tau$. The stress in a body with discrete relaxation spectrum is determined from (7.3):

$$\sigma = \dot{\varepsilon}_0 \sum_{i=1}^{n} H_i \left(1 - e^{-\frac{t}{\tau_i}}\right) \Delta\tau. \tag{7.5}$$

For the case where an equilibrium modulus exists,

$$\sigma = E_\infty \varepsilon + \dot{\varepsilon}_0 \sum_{i=1}^{n} H_i \left(1 - e^{-\frac{t}{\tau_i}}\right). \tag{7.6}$$

For the continuous relaxation spectrum in expression (7.6) we pass to the limit as $n \to \infty$, and hence as $\Delta\tau \to 0$:

$$\sigma = E_\infty \varepsilon + \dot{\varepsilon}_0 \lim_{\Delta\tau \to 0} \sum_{i=1}^{n} H_i \left(1 - e^{-\frac{t}{\tau_i}}\right) \Delta\tau =$$

$$= E_\infty \varepsilon + \dot{\varepsilon}_0 \int_0^\infty H(\tau) \left(1 - e^{-\frac{t}{\tau}}\right) d\tau. \tag{7.7}$$

Expression (7.7) can be rewritten as

$$\sigma = E_\infty \varepsilon + \dot{\varepsilon}_0 \int_0^\infty \int_0^t \frac{H(\tau)}{\tau} e^{-\frac{\xi}{\tau}} d\xi \, d\tau \tag{7.8}$$

or

$$\sigma = E_\infty \varepsilon + \dot{\varepsilon}_0 \int_{-\infty}^{+\infty} \int_0^t H(\tau) e^{-\frac{\xi}{\tau}} d\xi d\tau. \tag{7.9}$$

A different form is sometimes used as well in the linear theory of viscoelasticity:

$$\sigma = E_\infty \varepsilon + \int_0^t \Psi(t-\tau)\, \dot{\varepsilon}(\tau)\, d\tau, \tag{7.10}$$

where $\Psi(t)$ is the relaxation function. We can readily see that the relaxation function and the spectrum of relaxation times are related by the expression

$$\Psi(\xi) = \int_0^\infty \frac{H(\tau)}{\tau} e^{-\frac{\xi}{\tau}} d\tau. \tag{7.11}$$

The transverse modulus E_a calculated on a small deformation base ε_a is defined as follows:

$$E_a = \frac{\sigma_a}{\varepsilon_a} = E_\infty + \frac{1}{z} \int_0^\infty \int_0^z \frac{H(\tau)}{\tau} e^{-\frac{\xi}{\tau}} d\xi\, d\tau, \tag{7.12}$$

where $z = \varepsilon_a/\dot{\varepsilon}_0$ is the time expended in deformation of the specimen by an amount ε_a at a given strain rate $\dot{\varepsilon}_0$. The quantity ε_a that is taken as the base for calculating the transverse modulus E_a must be fairly small from consideration of the linearity of the relation between stress and strain. If we use the notation $E_a - E_\infty = E$, and $Ez = R$, (7.12) takes the form

$$R(z) = \int_0^\infty \int_0^z \frac{H(\tau)}{\tau} e^{-\frac{\xi}{\tau}} d\xi\, d\tau. \tag{7.13}$$

Whence

$$R'(z) = \frac{\partial R}{\partial z} = \int_0^\infty \frac{H(\tau)}{\tau} e^{-\frac{z}{\tau}} d\tau. \tag{7.14}$$

All existing approximate methods of calculating relaxation times reduce to evaluation of the integral

$$E(t) = E_\infty + \int_{-\infty}^{+\infty} H(\tau) e^{-\frac{t}{\tau}} d\ln\tau, \tag{7.15}$$

where $E(t)$ is the relaxation modulus, E_∞ is the equilibrium modulus, $H(\tau)$ is the spectrum of relaxation times. Calculation of the spectra of relaxation times from the results of experiments on uniform deformation according to (7.14) reduces to evaluation of an integral of the same form as in the case of stress relaxation.

The next problem is to determine H(t) from (7.14), knowing the function R'(z) determined experimentally over a wide range of variation in z. Let us introduce the new variable s: $\tau = 1/s$; we rewrite (7.14) as

$$R'(z) = \int_0^\infty H_1(s)\, e^{-sz}\, ds; \quad H_1(s) = \frac{H\left(\frac{1}{s}\right)}{s}. \tag{7.16}$$

If the variable z in (7.16) is treated as a Laplace transform parameter, this expression is a transformation of the function $H_1(s)$. Approximating R'(z) by a function that permits inversion, we get $H_1(s)$, and consequently $H(\tau)$ as well by inverse transformation. (7.16) at $z = 0$ gives

$$R'(0) = \int_{-\infty}^{+\infty} H(\tau)\, d\ln\tau. \tag{7.17}$$

We can readily see that $R'(0) = E_0 - E_\infty$, where E_0 is the asymptote of the Relation E vs. $\ln\dot{\varepsilon}$ as $\dot{\varepsilon} \to \infty$. Consequently the area bounded by the spectrum of $H(\tau)$ and axis $\ln\tau$ must be numerically equal to R'(0).

The sequence of computation in constructing the relaxation spectra is as follows: 1) calculation of R'(z) from experimental data for E_a vs. $f(\varepsilon)$; 2) approximation of the curve for R'(z) by the function $R'_a(z)$. The curve for R'(z) that is obtained from the experimental data and must satisfy the conditions

$$\begin{aligned} R_a'(z) &\longrightarrow 0, && z \longrightarrow \infty; \\ R_a'(z) &\longrightarrow E_0 - E_\infty, && z \longrightarrow 0, \end{aligned} \tag{7.18}$$

can be approximated by an infinite set of functions, and the choice of the approximation is quite arbitrary. Let us consider in more detail some approximations of R'(z) and their corresponding relaxation spectra.

1. We get the first approximation in evaluation of the relaxation spectrum after substituting e^{-sz} in (7.16):

$$e^{-sz} = \begin{cases} 1, & s \leqslant \frac{1}{z}; \\ 0, & s > \frac{1}{z}. \end{cases}$$

Integral relation (7.16) is replaced by the simpler experssion

$$R'(z) = \int_0^{\frac{1}{z}} H_1(s)\, ds. \tag{7.19}$$

Differentiating (7.19) with respect to z, we get for approximate evaluation of the spectrum

$$H_1(s) = -s^{-2}R''(s^{-1}). \tag{7.20}$$

2. Inverse Laplace transformation applies to mathematically incorrect problems, and therefore the spectrum of relaxation times that we get by inverse Laplace transformation may depend appreciably on approximation of the curve R'(z). Whether the spectra are realistic can be judged to a great extent by comparing the results found by different approximations and different methods. The curve R'(z) can be approximated with fair accuracy by the function

$$R'(z) = \sum_{i=1}^{n} A_i e^{-\alpha_i \sqrt[4]{z}}. \tag{7.21}$$

After inverse Laplace transformation, expression (7.21) gives a relaxation spectrum in the form

$$H(\tau) = \sum_{i=1}^{n} A_i \frac{\alpha_i}{2} \sqrt{\frac{\tau}{\pi}} e^{-\frac{\alpha_i^2}{4}\tau} \tag{7.22}$$

(hereafter the values of R'(z) and H(θ) computed from (7.21) and (7.22) will be denoted by $R_1'(z)$ and $H_1(\tau)$ respectively). Approximation of R'(z) in form (7.22) requires considerable computational work even for n = 3. Therefore it would be advisable to consider some simpler forms of approximation.

3. Conditions (7.18) are satisfied by the following approximation:

$$R_2'(z) = \frac{B}{\alpha + z^{0,5}}, \tag{7.23}$$

with conditions (7.18) implying

$$\frac{B}{\alpha} = E_0 - E_\infty.$$

The relaxation spectrum corresponding to (7.22) we get in the form

$$H_2(\tau) = \frac{B}{\tau}\left[\sqrt{\frac{\tau}{\pi}} - \alpha e^{\frac{\alpha^2}{\tau}}\left(1 - \mathrm{Erf}\frac{\alpha}{\sqrt{\pi}}\right)\right]. \tag{7.24}$$

4. If we approximate the function R'(z) by

$$R_3'(z) = \frac{A}{1 + bz^{\nu}}, \tag{7.25}$$

which satisfies conditions (7.18) at a value of the coefficient $A = R'(0) = E_0 - E_\infty$, then according to (7.17) the first approximation of the spectrum of relaxation times is

$$H_3 = \frac{Ab\nu\tau^\nu}{(1+b\tau^\nu)^2}. \tag{7.26}$$

Although the list of approximations could be extended, we will limit ourselves to those given above, and for purposes of illustration we will use the proposed approximations to calculate the relaxation spectrum of a fiberglass plastic specimen. The calculations were done with the dimensionless quantities

$$\bar{E} = \frac{E}{E_\infty}, \quad \bar{R}' = \frac{R'}{E_\infty \dot{\varepsilon}_0} \quad \text{and} \quad \bar{H}(t) = \frac{H_i(\tau)}{E_\infty}.$$

The given values of the coefficients of the approximations of curve R'(z) were calculated from the results of experiments [Ref. 53].

The coefficients of approximation R'(z) according to (7.21) and (7.23) were determined by the method of least squares; the coefficients of expression (7.25) were determined from the condition that divergence from the experimental curve does not exceed 5%. For expression (7.22) we get the corresponding values of the coefficients [Ref. 112]:

$$A_1 = 0{,}01, \quad A_2 = 0{,}20, \quad A_3 = 0{,}30, \quad A_4 = 0{,}04,$$
$$\alpha_1 = 0{,}158, \quad \alpha_2 = 14{,}2, \quad \alpha_3 = 100, \quad \alpha_4 = 50.$$

Then the spectrum of relaxation times is calculated by formula (7.22) as follows:

$$H(\tau) = \sqrt{\tau}(0{,}45 \cdot 10^{-3} \cdot e^{-0{,}62 \cdot 10^{-2}\tau} + 0{,}81e^{-50\tau} + 8{,}5e^{-2500\tau} + 0{,}56e^{-525\tau}). \tag{7.27}$$

If curve R'(z) is approximated according to (7.23) we get

$$B = 0.0125, \quad \alpha = 0.0262.$$

Finally, expression (7.25) has the corresponding coefficients

$$A = 0.48, \quad b = 29.9, \quad \nu = 0.4.$$

The spectrum of relaxation times in this case is calculated according to (7.26) with the following coefficients:

$$H_3(\tau) = \frac{56{,}1}{(1+29{,}9\tau^{0{,}4})}\tau^{0{,}4}. \tag{7.28}$$

The results of calculations of R'(z) from expressions (7.21), (7.23) and (7.25) and the spectra of relaxation times according to (7.22), (7.24)

Fig. 7.2. Curves for R'(z) calculated from formulas: 1--(7.23); 2--(7.21); 3--(7.25); 4---experiment [Ref. 112]

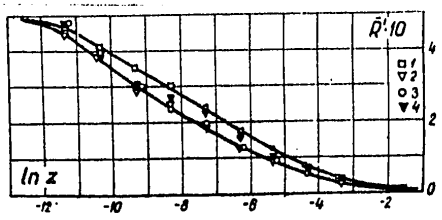

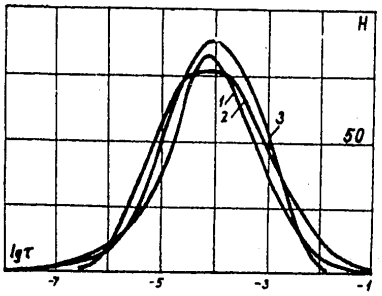

Fig. 7.3. Spectra of relaxation times for a glass cloth specimen calculated from formulas: 1--(7.22); 2--(7.24); 3--(7.26) [Ref. 53]

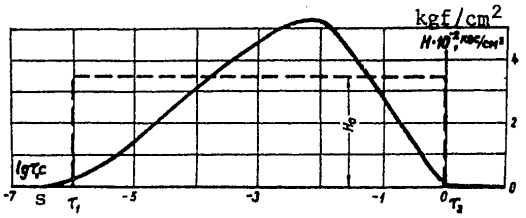

Fig. 7.4. Spectrum of relaxation times for low-density polyethylene calculated from formula (7.23). --- approximation of the spectrum by a rectangle.

and (7.24) with consideration of the values of the coefficients given above are shown in Fig. 7.2 and 7.3. As we can see from Fig. 7.3 and 7.4, using different functions to approximate the curve has little effect on the shape of the relaxation spectra. In some problems, even a quite considerable change in the shape of the spectrum has little influence on the final result for R'(z). Therefore in calculating the spectra of relaxation times one should choose the shape of the spectrum that is the simplest for computations, such as a rectangle of height H_0 and width $\tau_1 - \tau_2$. Fig. 7.4 shows two spectra. One has been obtained by using the approximation of the experimental relation R'(z) in form (7.22); and the other is a rectangle of height H_0 and width $\tau_1 - \tau_2$, where the height is the ratio $H_0 = \frac{E_0 - E_\infty}{\ln \tau_2/\tau_1}$. The approximation satisfies the requirement of equality of areas $\int_{-\infty}^{+\infty} H(\tau) d\ln\tau$ of both spectra.

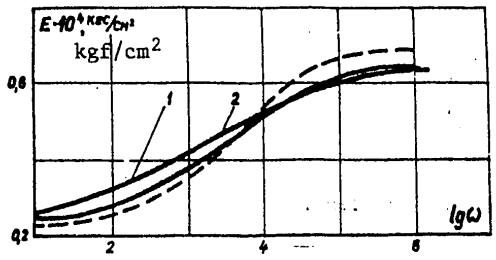

Fig. 7.5. Frequency dependence of the real part of the elastic modulus plotted by formulas: 1--(7.29); 2--(7.30); +-- experiment

We will show that corresponding to both spectra is approximately the same frequency dependence of the real part of the modulus of elasticity $E'(\omega)$, which can be expressed as

$$E'(\omega)=E_\infty+\int_{-\infty}^{\infty}\frac{H(\tau)\omega^2\tau^2}{1+\omega^2\tau^2}d\ln\tau. \tag{7.29}$$

For $H(\tau)=H_0=\text{const}$

$$E'(\omega)=E_\infty+\frac{H_0}{2}\ln\frac{1+\omega^2\tau_1^2}{1+\omega^2\tau_2^2}. \tag{7.30}$$

Fig. 7.5 shows the behavior of E' vs. lgω calculated from expressions (7.29) and (7.30). The values of the constants are as follows: $H_0=0.325\cdot10^3$ kg/cm^2; $\tau_1=10^{-6}$ s; $\tau_2=1$ s; $E_\infty=0.25\cdot10^4$ kgf/cm^2. We can see from the figure that in the case of comparatively narrow relaxation spectra, approximating the spectrum by a rectangle leads to slight deviation from the experimental data in accordance with which the spectrum was matched.

7.2. Validation of the Model of Mechanical Behavior of Polymers

The method of constructing a model of the mechanical behavior of materials considered in section 7.1 has a considerable disadvantage that shows up in the absence of proof of uniqueness of the selected law of strain. The same experimental initial behavior of E vs. lgε̇ taken as the basis of a linear model can be satisfied by a number of strain laws (see Fig. 7.3, 7.5). The method of constructing a model from the results of experiments over a wide range of strain rates or frequencies of oscillations must be supplemented by studies that confirm the subjectively chosen model of mechanical behavior. For instance the data of investigation of wave propagation in slender rods might be used for this purpse. The object of study in the given instance was rods enabling application of simple one-dimensional relations. Obviously analysis of the applicability of models based on two- or three-dimensional objects complicates the problem, and in a complex set of phenomena the effects associated with the

properties of the material are lost among similar effects due to the geometry of the specimen. To validate the model of mechanical behavior, the dynamic problem is solved on the basis of a model that is compared with an experiment on wave propagation. A conclusion as to the applicability of the model is drawn on the basis of this comparison. Given below are solutions of problems on wave propagation in viscoelastic rods. The solutions are based on the use of different models constructed from the results of experiments on creep, harmonic oscillations and quasi-static stretching. Where possible, the data of solution of the problems on wave propagation in rods have been compared with experimental results.

7.2.1. Model Based on Tests for Mechanical Vibrations

The results of experiments on harmonic oscillations are curves for the real part of the modulus of elasticity E' and tangent of the phase shift angle δ as functions of frequency. These functions are sufficient for constructing a mechanical model. Applying Fourier transformation to the Boltzmann equation

$$\sigma=\int_0^t \Psi(t-\tau)\frac{\partial \varepsilon}{\partial \tau}d\tau, \tag{7.31}$$

we get

$$\bar{\sigma}=i\omega\Psi\bar{\varepsilon}, \tag{7.32}$$

where ω is the parameter of the exponential Fourier transform (the lines over the symbols denote transformation). The ratio $\bar{\varepsilon}/\bar{\sigma}$ for small deformations is represented as

$$\frac{\bar{\sigma}}{\bar{\varepsilon}}=E(i\omega)=E'(\omega)e^{i\delta}, \tag{7.33}$$

where $E(i\omega)$ is the complex modulus of elasticity with real part $E'(\omega)$; δ is the phase shift angle. Let us note that

$$\Psi=\frac{E'(\omega)e^{i\delta}}{i\omega}; \quad \Psi(t)=\frac{1}{2\pi}\int_0^\infty \frac{E'(\omega)}{i\omega}e^{(i\omega t+i\delta)}d\omega.$$

Thus, knowing the experimental value of the functions $E'(\omega)$ and δ as the frequency varies from 0 to infinity we con construct the model:

$$\sigma=\frac{1}{2\pi}\int_0^t\int_0^\infty \frac{E'(\omega)e^{i(\omega t'+\delta)}}{i\omega}d\omega dt'\frac{\partial\varepsilon(t-t')}{\partial t'}. \tag{7.34}$$

To simplify the model, Kolsky [Ref. 141] and then a number of other researchers [Ref. 49, 149, 155] used the approximations

$$\begin{cases} c(\omega)=\dfrac{\sigma}{\rho V}=c^*\left(1+\dfrac{\operatorname{tg}\delta}{\pi}\ln\dfrac{\omega}{\omega^*}\right); \\ \delta=\text{const}, \end{cases} \tag{7.35}$$

where ρ is the density of the material, t^* is the phase velocity that corresponds to some fixed low frequency ω^*. The Fourier transform method is used to solve the problem of wave propagation with initial and boundary conditions: $U=0$ at $x=\infty$ and $t=0$; $U(0,t)$ at $x=0$, where U is displacement [Ref. 155]. Experiments have also been done that consist in registration of the force on the end face, and measurement of mass velocity in three cross sections of a polyethylene rod by using an induction pickup. Fig. 7.6 shows curves for dimensionless velocity $\tilde{V}=\rho c_0 V/\sigma_0$, where $V=\partial U/\partial t$, σ_0 is the amplitude value of the stress at $x=0$.

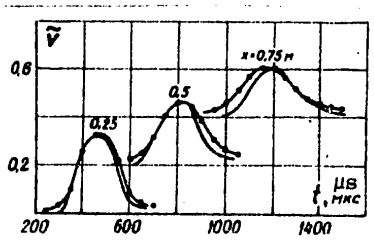

Fig. 7.6. Dimensionless velocity as a function of time in three cross sections of a rod [Ref. 155]

A model of mechanical behavior of polyethylene was constructed on the basis of experimental data for $E'(\omega)$ and $\delta(\omega)$ and approximation (7.35). The following conclusions can be drawn from a comparison of theoretical and experimental data (see Fig. 7.6): 1) satisfactory agreement between theory and experiment is observed near the end face that receives the impact. In virtue of the properties inherent in a Fourier transform, the theoretical solution leads to a velocity $V(x,t)$ that shows up in cross section x earlier than the wave with velocity c_0 arrives in this cross section; 2) as x increases, so does the discrepancy between the solution and experiment (the disparity may be caused both by the uncorrect model of the material, and by the unsatisfactory method of solving the problem). Agreement between the mechanical behavior of a quasistatic model obtained in experiments for harmonic oscillations on the one hand, and the data of experiments on wave propagation in slender rods on the other hand is also demonstrated in Ref. 49 and 149. In Ref. 149 such agreement is found for the case of wave propagation in a tapered PMMA rod. Using the Fourier method, Kolsky was the first to show the need for describing the mechanical properties of polymers by a model based on experiments over a wide range of times of action. It was he that showed that the dependence of phase velocity on very low to quite high frequencies leads to a considerable increase in the duration of a pulse as it propagates to considerable distances. Use of the Fourier transform method is quite effective in cases where the end face of the rod is comparatively smoothly loaded. As a consequence of slow convergence of the Fourier integral, the accumulation of errors in computation increases as x and t increase.

7.2.2. Model Based on Quasistatic Tests

Methods of constructing phenomenological models based on the results of experiments in creep, relaxation and uniform stretching are described in Ref. 62, 63, 84, 88, 95 and 100. Let us assume as before that validation of these models is given by agreement between the results of experiments on investigation of wave processes in rods and the corresponding theoretical solution of the problem on wave propagation. The most frequently used method of solving problems on wave propagation in viscoelastic rods is the Laplace transform method that was used in Ref. 143, 144, 150 and 164 to solve problems for the simplest models: Maxwell's [Ref. 143, 144] and the model of a standard body [Ref. 150, 164] which are special cases of the Boltzmann-Volterra strain law

$$\sigma=\int_0^t \Psi(t-\tau)\frac{\partial^2 U}{\partial x\partial\tau}d\tau. \tag{7.36}$$

The problem of wave propagation in a rod of material described by law (7.36) reduces to solution of the system

$$\begin{cases} \sigma=\int_0^t \Psi(t-\tau)\dfrac{\partial^2 U}{\partial x\partial\tau}d\tau; & (7.37a)\\ \dfrac{\partial\sigma}{\partial x}=\rho\dfrac{\partial^2 U}{\partial t^2};\quad \varepsilon=\dfrac{\partial U}{\partial x}. & (7.37b)\end{cases}$$

Equation (7.37a) corresponds to the behavior of the model shown in Fig. 7.1. To write the equation of motion for this model, we assume that each element is acted on by inertial force $\frac{E_i}{E_0}\rho\frac{\partial V}{\partial t}$, where ρ is the density of the material, $E_0=\sum_{i=1}^{n}E_i$; E_0 is the instantaneous modulus of elasticity; E_i is the modulus of elasticity of the i-th element. Summation over the individual elements of the model yields

$$\sum_{i=1}^{n}\frac{E_i}{E_0}\rho\frac{\partial V}{\partial t}=\rho\frac{\partial V}{\partial t}.$$

The equation of motion of the i-th element is

$$\frac{\partial\sigma_i}{dx}=\rho\frac{E_i}{E_0}\frac{\partial V}{\partial t};$$

with consideration of strain law (7.1) this is rewritten as

$$\frac{\partial^2\sigma_i}{\partial x^2}=\rho\frac{E_i}{E_0}\frac{\partial^2\varepsilon}{\partial t^2}=\rho\frac{E_i}{E_0}\left(\frac{1}{E_i}\frac{\partial^2\sigma_i}{\partial t^2}+\frac{\partial\sigma}{\partial t}\frac{1}{E_i\tau_i}\right). \tag{7.38}$$

Finally, (7.38) can be represented as follows:

$$c_0^2\frac{\partial^2\sigma_i}{\partial x^2}=\frac{\partial^2\sigma_i}{\partial t^2}+\frac{1}{\tau_i}\frac{\partial\sigma_i}{\partial t},\quad c_0=\sqrt{\frac{E_0}{\rho}}. \tag{7.39}$$

Corresponding to each equation (7.39) is a pair of characteristics

$$dx=\pm c_0dt \tag{7.40}$$

and the conditions thereon

$$d\sigma_i=\mp\frac{E_i}{E_0}\rho c_0dV-\sigma_i\frac{dt}{\tau_i}. \tag{7.41}$$

Considering that

$$\sigma_i=E_i\varepsilon-\int_0^t\frac{E_i}{\tau_i}e^{-\frac{t-\xi}{\tau_i}}\varepsilon(\xi)d\xi, \tag{7.42}$$

by summing the stresses over the elements and passing to the limit, we get

$$d\sigma=\mp\rho c_0dV-\varepsilon\int_0^\infty\frac{H(\tau)d\tau}{\tau^2}dt+$$
$$+dt\int_0^t\int_0^\infty\frac{H(\tau)}{\tau^3}d\tau e^{-\frac{t-\xi}{\tau}}\varepsilon(\xi)d\xi. \tag{7.43}$$

Using the notation

$$\Psi'(0)=\int_0^\infty\frac{H(\tau)}{\tau^2}d\tau;$$
$$\Psi'(t)=\frac{\partial}{\partial t}\int_0^\infty\frac{H(\tau)}{\tau}e^{-\frac{t}{\tau}}d\tau=-\int_0^\infty\frac{H(\tau)e^{-\frac{t}{\tau}}}{\tau^2}d\tau;$$
$$\Psi''(t)=\int_0^\infty\frac{H(\tau)}{\tau^3}e^{-\frac{t}{\tau}}d\tau; \tag{7.44}$$

we rewrite (7.43) as

$$z=t-\frac{x}{c_0}. \tag{7.45}$$

On the characteristic $dx = 0$; $x = x^*$

$$d\sigma=E_0 d\varepsilon-dt\left[\varepsilon\Psi(0)-\int_0^{z^*}\Psi'(z^*-\xi)\varepsilon(\xi)d\xi\right], \tag{7.46}$$

where $z^* = t - \frac{x^*}{c_0}$. Let us find the change in stress on the leading edge of the wave. Since on the leading edge

$$[\sigma]=-\rho c_0[V];\quad [\sigma]=E_0[\varepsilon],$$

we get from (7.46)

$$2d[\sigma]=-dt\frac{\Psi'(0)}{\Psi(0)}[\sigma], \tag{7.47}$$

where $E_0 = \rho c_0 = \Psi(0)$ is the instantaneous modulus of elasticity (the symbols in brackets denote discontinuities of the corresponding quantities). Integration of (7.47) gives*:

$$[\sigma]=\sigma_0\exp\left[-\frac{\Psi'(0)}{2\Psi(0)}\cdot\frac{x}{c_0}\right]. \tag{7.48}$$

Let us note that in order to account for equilibrium pliability it is necessary to substitute the constant $\Psi(0)$:

$$\Psi(0)=\int_{-\infty}^{+\infty}H(\tau)d\ln\tau=E_0-E_\infty.$$

Relations (7.45), (7.46) and (7.48) are sufficient for numerical solution of the problem with the given initial and boundary conditions.

It should be emphasized that the choice of functions $\Psi(t)$ at which $\Psi(0)\to\infty$ leads to infinite attenuation of discontinuities on the leading edge. Infinite attenuation of discontinuities of stresses on the leading

*The same result, obtained by the Laplace transform method, is given in Ref. 63.

edge of a wave takes place in the case of models with weakly singular waves. Let us assume that in the strain law

$$\sigma = E_0\varepsilon - (E_0 - E_\infty)\int_0^t \Psi'(t-\tau)\varepsilon(\tau)\,d\tau$$

the function $\Psi'(t)$ is selected according to Ref. 88:

$$\Psi'(t) = \frac{a^\beta e^{-at}}{\Gamma(\beta)\,t^{1-\beta}} \tag{7.49}$$

($a > 0$, $0 < \beta < 1$; $\Gamma(\beta)$ is the gamma function; α, β = const). In accordance with (7.48) one should expect an absence of discontinuities on the leading edge since $\Psi'(0) \to \infty$. In Ref. 6 a solution is found for the problem of wave propagation in a rod of material described by the model of A. R. Rzhanitsyn [Ref. 88]. Solutions found in Ref. 6 for initial and boundary conditions of $x = 0$, $\sigma(t) = \sigma_0 H(t)$; $x = \infty$, $t = 0$, $V = U = \sigma = 0$, where $H(t)$ is the heaviside function, have shown the following (Fig. 7.7, 7.8):

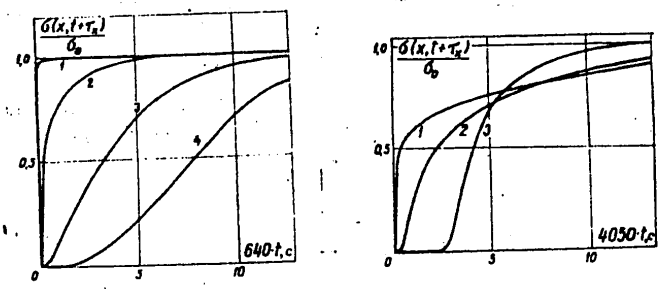

Fig. 7.7. Relations for σ vs. t at values of the constants $a = 10^{-3}$ s^{-1}; $\beta = 0.5$ at coordinates of the rod x, in meters: 1--1/6; 2--10/3; 3--50/3; 4--100/3 [Ref. 6]

Fig. 7.8. Curves for σ vs. t at $x = 10.3$ m and values of the constants $a = 10^3$ s^{-1}, and β: 1--0.7; 2--0.3; 3--0.05 [Ref. 6]

1) there are no discontinuities of stresses on the leading edge anywhere except in the cross section $x = 0$; 2) the influence that the kernel parameter β has on the propagation of a perturbation is expressed in the fact that the greater the value of β, the steeper the front of the curve for σ vs. t (at $\beta = 1$ there is a shock on the wavefront).

Thus it can be concluded that in order to choose models of mechnaical behavior, in addition to the requirement for the type of equation of motion (hyperbolic), it is necessary to introduce a condition that limits the function $\Psi(t)$ at $t = 0$. The physical premise of this condition is the fact that most known materials show pure elasticity during deformation,

which should cause propagation of discontinuities when a one-dimensional rod is loaded by steps.

Validation of model obtained from quasistatic tests over a wide range of strain rates. To sustain discontinuities on the leading edge of a wave, as we have shown, the model must have a corresponding finite value of $\Psi'(0)$. Corresponding to the condition of boundedness of $\Psi'(0)$ is a rectangular spectrum in the time interval τ_1-τ_2, since assignment of the limits of integration for $\Psi'(0)=\int_{\tau_1}^{\tau_2}\frac{H_0 d\tau}{\tau_2}$ leads to the situation that the integral becomes convergent for real functions H(t). For a rectangular spectrum

$$\frac{\Psi'(0)}{\Psi(0)}=\left(1-\frac{E_\infty}{E_0}\right)\left(1-\frac{\tau_1}{\tau_2}\right)\tau_1^{-1}\left(\ln\frac{\tau_2}{\tau_1}\right)^{-1},$$

and attenuation of the discontinuity on the leading edge occurs in accordance with the formula

$$[\sigma]=\sigma_0\exp\left[-\frac{\left(1-\frac{E_\infty}{E_0}\right)\left(1-\frac{\tau_1}{\tau_2}\right)}{2\tau_1\ln\frac{\tau_2}{\tau_1}}\frac{x}{c_a}\right]. \tag{7.50}$$

As $\tau_1\to\tau_2$ we have a transition to a spectrum in the form of a δ-function, which corresponds to a model with one relaxation time τ, and

$$[\sigma]=\sigma_0\exp\left[-\frac{\left(1-\frac{E_\infty}{E_0}\right)\frac{x}{c_0}}{2\tau}\right]. \tag{7.51}$$

Expression (7.51) agrees with known solutions [Ref. 63, 144, 150, 164].

Given below is the validation of an idealized model that corresponds to a relaxation spectrum in the form of a rectangle (see Fig. 7.4), and also a method of experimentally finding the constants of the material (E_0, E_∞, τ_1 and τ_2) that completely determine a rectangular spectrum with height $H_0=\frac{E_0-E_\infty}{\ln\tau_2/\tau_1}$. Corresponding to a rectangular spectrum of width τ_1-τ_2 and height H_0 is a discrete model (Fig. 7.1) in which the relaxation times $\tau_i=\eta_i/E_i$ vary over a range of $\tau_1\leqslant\tau_i\leqslant\tau_2$, and the moduli of elasticity of the elements are $E_i=H_0 d\ln\tau_i$. The constants E_∞ and τ_2 are determined from static experiments, while E_0 and τ_1 are determined from dynamic experiments. Ideally, these experiments should be done at strain rates of

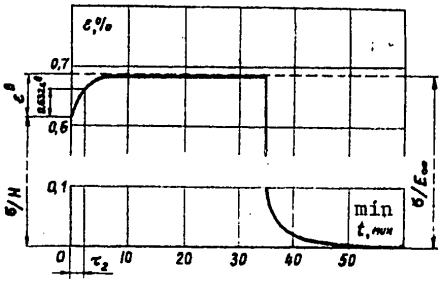

Fig. 7.9. On the method of determining constants E_∞ and τ_2 from the creep curve [Ref. 68]

$\dot{\varepsilon} \to 0$ and $\dot{\varepsilon} \to \infty$. Experiments on uniform stretching, creep or relaxation can serve as static tests, and experiments on studying the propagation of waves are in the dynamic class.

The approximating constants are validated as follows.

Experimental determination of the constants. The technique for determining the constants E_∞ and τ_2 for materials that show equilibrium pliability during creep [Ref. 68] is illustrated by Fig. 7.9. E_∞ can be determined with adequate precision in practice. It is not possible to determine the constant E_0 with acceptable accuracy from experiments on creep. However, from these experiments we can get a rough idea of E_0 that can then be corrected in accordance with the experimental results on studies of wave propagation. Fig. 7.9 also shows a method of determining the constant τ_2 in an approximate treatment of the material as a linear standard body at low strain rates. Hereafter the value of τ_2 will be given the meaning of the right-hand boundary of the rectangular spectrum (see Fig. 7.4). It should be noted that the assumption that the material is described by a single characteristic relaxation time during creep leads to neglect of relaxation processes at large times which, it can be assumed, do not affect the dynamic behavior of polymers during impact.

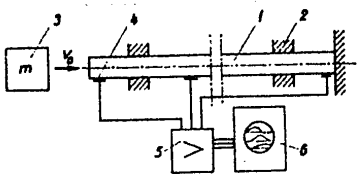

Fig. 7.10. Diagram of experiment to study wave propagation in a rod: 1--specimen; 2--supports; 3--impacting mass; 4--strain gage; 5--strain-gage amplifier; 6--oscilloscope

Experimental determination of constants E_0 and τ_1 based on studying wave propagation [Ref. 52]. A diagram of an experiment with fiberglass plastic rods (diameter 10 mm, length 1 m) is shown in Fig. 7.10. Impact was by a mass against the end face of the rod. The other end rested on a massive rigid plate. Strain gages with a 5 mm base were cemented to the middle of the rod and close to the end faces. Signals from the strain gages, amplified by a three-channel strain-gage amplifier, were sent to the input of an oscilloscope. Fig. 7.11 shows a typical deformation-time oscillogram obtained upon impact of a

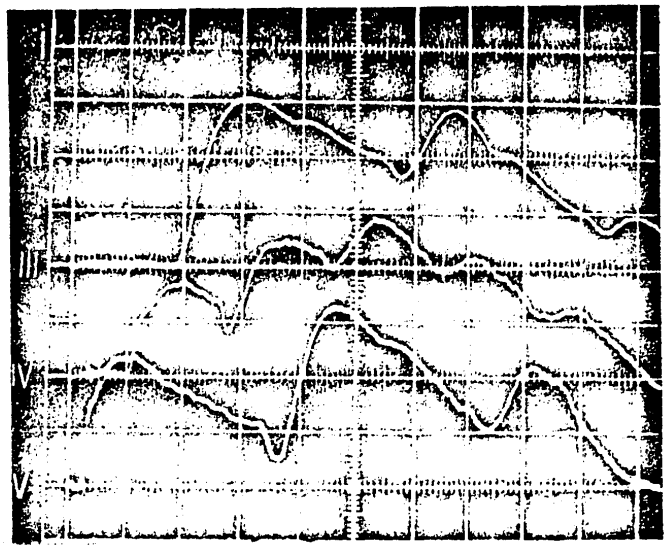

Fig. 7.11. Typical oscillograms of ε vs. t on the ends of a rod (beams I and III) and in cross section $x = L/2$ (beam II). Scales of the oscillograms: along the horizontal $t = 200$ 1/div; along the vertical $\varepsilon = 2 \cdot 10^{-4}$ 1/div.

mass of $m = 0.3$ kg with initial velocity $V_0 = 1.8$ m/s. From the oscillograms we can clearly see the wave nature of the process of rod loading. Calculation of the rate of propagation of the leading edge of the wave enables determination of the constant E_0. The dependence of ε vs. t at $t = 0$ is used to determine τ_1.

Method of determining constant τ_1. The mechanical behavior of a polymer for small t is described in the form

$$\dot{\sigma} = E_0 \dot{\varepsilon} - \frac{\sigma - E_\infty \varepsilon}{\tau_1}. \tag{7.52}$$

Boundary and initial conditions of the problem. To solve the problem, the boundary condition at $x = 0$

$$F \int_0^t \sigma dt = -m \left(V_0 - \frac{\partial U}{\partial t} \right) \tag{7.53}$$

can be transformed to the condition $V(t) = V_0 - \nu t + \beta t^2 - \ldots$, where the function V(t) is expressed in the form of an infinite series, F is the cross sectional area of the rod, ν, $\beta = \text{const}$. Limiting ourselves for small t to the first two terms of the expansion, we find

$$V(t) \simeq V_0 - \frac{M[\sigma]}{\rho L} t, \tag{7.54}$$

where $[\sigma]$ is discontinuity of the stress on the leading edge at $x = 0$, M is the ratio of masses of the rod and striker, L is the length of the rod. Finally we can express V(t) as

$$V(t) \simeq V_0\left(1 - \frac{Mc_0 t}{L}\right). \tag{7.55}$$

The second boundary condition: $x = L$, $U = 0$.

In the following it is necessary to use dimensionless time $\tilde{t} = t/\tau_0$ along with equation (7.52) under boundary conditions (7.55). Initial conditions: at $t = 0$, $U = \sigma = \varepsilon = 0$.

Solution of the problem for $x = 0$. The problem consists in solution of a system comprised of (7.52 and the equation $\frac{\partial \sigma}{\partial x} = \rho \frac{\partial V}{\partial t}$ with consideration of boundary conditions (7.55). The solution reduces to finding the original for the expressions

$$\sigma(0, s) = \frac{\rho c_0 V_0}{s}\left(1 - \frac{Mc_0}{Ls}\right)\left(\frac{s + \frac{1}{\tau_1}}{s + \frac{1-\lambda}{\tau_1}}\right); \tag{7.56a}$$

$$\bar{\varepsilon}(0, s) = \frac{\bar{\sigma}}{E_0} \frac{s + \frac{1}{\tau_1}}{s - \frac{1-\lambda}{\tau_1}}, \tag{7.56b}$$

where $\lambda = 1 - \frac{E_\infty}{E_0}$. Inverse transformation of (7.56a) and (7.56b) gives:

$$\sigma(0, \tilde{t}) = -\rho c_0 V_0\left[e^{-\frac{2-\lambda}{2}\tilde{t}} I_0\left(\frac{\lambda \tilde{t}}{2}\right) + \right.$$
$$+\left(1 - \lambda - \frac{Mc_0\tau_1}{L}\right) \times \int_0^{\tilde{t}} e^{-\frac{2-\lambda}{2}\tilde{t}} I_0\left(\frac{\lambda \tilde{t}}{2}\right) d\tilde{t} -$$
$$\left. - (1-\lambda)\frac{Mc_0\tau_1}{L} \int_0^{\tilde{t}}\left(\int_0^{\tilde{t}} e^{-\frac{2-\lambda}{2}\xi} I_0\left(\frac{\lambda\xi}{2}\right) d\xi\right) d\theta\right]; \tag{7.57a}$$

$$-\varepsilon(\Theta, \tilde{t}) = \frac{V_0}{c_0}\left[e^{-\frac{2-\lambda}{2}\tilde{t}} J_0\left(\frac{\lambda \tilde{t}}{2}\right) + \left(1 - \frac{Mc_0\tau}{L}\right)\int_0^{\tilde{t}} e^{-\frac{2-\lambda}{2}\tilde{t}} J_0\left(\frac{\lambda \tilde{t}}{2}\right) d\tilde{t} - \right.$$

$$\left. - \frac{Mc_0}{L}\tau \int_0^{\tilde{t}} \left(\int_0^{\Theta} e^{-\frac{2-\lambda}{2}\xi} J_0\left(\frac{\lambda\xi}{2}\right) d\xi \right) d\Theta \right]. \qquad (7.57b)$$

where J_0 is the zero-order Bessel function of the purely imaginary argument. For $M = 0$ we have $V = V_0 = \text{const}$; solutions (7.57a) and (7.57b) coincide with the relations obtained in Ref. 144, 150, 164]. At $\lambda = 1$ we arrive at Maxwell's model. For $\lambda = 1$, $M = 0$ the solution coincides with the expression for σ and ε found in Ref. 143. Stresses and strains were calculated on a computer using formulas (7.57a) and (7.57b) for a set of values of constants τ_1 (Fig. 7.12). As a result of comparison of theoretical curves for different τ with experiment, the value of τ_1 was found to be 42.5 μs for fiberglass plastic with 50% filler, and about 10 μs for PMMA. For unidirectional fiberglass plastic $\tau_1 = 70$ μs. It should be noted that the given solution implies that expression (7.57a) is little dependent on the coefficient τ (see Fig. 7.12), which means that deformations can be resolved into elastic and viscous components (Fig. 7.13). The quantity τ_1 is an important characteristic of material since it can be considered as a limit on the time axis of the relaxation spectrum of the material.

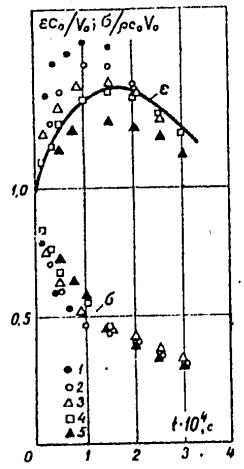

Fig. 7.12. Curves for σ vs. t and ε vs. t at $x = 0$. The calculations were done at values of the constants τ in μs of: 1--16.7; 2--25; 3--32; 4--42; 5--62; --- experiment.

Thus we can consider all four constants that characterize rectangular distribution of relaxation times experimentally determined. However, validation of the limits of the spectrum and its height is necessary, but not sufficient for substantiation of the model as a whole. To validate the model we must compare experimental registration of the wave process with solution of the problem of wave propagation in the material whose properties are assigned by the spectrum.

Numerical solution of the problem of impact of a rigid mass against a viscoelastic rod. Henceforth we use rectangular distribution of relaxation times with height H_0 in interval τ_1-τ_2 which corresponds to the Laplace transform of function Ψ

(7.58)

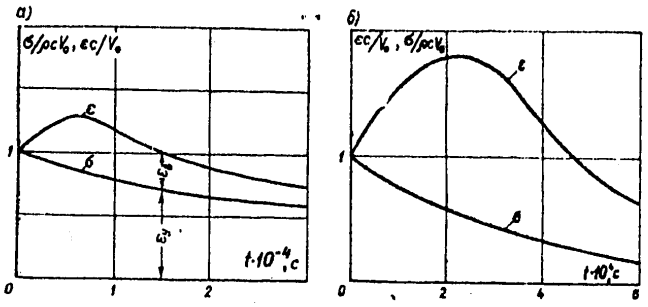

Fig. 7.13. Functions σ vs. t and ε vs. t calculated for unidirectional fiberglass plastic at τ = 70 μs (a) and PMMA at τ = 10 μs (b). The graph (a) shows the possibility of approximate separation of deformation into elastic ε_y and viscous ε_θ components.

where E_∞ is the equilibrium modulus.

Impact of a rigid body against an elastic rod was considered by St. Venant [see Ref. 22]. The assumptions that he made included consideration of only uniform propagation of waves in the rod, disregard of the process of oscillations in the struck body, and the assumption of ideally plane contact surfaces. An analogous problem is considered below. The processes following cessation of contact of the striking body with the end face of the rod are not considered. Just as St. Venant did, let us take the boundary conditions and initial conditions

$$\begin{aligned} &x=L; \quad U=0; \\ &x=0; \int_0^t P dt = -m\left(V_0 - \frac{\partial U}{\partial t}\right); \\ &t=0; \quad U=\sigma=V=0. \end{aligned} \tag{7.59}$$

In the following we will use the Laplace transform

$$f(s)=\int_0^\infty F(t)e^{-st}dt$$

with transformation parameter s. The transformed equation of motion for an elastic rod with elastic modulus E will have the form

$$\frac{d^2U}{dx^2}=s^2\frac{U}{c_0^2}, \tag{7.60}$$

and solution of the problem corresponds to

$$U = c_1 e^{-\frac{xs}{c_0}} + c_2 e^{\frac{xs}{c_0}}. \tag{7.61}$$

Transforming the boundary conditions, we get

$$\frac{dU}{dx} = -\frac{L}{Mc_0^2}(V_0 - Us^2), \tag{7.62}$$

where c_0 is the velocity of propagation of elastic waves, $M = \rho FL/m$ (ρFL is the mass of the rod). From (7.61) and (7.62) with consideration of the second boundary condition for U we have

$$c_1 = -c_2 e^{-\frac{2Ls}{c_0}} =$$

$$= \frac{V_0 L}{Mc_0 s\left(1+\frac{Ls}{Mc_0}\right)}\left(1+\frac{1-\frac{Ls}{Mc_0}}{1+\frac{Ls}{Mc_0}}e^{-\frac{2Ls}{c_0}}\right)^{-1}.$$

Representing

$$\left(1+\frac{1-\frac{Ls}{Mc_0}}{1+\frac{Ls}{Mc_0}}e^{-\frac{2Ls}{c_0}}\right)^{-1}$$

as the sum of a geometric series

$$\sum_{n=0}^{\infty}(-1)^n\left(\frac{1-\frac{Ls}{Mc_0}}{1+\frac{Ls}{Mc_0}}\right)^n e^{-\frac{2Ls}{c_0}n},$$

we get

$$U = -\frac{V_0 L}{Mc_0}\frac{e^{-\frac{sx}{c_0}} - e^{-\frac{s(2L-x)}{c_0}}}{s\left(1+\frac{Ls}{Mc_0}\right)}\sum_{n=0}^{\infty}(-1)^n\left(\frac{1-\frac{Ls}{Mc_0}}{1+\frac{Ls}{Mc_0}}\right)^n e^{-\frac{2Ls}{c_0}n}. \tag{7.63}$$

Inverse transformation of relation (7.63) for n = 0, 1, 2, 3... completely coincides with the St. Venant solution for times that do not exceed the duration of contact of the end face of the rod with mass m.

Consider the case of impact against a viscoelastic rod. Applying Laplace transformation with respect to variable t to strain law (7.36), we get

$$\bar{\sigma}=\Psi s\bar{\varepsilon}=\bar{\Psi}s\frac{d\bar{U}}{dx}. \tag{7.64}$$

Substituting in (7.64) the value of Ψ corresponding to a rectangular relaxation spectrum, we get

$$\bar{\sigma}=\rho c^2(s)\bar{\varepsilon}, \tag{7.65}$$

where

$$c(s)=\sqrt{\frac{\bar{\Psi}s}{\rho}}=\sqrt{c_\infty^2+\frac{H_0}{\rho}\ln\frac{1+\tau_2 s}{1+\tau_1 s}};\quad c_\infty=\sqrt{\frac{E_\infty}{\rho}}.$$

Solving (7.65) simultaneously with the equation of motion in its transformed representation with consideration of the same initial values as in the preceding case we get

$$\frac{d^2\bar{U}}{dx}=s^2\frac{\bar{U}}{c^2(s)}. \tag{7.66}$$

Thus in the space of images the solution of the problem of impact against a viscoelastic rod will have the same form as in (7.63) with the difference that in the latter case c(s) should be substituted in (7.63) instead of c_0. Inversion of the resultant dependence meets with a number of difficulties that we have obviated by using a method of numerical inversion for which a computer program was set up and a number of graphs were plotted (Fig. 7.14).

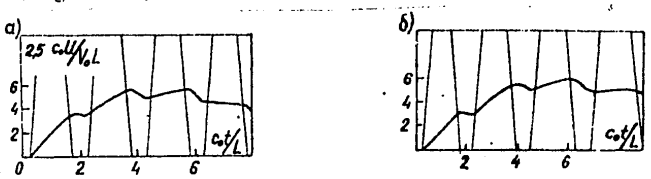

Fig. 7.14. Results of numerical calculations for displacements in one cross section of a rod with material described by a rectangular spectrum with constants: a--$c_0=5000$ m/s; $c_\infty=E_\infty/\rho=4000$ m/s; $\tau_1=10^{-4}$ s; $\tau_2=10^{-1}$ s; b--$c_0=E_0/\rho=1600$ m/s; $c_\infty=E_\infty/\rho=800$ m/s; $\tau_1=10^{-3}$ s; $\tau_2=10^{-1}$ s; $m/M=12$.

Comparison of theory [Ref. 54, 56] and experiment [Ref. 38] (Fig. 7.15) at a ratio of $L/M=20$ m and $V_0=0.5$ m/s is shown in Fig. 7.16. The satisfactory agreement of experimental and calculated data (Fig. 7.16) is evidence that the model is sound.

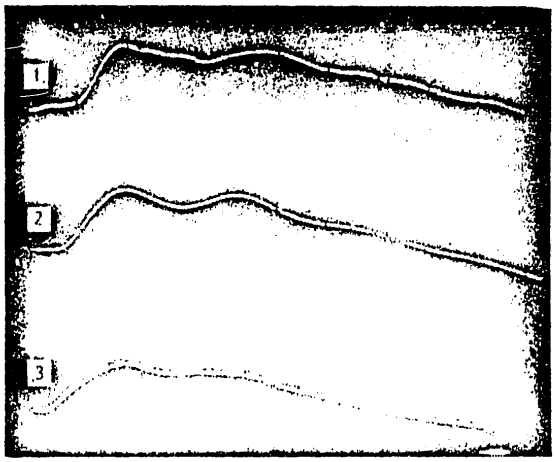

Fig. 7.15. Oscillograms of U vs. t for rod cross sections of 0.03, 0.6 and 0.9 m corresponding to amplification of 1:1, 2:1 and 3:1 (curves 3-1)

Fig. 7.16. Theoretical (———) and experimental (- - -) relations for U vs. t

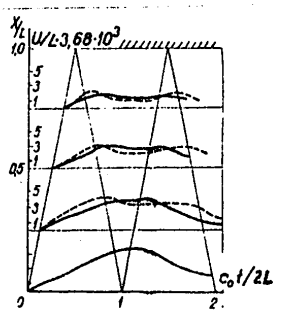

7.3. Validation of Model from a Study of Propagation of Added Load Pulses

To describe nonlinear behavior of materials one most frequently uses a model of the Malvern-Sokolovskiy type [see Ref. 86]:

$$\dot{\sigma}=E_0\dot{\varepsilon}-g[\sigma-f(\varepsilon)], \tag{7.67}$$

where $\sigma = f(\varepsilon)$ is the static stress-strain diagram; g(z) is some nonlinear function. In the nonlinear theory of viscoelasticity equation (7.67) occupies a special place since it can be compared with physically validated strain laws such as the Gurevich equation

$$\dot{\varepsilon}=\frac{\dot{\sigma}}{E}+\frac{\sigma-E_*\varepsilon^b}{\eta(\sigma,\ T)}, \tag{7.68}$$

where ε^b and E_* are viscous deformation and the long-term elastic modulus; $\eta(\sigma, T) = E_*\tau$ is the viscosity, which is a function of stress and temperature. Since $\varepsilon^b = \varepsilon - (\sigma/E)$, (7.68) can be written as

$$\dot{\varepsilon} = \frac{\dot{\sigma}}{E} + \frac{1}{\eta(\sigma, T)}\left[\sigma\left(1 + \frac{E_*}{E}\right) - E_*\varepsilon\right]. \tag{7.69}$$

The physical justification for using (7.69) may be experimental results of quasistatic tests of polymers over a wide range of strain rates. In particular, the dependence of characteristic relaxation times on stress, taken in the form

$$\tau(\sigma, T) = \tau_0 \exp\frac{U_0 - \gamma\sigma}{RT},$$

leads to an Eyring equation (see chapter 6) that agrees with experiment. It has been shown [Ref. 13] that equation (7.69) leads to the form

$$\varepsilon(t) = \frac{\sigma(t)}{E_t} + \int_0^t \sigma(z) D'[\xi(t) - \xi(z)]\, a(z)\, dz;$$

$$\xi(t) = \int_0^t a\, dt', \tag{7.70}$$

where $a = \frac{\eta_0}{\eta} = \frac{\tau_0}{\tau}$; $D(\xi)$ is the creep function. For model (7.69)

$$D'(\xi) = \frac{1}{E} + \frac{1}{E_*}\left(1 - e^{-\frac{\xi}{\tau_0}}\right); \quad \tau_0 = \frac{\eta_0}{E_*}. \tag{7.71}$$

Nonlinear relation between stress and strain may be formally complicated if a complex creep function is used instead of the very simple function $D(\xi)$ of (7.71). In this case (7.70) describes the stress-strain dependence over a wide time range. The simple function $D'(\xi)$ is suitable for describing mechanical behavior over a narrow time range, and equation (7.70) can be expressed in form (7.67). The feasibility of using equation (7.67) to describe wave propagation is considered below. The simplest relation between stress and strain is considered in which $g(z) = z$.

Studies of added load pulses in a rod of material corresponding to a nonlinear convex stress-strain diagram prove the following.

1. The following nonlinear model, which is a special case of relation (7.67) is taken for quantitative description over a narrow range of strain rates:

$$\dot{\sigma} = E\dot{\varepsilon} - \frac{\sigma - f(\varepsilon)}{\tau}; \tag{7.72}$$

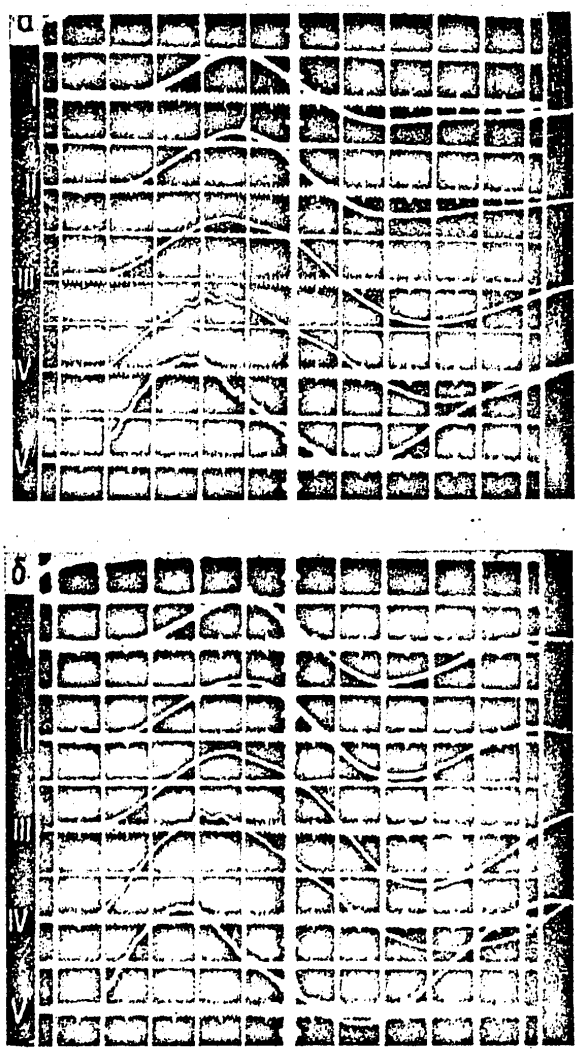

Fig. 7.17. Oscillograms of P vs. t and V vs. t for preliminary stresses $\varepsilon = 0.83\%$ (a) and $\varepsilon = 2.0\%$ (b). Oscilloscope beams: I--V vs. t at x = 1.5 m; II--V vs. t at x = 1.0 m; III--V vs. t at x = 0.5 m; IV--V vs. t at x = 0; V--P vs. t at x = 0

where τ is relaxation time ($\tau = \text{const}$), $\sigma = f(\varepsilon)$ is the static stress-strain diagram.

The quasilinear wave equation stemming from (7.72) and the equations of motion $\frac{\partial \sigma}{\partial x} = \rho \frac{\partial V}{\partial t}$ correspond to the characteristics and conditions thereon:

$$\begin{aligned} dx &= \pm c_0 dt; \quad d\sigma = \pm \rho c_0 dV - \frac{\sigma - f(\varepsilon)}{\tau} dt; \\ dx &= 0; \quad d\sigma = E_0 d\varepsilon - \frac{\sigma - f(\varepsilon)}{\tau} dt. \end{aligned} \tag{7.73}$$

For the case of low-amplitude added load pulses equation (7.72) is linearized: $f(\varepsilon) = E(\sigma_{CT})\varepsilon$, where $E(\sigma_{CT})$ is the value of $\partial\sigma/\partial\varepsilon$ at the point corresponding to pretensioning on the stress-strain diagram.

As shown by B. M. Malyshev [Ref. 69], registration of velocities by induction sensors enables determination of stress by using the conditions on characteristics (7.68) written in piecewise-difference form.

Fig. 7.17 shows the results of an experiment [Ref. 49] on studying propagation of added loading pulses in a polyethylene rod 1.5 m long and 3 mm in diameter. Velocities were recorded for four cross sections of the specimen. To compare the computed stress based on (7.73) with the actual value, data are given for force registration by a piezoelectric sensor on the end face. It was established as a result of the studies that the process of wave propagation is affected by pretensioning; as the force of pretensioning increases, there is an increase in the coefficient τ in (7.67); at large values of t/τ (1.75-2.0) the slope of dynamic diagrams plotted from (7.73) does not differ from that on the static diagram (see Fig. 7.18).

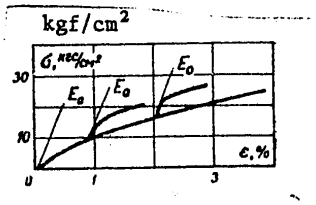

Fig. 7.18. Stress-strain diagrams obtained by studying added load pulses. The static diagram is on the lower part of the graph

2. Linearization of the nonlinear model (7.67) is sensible at sufficiently short times and at a short distance from the end. To describe wave phenomena in the rod that are far from the leading edge, the given linearization does not give satisfactory agreement between experiment and theory.

Experimental data [Ref. 49] have been compared with the results of numerical computer solutions* on wave propagation in a rod whose behavior is described by model (7.67) with initial conditions of the problem: $t = 0$,

*The calculations were done by V. P. Shapeyev and S. V. Meleshko at the Computing Center, Siberian Affiliate, USSR Academy of Sciences.

$\sigma = U = V = 0$. The boundary condition was the experimental behavior of σ vs. t (see Fig. 7.17), i. e. at $x = 0$ $\sigma = f_1(t)$. The function $\sigma = f(\varepsilon)$ was determined from static experiments. In the solution, the $g(\sigma,\varepsilon)$ were not assigned in analytical form. The function $g(\sigma,\varepsilon)$ was determined from experiment (see Fig. 7.17a) (pretensioning 0.83%) in such a way that the experimental results for the velocities V of the four cross sections differ minimally from the calculated values (Fig. 7.19). To check the certainty of the resultant function $g(\sigma,\varepsilon)$, V was calculated for the same cross sections with pretensioning of 2%, where $g(\sigma,\varepsilon)$ was already known. Successful agreement of the solution with the experiment can be taken as substantiation of the function $g(\sigma,\varepsilon)$ (Fig. 7.20), and hence of the model as a whole.

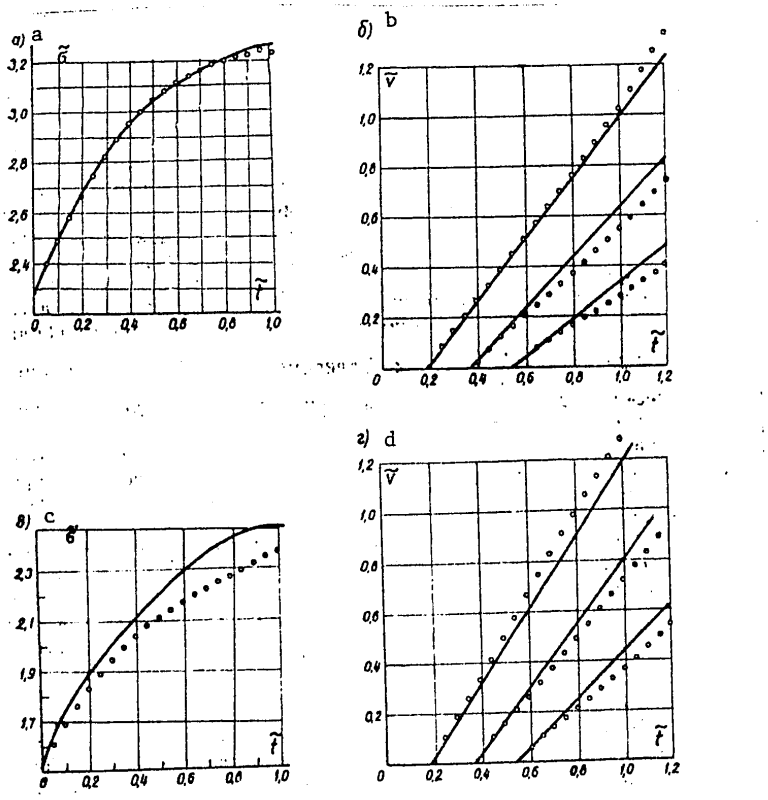

Fig. 7.19. Dimensionless relations $\tilde{\sigma}$ vs. $\tilde{t}$ and $\tilde{V}$ vs. $\tilde{t}$. Numerical calculations (points) and experiment (- - -) for values of $\varepsilon_{CT} = 0.83\%$ (a, b) and $\varepsilon_{CT} = 2.0\%$ (c, d). Values of the dimensionless variables: $\tilde{\sigma} = \sigma/6.6$, $\tilde{t} = t/2.25 \cdot 10^{-4}$, $\tilde{V} = V$.

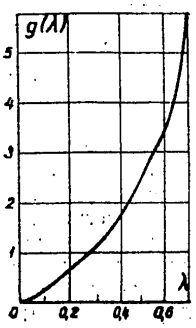

Fig. 7.20. Function $g(\lambda)$: $\lambda = 1/6.6\ [\sigma - f(\varepsilon)]$ kgf/cm^2; $g = 1/2.25\ 10^{-3}$ g, kgf/cm^2·s.

* * *

The behavior of mechanical properties of amorphous and crystalline polymer materials as a function of strain rate is determined by relaxation processes that take place during deformation. The relaxation transitions in polymers can be studied from the dependence of mechanical behavior over a wide range of strain rates. Based on a study of the mechanical properties of amorphous polymers with wide variation of temperature and strain rate, the feasibility of using temperature-time analogy is proved. The dependence of the yield stress of amorphous polymers on the logarithm of the strain rate takes the form of two straight lines with a small transition section. The behavior of σ_s/T vs. $\lg\dot{\varepsilon}$ is satisfactorily described by the Eyring equation that accounts for simultaneous occurrence of two relaxation processes (α and β). For a polymer such as polystyrene that does not show secondary relaxation processes in addition to the main process, the yield stress is a linear function of the logarithm of the strain rate.

The strength properties of amorphous polymers strained at different rates and temperatures are basically described by the kinetic theory of strength of solids right down to the short-term loads at which testing time becomes commensurate with the time required for crack propagation over the width of a specimen.

The curves that characterize the mechanical properties of crystalline polymers are more complicated than those that reflect the behavior of amorphous polymers because of three pronounced relaxation transitions (α, β and γ). Corresponding to these transitions, the curve for σ_s vs. $\lg\dot{\varepsilon}$ has three sections for most crystalline polymers.

Some polymer materials (fluorocarbon, polyformaldehyde) are typified by only α- and γ-transitions, and accordingly there are two sections on the curve for σ_s vs. $\lg\dot{\varepsilon}$.

The laws of strength of crystalline polymers do not conform to existing concepts of the theory of kinetic strength since destruction of the polymers involves the considerable influence of a change in supermolecular structure. The dependences of mechanical characteristics (including strength) of strongly crystallized polymers such as polyformaldehyde correspond to the patterns of amorphous polymers. Peculiarities of the influence that strain rate has on the mechanical properties of reinforced materials are a reduction in the degree of anisotropy as strain rate increases, and linear dependence of the modulus of elasticity and tensile strength on strain rate. The limits of strength are nearly linearly dependent on durability in logarithmic coordinates.

It is proposed that the materials of investigation of wave propagation in rods be used to validate models constructed on the basis of data of quasistatic experiments. A model is considered validated if it satisfactorily describes wave processes. A model derived from experiments on harmonic oscillations describes wave propagation far from the end face that takes the impact, and also when the rod is loaded by a continuous function that is fairly smooth in time.

A model of mechanical behavior derived from quasistatic tensile experiments, which is described by a relaxation spectrum in the form of a rectangle with height H_0 in the time interval τ_1-τ_2, gives a good description of wave propagation in a rod in the case of additional validation of the constants τ_1, τ_2 and $H = \frac{E_0 - E_\infty}{\ln \tau_1/\tau_2}$.

A nonlinear law of the Sokolovskiy-Malvern type gives a good description of wave propagation for added load pulses in a polyethylene rod.

REFERENCES

1. L. Aynola, U. Nigul, "Wave Processes in Deformation of Elastic Plates and Shells," IZVESTIYA AKADEMII NAUK ESSR, SERIYA FIZIKO-MATEMATICHESKIKH I TEKHNICHESKIKH NAUK, Vol 14, No 1, 1965, pp 3-63.

2. A. A. Askadskiy, "Deformatsiya polimerov" [Deformation of Polymers], Moscow, "Khimiya," 1973, 448 pp.

3. L. V. Andreyev, I. N. Krushel'nitskiy, I. D. Pavlenko et al., "Dynamic Stability of Reinforced Cylindrical Shells Under Loading by an External Pressure Pulse," MEKHANIKA TVERDOGO TELA, No 1, 1974, pp 118-125.

4. N. A. Zlatin, G. I. Mishin, editors, "Ballisticheskiye ustanovki i ikh primeneniye v eksperimental'nykh issledovaniyakh" [Ballistic Installations and Their Use in Experimental Research], Moscow, Nauka, 1974, 344 pp.

5. J. Bell, "Experimental Verification of the Quasistatic Hypothesis in an Experiment on a Hopkinson Split Bar Using Diffraction Gratings," MEKHANIKA, Vol 3, No 5, 1968, pp 138-156.

6. M. A. Belov, A. Ye. Bogdanovich, "Numerical Generalization of Laplace Transformation by the Method of Asymptotic Expansion of an Interval in Dynamic Problems of Viscoelasticity," MEKHANIKA POLIMEROV, No 5, 1976, pp 864-870.

7. Yu. A. Belyayev, A. F. Mel'shanov, "Method of Dynamic Testing of Some Materials at High Loading Rates and Low Temperatures," ZAVODSKAYA LABORATORIYA, Vol 34, No 12, 1968, pp 1501-1504.

8. D. Berry, "Brittleness of Solid Polymers" in: "Razrusheniye tverdykh polimerov" [Destruction of Solid Polymers], edited by B. Rouzen, Moscow, Khimiya, 1971, pp 155-187.

9. M. L. Bogorad, M. A. Loshkarev, "A New Pulse Loading Technique for Studying Dynamic Strength of Polymer Materials," MEKHANIKA POLIMEROV, No 1, 1966, pp 139-142.

10. R. F. Boyler, "Transitions and Relaxation Phenomena in Polymers" in: "Perekhody i relaksatsionnyye yavleniya v polimerakh" [Transitions and Relaxation Phenomena in Polymers], Moscow, Mir, 1968, pp 11-24.

11. A. M. Bragov, "Destruction of Metals for [Durabilities] in the Microsecond Range," author's abstract of dissertation for a degree as Candidate of Technical Sciences, Leningrad, 1975, 17 pp.

12. U. Brown, J. Sroley, "Ispytaniya vysokoprochnykh metallicheskikh materialov na vyazkost' razrusheniya pri vysokoy deformatsii" [Tests of High-Strength Metallic Materials for Breaking Toughness at High Deformation], Moscow, Mir, 1972, 224 pp.

13. I. I. Bugakov, "Relation Between the Gurevich Equation and the Creep Equation," VESTNIK LENINGRADSKOGO UNIVERSITETA, No 1, 1976, pp 78-80.

14. R. Buntzen, "Using Exploding Wires to Study Low-Power Underwater Blasts" in: "Elektricheskiy vzryv provodnikov" [Electrical Explosion of Conductors] edited by A. A. Rukhadze, I. S. Shpigel', Moscow, Mir, 1965, pp 225-238.

15. S. Wenzi, A. Priest, M. May, "Influence of an Inertial Load in Impact Tests with Oscillographic Registration" in: "Udarnyye ispytaniya metallov" [Impact Testing of Metals], edited by B. A. Drozdovskiy, Ye. M. Morozov, Moscow, Mir, pp 175-188.

16. V. V. Viktorov, "Experimental Investigation of the Elastic Dynamic Behavior of Materials and Structures," author's abstract of dissertation for degree as Candidate of Technical Sciences, Moscow, 1972, 16 pp

17. V. V. Viktorov, G. S. Shapiro, "Long-Term Strength of Fiberglass Plastic Under Static and Quasistatic Loading" in: "Mekhanika deformiruyemykh tel i konstruktsiy" [Mechanics of Deformable Bodies and Structures], Moscow, Mashinostroyeniye, 1975, pp 99-102.

18. I. Vitkovskiy, P. Bey, U. Faust et al., "An Exploding Wire as a Source of X-Radiation" in: "Elektricheskiy vzryv provodnikov," edited by A. A. Rukhadze, I. S. Shpigel', Moscow, Mir, 1965, pp 108-118.

19. G. A. Voloskov, G. G. Popov, "Influence that Strain Rate has on Strength Indices and Rigidity of Cold-Setting Fiberglass Plastics," TRUDY INSTITUTA ZHELEZNO-DOROZHNOGO TRANSPORTA, No 322, Transzheldorizdat, 1966, pp 45-53.

20. Yu. Ya. Voloshenko-Klimovitskiy, "Dinamicheskiy predel tekuchesti" [Dynamic Yield Stress], Moscow, Nauka, 1958, 179 pp.

21. Yu. I. Golovin, Yu. A. Brusentsov, V. M. Finkel', "A Facility for Producing Stress Waves with a Plane Front," ZAVODSKAYA LABORATORIYA, Vol 40, No 8, 1974, pp 1031-1032.

22. W. Goldsmith, "Udar" [Impact], Moscow, Stroyizdat, 1965, 448 pp.

23. W. Holke, "Physical Investigation of High-Strain Rate Deformation of Metals" in: "Fizika bystroprotekayushchikh protsessov" [Physics of High-Speed Processes], Vol 2, Moscow, Mir, 1971, pp 69-100.

24. E. I. Grigolyuk, I. T. Selezov, "Neklassicheskiye teorii kolebaniy sterzhney, plastin i obolochek" [Nonclassical Theories of Vibrations of Rods, Plates and Shells], Seriya "Itogi nauki" Vol 5, Moscow, 1973, 272 pages.

25. G. Gross, "Influence that the Strength and Thickness of Notched Specimens have on Impact Toughness" in: "Udarnyye ispytaniya metallov," edited by B. A. Drozdovskiy, Ye. M. Morozov, Moscow, Mir, 1973, pp 30-63.

26. V. Ye. Gul', "Struktura i prochnost' polimerov" [Structure and Strength of Polymers], Moscow, Khimiya, 1971, 334 pp.

27. S. Gurley, H. Keskulla, "Investigation of Multiple Transitions in Polymers by a Dynamic Method" in: "Perekhody i relaksatsionnyye yavleniya v polimerakh," Moscow, Mir, 1968, pp 86-108.

28. N. N. Davidenkov, "Dinamicheskiye ispytaniya metallov" [Dynamic Tests of Metals], Moscow, 1936, 360 pp.

29. R. M. Davis, "Volny napryazheniy v tverdykh telakh" [Stress Waves in Solids], Moscow IL, 1961, 102 pp.

30. O. Jones, E. Ellis, "Propagation of Longitudinal Strain Pulses in Wide Rectangular Rods," PRIKLADNAYA MEKHANIKA, No 1, 1963, pp 61-72.

31. O. Jones, K. Norwood, "Propagation of Strains and Stresses in the Cross Section of an Elastic Cylindrical Rod Under Conditions of Axisymmetric Loading," PRIKLADNAYA MEKHANIKA, No 3, 1967, pp 280-292.

32. N. A. Zlatin, S. M. Mochalov, G. S. Pugachev, A. M. Bragov, "Time Patterns of the Process of Destruction of Metals Under Intense Loads," FIZIKA TVERDOGO TELA, Vol 16, No 6, 1974, pp 1752-1755.

33. N. A. Zlatin, G. S. Pugachev, S. M. Mochalov, A. M. Bragov, "Time Dependence of Strength of Metals with Durability in the Microsecond Range," FIZIKA TVERDOGO TELA, Vol 17, No 9, 1975, pp 2599-2602.

34. L. B. Zuyev, V. Ye. Gromov, V. P. Sergeyev, "A Device for Pulse Loading of Single Crystals," ZAVODSKAYA LABORATORIYA, Vol 40, No 9, 1974, pp 1155-1156.

35. A. B. Zlochevskiy, V. S. Volkov, L. A. Bondarovich, A. V. Kargin, "Particulars of Strain-Gage Measurement of Elastoplastic Deformations Under Impact Loading," ZAVODSKAYA LABORATORIYA, Vol 40, No 11, 1974, pp 1382-1386.

36. Ye. G. Isakovich, M. A. Gol'derman, "Sovremennyye sredstva vysokoskorostnykh ispytaniy materialov" [Modern Facilities for High-Speed Testing of Materials], Moscow, 1970, 61 pp.

37. A. I. Kalimov, Ye. K. Pochtennyy, "A Facility for Dynamic Testing of Materials," ZAVODSKAYA LABORATORIYA, Vol 25, No 1, 1969, pp 114-115.

38. P. P. Kalnin', S. M. Kokoshvili, "Experimental Study of Correspondence Between Quasistatic Stretching and Propagation of Longitudinal Waves in a Polyethylene Rod," MEKHANIKA POLIMEROV, No 3, 1971, pp 564-567.

39. L. Kennedy, O. E. Jones, "Propagation of Longitudinal Waves in a Circular Rod Suddenly Loaded on the End by Pressure that Varies in the Radial Direction," PRIKLADNAYA MEKHANIKA, SER. E., Vol 36, 1969, pp 92-101.

40. J. Kersavag, "Pressures Produced Upon Underwater Explosion of Wires" in: "Elektricheskiy vzryv provodnikov," edited by A. A. Rukhadze, I. S. Shpigel', Moscow, Mir, 1965, pp 260-269.

41. I. A. Kiyko, "Cylindrical Shell Exposed to an Axial Impact Load," MEKHANIKA TVERDOGO TELA, No 2, 1969, pp 135-138.

42. N. A. Kil'chevskiy, "Dinamicheskoye kontaktnoye szhatiye tverdykh tel" [Dynamic Contact Compression of Solids], Kiev, Naukova dumka, 1976, 314 pp.

43. H. Kinopfel, "Sverkhsil'nyye impul'snyye magnitnyye polya" [Ultrastrong Pulsed Magnetic Fields], Moscow, IL, 1972, 320 pp.

44. V. V. Kovriga, V. N. Chalidze, "A Facility for Studying Polymers Under Short-Term Action," MEKHANIKA POLIMEROV, No 5, 1969, pp 919-921.

45. G. M. Kozlov, "Investigation of Strength and Ductility of Metals Under Impact Loading," ZAVODSKAYA LABORATORIYA, Vol 26, No 11, 1960, pp 1284-1288.

46. H. Kolsky, "Volny napryazheniy v tverdykh telakh" [Stress Waves in Solids], Moscow, IL, 1955, 192 pp.

47. H. Kolsky, D. Raider, "Stress Waves and Fractures" in: "Razrusheniye" [Fracture], edited by A. Yu. Ishlinskiy, Vol 1, Moscow, Mir, 1973, 616 pp.

48. S. M. Kokoshvili, "Mechanical Behavior of Some Crystalline Polymers with Wave Propagation and Dynamic Stretching," author's abstract of dissertation for degree as Candidate of Technical Sciences, Riga, 1969, 17 pp.

49. S. M. Kokoshvili, P. P. Kalnin', "Investigation of Wave Propagation in a Polyethylene Rod," MEKHANIKA POLIMEROV, No 1, 1970, pp 59-67.

50. S. M. Kokoshvili, P. P. Kalnin', "A Piezoelectric Dynamometer" Soviet Patent No 309259, OTKRYTIYA, IZOBRETENIYA, PROMYSHLENNYYE OBRAZTSY, TOVARNYYE ZNAKI (Patent Bulletin), No 22, 1971, p 160.

51. S. M. Kokoshvili, P. P. Kalnin', "A Piezoelectric Dynamometer," Soviet Patent No. 302969, Patent Bulletin No 27, 1972, p 224.

52. S. M. Kokoshvili, P. P. Kalnin', "Plotting the Stress-Strain Relations of Fiberglass Plastics from an Experimental Study of Wave Processes," MEKHANIKA POLIMEROV, No 4, 1974, pp 704-705.

53. S. M. Kokoshvili, P. P. Kalnin', Yu. O. Yanson, "Quasistatic Methods of Studying Dynamic Properties of Rigid Polymers," MEKHANIKA POLIMEROV, No 4, 1974, pp 683-685.

54. S. M. Kokoshvili, V. P. Muzychenko, V. P. Tamuzh, "Numerical Solution of the Problem of Impact of a Rigid Mass Against a Rod of Finite Length," MEKHANIKA POLIMEROV, No 3, 1971, pp 453-456.

55. S. M. Kokoshvili, "Investigation of Mechanical Properties of Polyethylene and Fluorocarbon over a Wide Range of Strain Rates," MEKHANIKA POLIMEROV, No 1, 1968, pp 45-52.

56. S. M. Kokoshvili, V. P. Muzychenko, V. P. Tamuzh, "Numerical Solution of the Problem of Impact of a Rigid Mass Against a Viscoelastic Rod of Finite Length" in: "Tezisy dokladov Pyatogo Vsesoyuznogo simpoziuma po rasprostraneniyu uprugikh i uprugo-plasticheskikh voln" [Abstracts of Reports to the Fifth All-Union Symposium on Propagation of Elastic and Elasto-Plastic Waves], Alma-Ata, 1971, pp 107-108.

57. S. M. Kokoshvili, Yu. Ya. Riba, V. P. Tamuzh, P. V. Tikhomirov, "Pulse Loading of Fiberglass Plastic Beams by a Distributed Load Using Electromagnetic Fields," MEKHANIKA POLIMEROV, No 5, 1974, pp 868-873.

58. S. M. Kokoshvili, V. P. Tamuzh, "Influence of Strain Rate on the Mechanical Properties of Polyformaldehyde," MEKHANIKA POLIMEROV, No 6, 1966, pp 937-940.

59. S. M. Kokoshvili, V. P. Tamuzh, G. S. Shapiro, "Dynamic Loading of Polymer Materials," MEKHANIKA POLIMEROV, No 2, 1970, pp 326-340.

60. S. M. Kokoshvili, V. P. Tamuzh, Yu. O. Yanson, "Calculation of Relaxation Spectra from the Results of Dynamic Tests," MEKHANIKA POLIMEROV, No 2, 1971, pp 349-353.

61. S. M. Kokoshvili, P. V. Tikhomirov, P. P. Kalnin' "Impact of a Massive Body Against a Fiberglass Plastic Beam," MEKHANIKA POLIMEROV, No 5, 1974, pp 860-867.

62. M. A. Koltunov, "On the Choice of Kernels in Solving Problems with Consideration of Creep and Relaxation," MEKHANIKA POLIMEROV, No 4, 1966, pp 483-497.

63. R. M. Kristensen, "Vvedeniye v teoriyu vyazkouprugosti" [Introduction to the Theory of Viscoelasticity], Moscow, Mir, 197?, 338 pp.

64. K. Lecont, "High-Speed Throwing" in: "Fizika bystroprotekayushchikh protsessov," Vol 2, Moscow, Mir, 1971, pp 247-275.

65. V. S. Lenskiy, "Interaction of Bodies with High Velocities" in: "Materialy Vsesoyuznogo simpoziuma po rasprostraneniyu uprugo-plasticheskikh voln v sploshnykh sredakh" [Materials of the All-Union Symposium on Propagation of Elastoplastic Waves in Continuous Media], Baku, Academy of Sciences of the Azerbaijan SSR, 196?, pp 27-65.

66. V. N. Loginov, "Elektricheskiye izmereniya mekhanicheskikh velichin" [Electric Measurements of Mechanical Quantities], Moscow, Energiya, 1970, 104 pp.

67. J. Lewis, W. Goldsmith, "A Biaxial Hopkinson Bar for Simultaneous Twisting and Compression," PRIBORY DLYA NAUCHNYKH ISSLEDOVANIY, No 7, 1973, pp 22-26.

68. A. K. Malmeyster, "Uprugost' i neuprugost' betona" [Elasticity and Inelasticity of Concrete], Riga, Latv SSR Academy of Sciences, 1957, 202 pp.

69. B. M. Malyshev, "Propagation of Added Load Pulses over a Tensioned Rod," IZVESTIYA AKADEMII NAUK SSSR: MEKHANIKA I MASHINOSTROYENIYE, No 2, 1960, pp 120-124.

70. C Maiden, S. Green, "Testing for High-Speed Deformation Under Compression for Six Materials at Strain Rates from 10^{-3} to 10^{4} s^{-1}," PRIKLADNAYA MEKHANIKA, No 3, 1966, pp 20-30.

71. A. V. Mironenko, "Fotoelektricheskiye izmeritel'nyye sistemy (izmereneiye lineynykh i uglovykh velichin)," [Photoelectric Measurement Systems (Measurement of Linear and Angular Quantities)], Moscow, Energiya, 1967, 360 pp.

72. V. P. Muzychenko, S. M. Kokoshvili, "Rezul'taty izucheniya rasprostraneniya prodol'nykh vyazko-uprugikh voln chislennymi metodami" [Results of Measurement of Longitudinal Viscoelastic Wave Propagation by Numerical Methods], NAUCHNO-TEKHNICHESKIY SBORNIK RVVIU IMENI ALKSNISA, Riga, No 11, 1973, pp 3-7.

73. U. K. Nigul, "Application of the Three-Dimensional Theory of Elasticity to Analysis of the Wave Process of Bending of a Semi-Infinite Plate with Short-Term Action of an Edge Load," PRIKLADNAYA MATEMATIKA I MEKHANIKA, Vol 17, No 6, 1963, pp 583-588.

74. T. Nikolas, "Analysis of Applicability of the Hopkinson Split Bar Method to Investigation of Materials with Characteristics that Depend on Strain Rate," PRIKLADNAYA MEKHANIKA, SER. E., No 1, 1973, pp 288-295.

75. V. P. Ol'shanskiy, A. R. Filipov, "Oscillations of a Sandwich Strip Beam Under Impact," PRIKLADNAYA MEKHANIKA, Vol 4, No 12, 1970, pp 92-96.

76. V. G. Petushkov, "Choosing a Specimen for High-Strain Rate Tensile Testing," PROBLEMY PROCHNOSTI, No 4, 1970, pp 97-99.

77. V. G. Petushkov, G. V. Stepanov, "A Facility for Tensile Testing Materials with High Strain Rates," PRIKLADNAYA MEKHANIKA, Vol 5, No 7, 1969, pp 99-102.

78. V. G. Petushkov, G. V. Stepanov, "Some Patterns of Longitudinal Elastic Stress Waves in Rods," PROBLEMY PROCHNOSTI, No 1, 1971, pp 78-81.

79. V. G. Petushkov, G. V. Stepanov, N. A. Fot, "A Method of Experimental Investigation of the Influence of Strain Rate on the Mechanical Properties of Materials," PROBLEMY PROCHNOSTI, No 5, 1970, pp 59-62.

80. V. G. Petushkov, N. A. Fot, "On Using Strain Gages to Measure Dynamic Stresses," PROBLEMY PROCHNOSTI, No 4, 1971, pp 113-115.

81. S. D. Ponomarev, V. L. Biberman, K. K. Likharov et al., "Osnovy sovremennykh metodov rascheta na prochnost' v mashinostroyenii" [Principles of Modern Methods of Strength Calculation in Machine Building], Moscow, "Masgia," 1952, 862. pp.

82. L. M. Puchkov, "Experimental Investigation of the Impact Strength of Kaprolon in the Linear and Plane Stressed States," author's abstract of dissertation for degree as Candidate of Technical Sciences, Leningrad, 1970, 16 pp.

83. L. M. Puchkov, "Experimental Investigation of the Impact Strength of Kaprolon in the Linear and Plane Stressed States," MEKHANIKA POLIMEROV, No 2, 1971, pp 332-334.

84. Yu. N. Rabotnov, "Polzuchest' elementov konstruktsiy" [Creep of Structural Elements], Moscow, Nauka, 1966, 752 pp.

85. S. Randzhanat, "Transverse Impact of a Semi-Infinite Elastic Rod on an Infinite Elastic Beam," PRIKLADNAYA MEKHANIKA, Vol 38, No 2, 1971, pp 162-167.

86. Kh. A. Rakhmatulin, Yu. A. Dem'yanov, "Prochnost' pri intensivnykh kratkovremennykh nagruzkakh" [Strength Under Intense Short-Term Loads], Moscow, Fizmatgiz, 1961, 339 pp.

87. V. V. Regel', A. I. Slutsker, E. Ye. Tomashevskiy, "Kineticheskaya priroda prochnosti tverdykh tel" [Kinetic Nature of Strength of Solids], Moscow, Nauka, 1974, 560 pp.

88. A. R. Rzhanitsyn, "Teoriya polzuchesti" [Theory of Creep], Moscow, Stroyizdat, 1968, 416 pp.

89. V. P. Rusov, "Methods of Testing Plastics on Charpy and Izod Hammers and the Dinstat Machine," IZVESTIYA VUZov: STROITEL'STVO I ARKHITEKTURA, No 4, 1973, pp 155-159.

90. V. A. Ryzhanskiy, V. N. Mileyev, V. I. Tsypkin et al., "Experimental Investigation of Explosive Expansion of Thin Annealed Aluminum Alloy

Rings," FIZIKA GORENIYA I VZRYVA, Vol 12, No 1, 1976, pp 120-124.

91. G. V. Stepanov, "A Method of Exciting Planar Elastoplastic Waves in Solids," PROBLEMY PROCHNOSTI, No 9, 1971, pp 75-78.

92. G. V. Stepanov, "Influence that the Loading Scheme has on Stretching and Compression in High-Strain Rate Tests," PROBLEMY PROCHNOSTI, No 2, 1974, pp 63-65.

93. G. V. Stepanov, "Analysis of a Technique for Measuring Pressure in Intense Waves by Dielectric Sensors," PROBLEMY PROCHNOSTI, No 4, 1974, pp 100-103.

94. S. Strella, "Behavior of Polymers Under Impact Loads" in: "Konstruktsionnyye svoystva plastmass" [Structural Properties of Plastics], Moscow, Khimiya, 1967, pp 379-400.

95. B. I. Taratorin, V. V. Kryzhanovskiy, "Investigation of Relaxation and Optical Properties of Hardened Epoxy Resin," MEKHANIKA POLIMEROV, No 1, 1970, pp 15-23.

96. Yu. M. Tarnopol'skiy, T. Ya. Kintsis, "Metody staticheskikh ispytaniy armirovannykh plastikov" [Methods of Static Tests of Reinforced Plastics], Moscow, Khimiya, 1975, 264 pp.

97. K. Turner, "Measurement of Breaking Toughness in Impact Testing with Oscilloscopic Registration" in: "Udarnyye ispytaniya metallov," edited by B. A. Drozdovskiy, Ye. M. Morozov, Moscow, Mir, 1973, pp 100-122.

98. S. P. Timoshenko, "Kolebaniya v inzhenernom dele" [Vibrations in Engineering], Moscow, Nauka, 1967, 444 pp.

99. A. Tobol'skiy, "Svoystva i struktura polimerov" [Properties and Structure of Polymers], Moscow, Khimiya, 1969, 332 pp.

100. I. M. Tyuneyeva, "Relaxation Characteristics of Fiberglass Plastics," MEKHANIKA POLIMEROV, No 3, 1970, pp 560-562.

101. H. Walling, M. Forrestal, "Elastoplastic Stretching of 6061-T6 Aluminum Alloy Rings," RAKETNAYA TEKHNIKA I KOSMONAVTIKA, Vol 11, No 8, 1973, pp 174-175.

102. J. S. Ufland, "Wave Propagation with Transverse Vibrations of Rods and Plates," PRIKLADNAYA MATEMATIKA I MEKHANIKA, Vol 12, No 3, 1948, pp 287-300.

103. A. P. Fillipov, "Kolebaniya deformiruyemykh sistem" [Vibrations of Deformable Systems], Moscow, "Mashinostroyeniye, 1970, 736 pp.

104. A. Florest, R. Fers, "Rigid-Ductile Beams Under the Action of a Uniformly Distributed Pulse Load," PRIKLADNAYA MEKHANIKA, SER. E, No 3, 1965, pp 3-10.

105. M. Forrestal, H. Walling, "Axisymmetric Plastic Deformation of Rings Under the Action of Short Pressure Pulses," RAKETNAYA TEKHNIKA I KOSMONAVTIKA, Vol 10, No 10, 1972, pp 142-144.

106. F. Franch, "Development of a Pendulum Hammer for Dynamic Testing with a Falling Weight" in: "Udarnyye ispytaniye metallov" edited by B. A. Drozdovskiy, Ye. M. Morozov, Mir, 1973, pp 297-305.

107. J. Haberstead, "Numerical Solution of the Two-Dimensional Problem of Elastic Wave Propagation in Rods of Different Configurations," PRIKLADNAYA MEKHANIKA, SER. E, No 1, 1971, pp 62-69.

108. J. Haberstead, K. Hodge, "Influence that Disruption of Continuity of the Cross Section has on Transmission of an Elastic Pulse," PRIKLADNAYA MEKHANIKA, SER. E, No 1, 1971, pp 266-267.

109. L. M. Shestopalov, "Deformirovaniye metallov i volny plastichnosti v nikh" [Deformation of Metals and Plasticity Waves in them], Moscow, USSR Academy of Sciences, 1958, 268 pp.

110. V. A. Shushkevich, "Osnovy elektrotenzometrii" [Principles of Electric Strain Measurement], Minsk, Vysheyshaya shkola, 1975, pp 32-96.

111. L. A. Yutkin, "Elektrogidravlicheskiy effekt i nekotoryye vozmozhnosti yego primeneniya" [The Electrohydraulic Effect and Some Possibilities of its Application], Leningrad, 1969, 16 pp.

112. Yu. O. Yanson, "Determining the Spectra of Relaxation Times and Dissipated Energy of Some Rigid Polymer Materials Under Impact Loading," Author's abstract of dissertation for degree as Candidate of Technical Sciences, Riga, 1973, 12 pp.

113. A. E. Armenakas, C. A. Sciamarella "Response of Glass-Fiber Reinforced Epoxy Specimens to High Rates of Tensile Loading," EXP. MECH., Vol 13, No 10, 1973, pp 433-440.

114. J. R. Asay, "Shock-Induced Melting in Bismuth," J. APPL. PHYS., Vol 45, No 10, 1974, pp 4441-4452.

115. J. Bell, "Determination of Dynamic Plastic Strain Through the Use of Diffraction Gratings," J. APPL. PHYS., Vol 27, No 10, 1956, pp 1109-1113.

116. J. Bell, "The Experimental Foundations of Solid Mechanics," New York - Berlin, Springer-Verlag, 1973, 813 pp.

117. L. D. Bertholf, C. H. Karnes, "Two-Dimensional Analysis of the Hopkinson Pressure Bar System," J. MECH. PHYS. SOLIDS, Vol 23, 1975, pp 1-19.

118. B. A. Boley, "On the Use of Sine Transforms in Timoshenko Beam Impact Problems," J. APPL. MECH., Vol 24, No 1, 1957, pp 152-153.

119. B. A. Boley, C. C. Chao, "Some Solutions on Timoshenko Beam Equations," J. APPL. MECH., Vol 22, No 4, 1955, pp 579-586.

120. L. J. Broutman, T. Kobayashi, "Dynamic Crack Propagation Studies in Polymers," Dynamicrack Prop., Holand, 1975, pp 215-225.

121. J. D. Cambell, A. R. Dowling, "The Behavior of Materials Subjected to Dynamic Incremental Shear Loading," J. MECH. PHYS. SOLIDS, Vol 18, 1970, pp 43-63.

122. S. S. Chiu, V. H. Neubert, "Difference Method for Wave Analysis of the Split Hopkinson Pressure Bar with a Viscoelastic Specimen," J. MECH. PHYS. SOLIDS, Vol 12, 1964, pp 317-335.

123. C. C. Chou, K. D. Robertson, J. H. Rainey, "The Effect of Strain Rate and Heat Developed During Deformation on the Stress-Strain Curve of Plastics," EXP. MECH., No 10, 1973, pp 127-132.

124. G. L. Commerford, J. S. Whittier, "Uniaxial Strain Wave Propagation Loading," EXP. MECH., No 3, 1970, pp 120-126.

125. G. R. Cowper, "The Shear Coefficient in Timoshenko's Beam Theory," J. APPL. MECH., Vol 33, Ser. E, No 2, 1966.

126. E. D. Davies, S. C. Hunter, "The Dynamic Compression Testing of Solids by the Method of the Split Hopkinson Pressure Bar," J. MECH. PHYS. SOLIDS, Vol 11, 1963, pp 165-179.

127. G. P. de Vault, "The Effect of Lateral Inertia on the Propagation of Plastic Strain in a Cylindrical Rod," J. MECH. PHYS. SOLIDS, Vol 13, 1965, pp 55-68.

128. Taichi Fujii, Mitsumori Miki, "The Studies on Impact Behavior for Unidirectional Fiber-Reinforced Plastic," MEM. FAC. ENG., Osaka City University, No 14, 1973, pp 25-35.

129. G. Gerard, R. Papirno, "Dynamic Biaxial Stress-Strain Characteristics of Aluminum and Mild Steel," TRANS. AMER. SOC. METALS, No 49, 1957, pp 178-183.

130. A. K. Green, P. L. Pratt, "Measurement of the Dynamic Fracture Toughness of Polymethyl Methacrylate by High-Speed Photography," ENG. FRACTURE MECH., Vol 6, 1974, pp 71-90.

131. N. L. Hancox, "Izod Impact Testing of Carbon-Fiber Reinforced Plastics," COMPOSITES, Vol 2, No 1, 1971, pp 41-45.

132. F. Hauser, "Techniques for Measuring Stress-Strain Relation at High Strain Rates," EXP. MECH., Vol 6, No 8, 1966, pp 395-402.

133. K. G. Hoge, "Influence of Strain Rate on Mechanical Properties of 6061-T6 Aluminum Under Uniaxial and Biaxial States of Stress," PROC. SOC. ESA, No 1, 1966, pp 13-18.

134. D. L. Holt, "The Modulus and Yield Stress of Glassy Poly(methyl) Methacrylate at Strain rates up to 100 inch/inch/second," J. APPL. POLYM. SCI., Vol 12, No 7, 1968, pp 1653-1659.

135. C. C. Hsiao, "Time Dependent Tensile Strength of Solids," NATURE, No 4, 759, 1961, pp 131-132.

136. A. Izraeli, J. M. Lifshitz, "Experimental Investigation of Longitudinal Pulse Propagation in Unidirectional Composite Rods," FIBER SCI. TECHNOL., Vol 7, No 2, 1974, pp 99-110.

137. P. C. Johnson, R. S. Stein, "Measurement of Dynamic Flow Properties Under Uniform Stress," Symp. on the Dynamic Behavior of Materials, 1963, No 336, pp 195-207.

138. D. H. Kaelble, "Dynamic and Tensile Properties of Epoxy Resins," J. APPL. POLYM SCI., Vol 9, No 4, 1965, pp 1213-1225.

139. T. Kaneko, "On Timoshenko's Correction for Shear in Vibrating Beams," J. APPL. PHYS., Vol 8, No 16, 1965, pp 1927-1936.

140. K. Kishida, K. Senda, "New Exponential Method for Determining Dynamic Stress-Strain Relations on Metals," EXP. MECH., No 12, 1968, pp 567-571.

141. H. Kolsky, "The Propagation of Stress Pulses in Viscoelastic Solids," PHIL. MAG., Vol 1, No 8, 1956, pp 693-710.

142. A. Kumar, "Strain Rate Effects in Materials," APPL. POLYMER SCI., No 12, 1969, pp 67-96.

143. E. H. Lee, J. Kanter, "Wave Propagation in Finite Rods of Viscoelastic Materials," J. APPL. PHYS., Vol 24, 1953, pp 1115-1122.

144. E. H. Lee, J. H. Morrison, "A comparison of the Propagation of longitudinal Waves in Rods of Viscoelastic Materials," J. POLYM. SCI., Vol 19, 1956, pp 93-110.

145. U. S. Lindholm, "Some Experiments with the Split Hopkinson Pressure Bar," J. MECH. PHYS. SOLIDS, Vol 12, 1964, pp 317-335.

146. U. S. Lindholm, L. M. Yeakley, "A Dynamic Biaxial Testing Machine," PROC. SOC. ESA, 1967, No 1, pp 179-181.

147. U. S. Lindholm, L. M. Yeakley, "High Strain Rate Tension and Compression," EXP. MECH., No 1, 1968, pp 1-9.

148. J. J. Lohr, "Time-Temperature-Strain Rate Equivalence for Various Engineering Thermoplastics," HIGH SPEED TESTING, Vol 5, No 1, 1965, pp 55-70.

149. M. Mao, D. Rader, "Longitudinal Stress Pulse Propagation in Non-uniform Elastic and Viscoelastic Bars," INT. J. SOLIDS STRUCTURE, Vol 6, 1970, pp 519-538.

150. J. A. Morrison, "Wave Propagation in Rods with Voigt Materials and Viscoelastic Materials with Three Parameter Models," QUART. J. MATH., Vol 14, 1956, pp 153-169.

151. E. McAbee, M. Chmura, "Static and High-Rate Tensile Behavior of Various Resin-Reinforcement Combinations," HIGH SPEED TESTING, Vol 5, 1965, pp 85-98.

152. E. McAbee, D. W. Levi, "Problems of Mechanical Properties of Polymers. Tensile Strength of Glass-Reinforced Plastics," J. APPL. POLYM. SCI., Vol 13, 1969, pp 1899-1908.

153. J. Miklowitz, "Flexure Stress in an Infinite Elastic Plate due to a Suddenly Applied Concentrated Transverse Load," J. APPL. MECH., Vol 27, No 4, 1958, pp 681-689.

154. T. Nicholas, J. E. Lawson, "On the Determination of the Mechanical Properties of Materials at High Shear-Strain Rates," PHYS. SOLIDS, Vol 20, 1972, pp 57-64.

155. D. M. Norris, "Propagation of a Stress Pulse in a Viscoelastic Rod," EXP. MECH., Vol 7, No 7, 1967, pp 297-301.

156. N. G. Ohlson, "A High-Speed Testing Machine for Biaxial States of Stress," REV. SCI. INSTRUM., Vol 45, No 6, 1974, pp 827-833.

157. J. H. Percey, "New Techniques for Testing Materials at High Strain Rates," Proc. Conf. Stress and Strain Eng., Brisbane, 1973, Sydney, S.A., pp 219-223.

158. N. Perrone, "On the Use of Ring Tests for Determining Rate-Sensitive Material Constants," EXP. MECH., Vol 5, 1968, pp 232-236.

159. D. C. Phillips, A. S. Tetelman, "The Fracture Toughness of Fiber Composites," COMPOSITES, No 9, 1972, pp 216-223.

160. H. J. Plass, "Some Solutions of the Timoshenko Beam Equation for Short Pulse-Type Loading," J. APPL. MECH., Vol 25, No 3, 1958, pp 379-385.

161. J. A. Roetling, "Yield Stress Behavior of Polymethyl Methacrylate," POLYMER, Vol 6, No 6, 1965, pp 311-317.

162. J. A. Roetling, "Yield Stress Behavior of Some Thermoplastic Polymers," APPL. POLYMER SYMP., No 5, 1967, pp 161-169.

163. C. A. Sciamarella, H. Nyuoka, "Two New Optical Techniques to Measure Strain," EXP. MECH., Vol 14, No 8, 1974, pp 311-316.

164. J. C. Smith, "Wave Propagation in Three-Element Linear Spring and Dashpot Model Filament," J. APPL. PHYS., Vol 37, 1966, pp 1697-1704.

165. T. L. Smith, "Viscoelastic Behavior of Polyisobutylene Under Constant Rates of Elongation," J. POLYM. SCI., Vol 20, 1956, pp 89-100.

166. T. L. Smith, "Dependence of the Ultimate Properties of a GR-S Rubber on Strain Rate and Temperature," J. POLYM. SCI., Vol 32, 1958, pp 99-113.

167. C. Sve, S. Okubo, "Experiments on Pulse Propagation in an Obliquely Laminated Composite," TRANS. ASME, SER. E, Vol 41, No 4, 1974, pp 1052-1056.

168. H. P. Tardif, H. Marquis, "Some Dynamic Properties of Plastics," CANAD. AERONAUTICS SPACE J., Vol 9, No 7, 1963, pp 205-213.

169. Y. M. Tsai, H. Kolsky, "Surface Wave Propagation for Linear Viscoelastic Solids," J. MECH. PHYS. SOLIDS, Vol 16, 1968, pp 99-103.

170. H. C. Walling, M. J. Forrestal, W. K. Tucker, "An Experimental Method of Impulsively Loading Ring Structures," INT. J. SOLIDS STRUCT., Vol 8, No 6, 1968, pp 825-831.

SUBJECT INDEX

END

6610
CSO: 8144/1704